

Best Available Copy

AFFDL-TR-79-3152  
VOLUME I

AC 85117  
VULT

LEVEL III

2  
42

PERIPHERAL JET AIR CUSHION LANDING  
SYSTEM SPANLOADER AIRCRAFT

Lockheed-Georgia Company  
Marietta, Georgia 30063

December 1979

TECHNICAL REPORT AFFDL-TR-79-3152, VOLUME I

Final Report for Period July 1979 - December 1979

Approved for Public Release, Distribution Unlimited

DTIC  
ELECTE  
JUN 4 1980  
A

AIR FORCE FLIGHT DYNAMICS LABORATORY  
AIR FORCE WRIGHT AERONAUTICAL LABORATORIES  
AIR FORCE SYSTEMS COMMAND  
WRIGHT PATTERSON AIR FORCE BASE, OHIO 45433

80 6 2 07

ADA 085203

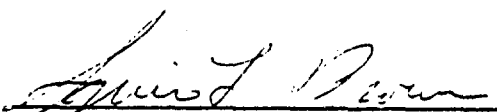
DDC FILE COPY

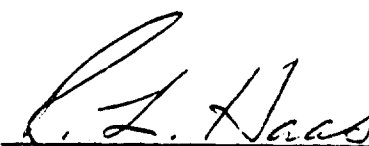
## NOTICE


When Government drawings, specifications, or other data are used for any purpose other than in connection with a definitely related Government procurement operation, the United States Government thereby incurs no responsibility nor any obligation whatsoever; and the fact that the government may have formulated, furnished, or in any way supplied the said drawings, specifications, or other data, is not to be regarded by implication or otherwise as in any manner licensing the holder or any other person or corporation, or conveying any rights or permission to manufacture, use, or sell any patented invention that may in any way be related thereto.

This report has been reviewed by the Information Office (OI) and is releasable to the National Technical Information Service (NTIS). At NTIS, it will be available to the general public, including foreign nations.

This technical report has been reviewed and is approved for publication.

  
SQUIRE L. BROWN, Project Engineer  
FOR THE COMMANDER

  
RAYMOND L. HAAS, Chief  
Vehicle Synthesis Branch

  
PETER J. BUTKEWICZ, Colonel, USAF  
Chief, Aeromechanics Division

If your address has changed, if you wish to be removed from our mailing list, or if the addressee is no longer employed by your organization please notify AFWAL/FIMB, W-PAFB, OH 45433 to help us maintain a current mailing list.

Copies of this report should not be returned unless return is required by security considerations, contractual obligations, or notice on a specific document.

1. REPORT DOCUMENTATION PAGE		READ INSTRUCTIONS BEFORE COMPLETING FORM	
2. GOVT ACCESSION NO.	3. RECIPIENT'S CATALOG NUMBER		
4. AUTHOR	5. TYPE OF REPORT & PERIOD COVERED		
6. PERIPHERAL JET AIR CUSHION LANDING SYSTEM- SPANLOADER AIRCRAFT, VOLUME I	7. AUTHOR		
8. J. W. Moore, L. Barnett, B. T. Farmer, E. E. McBride, B. I. Reynolds and R. E. Stephens	9. Final Report, Jul-Dec 79		
10. PERFORMING ORGANIZATION NAME AND ADDRESS	11. PROGRAM ELEMENT, PROJECT, TASK AREA & WORK UNIT NUMBERS		
Lockheed-Georgia Company Marietta, Georgia 30063	Project 2404 Task 01 Work Unit 56		
12. CONTROLLING OFFICE NAME AND ADDRESS	13. REPORT DATE		
Air Force Flight Dynamics Laboratory (FXB) Air Force Wright Aeronautical Laboratories (AFSC) Wright-Patterson AFB, Ohio 45433	December 1979		
14. MONITORING AGENCY NAME & ADDRESS (if different from Controlling Office)	15. SECURITY CLASS. (of this report)		
12 154	Unclassified		
16. DISTRIBUTION STATEMENT (of this Report)			
Approved for public release; distribution unlimited			
17. DISTRIBUTION STATEMENT (of the abstract entered in Block 20, if different from Report)			
16 2404 17 01			
18. SUPPLEMENTARY NOTES			
19. KEY WORDS (Continue on reverse side if necessary and identify by block number)			
<ul style="list-style-type: none"> <li>o Peripheral Jet</li> <li>o Air Cushion Landing System</li> <li>o Spanloader</li> <li>o Military Aircraft</li> <li>o Cargo Aircraft</li> <li>o Advanced Technology</li> </ul>			
20. ABSTRACT (Continue on reverse side if necessary and identify by block number)			
<p>Inherent in the design optimization of wing span-distributed load (spanloader) aircraft is the lack of ground operational down bending load reaction capability of the wing structure. It is necessary to provide a means to react these down bending loads if the wing structural weight is minimized. Recent studies have provided wide tread landing gears as a means to react these down bending loads, limiting the operational capability</p>			

210065 Am

1. REPORT DOCUMENTATION PAGE		READ INSTRUCTIONS BEFORE COMPLETING FORM	
1. REPORT NUMBER (18) AFFDL-TR-79-3152, <u>V8L-1</u>	2. GOVT ACCESSION NO. AD-A085203	3. RECIPIENT'S CATALOG NUMBER	
4. TITLE (and Subtitle) (6) PERIPHERAL JET AIR CUSHION LANDING SYSTEM- SPANLOADER AIRCRAFT, VOLUME I		5. TYPE OF REPORT & PERIOD COVERED (9) Final Report. Jul-Dec 79	
7. AUTHOR(s) (10) J. W. Moore, L. Barnett, B. T. Farmer, E. E. McBride, B. I. Reynolds, and R. E. Stephens		6. PERFORMING ORG. REPORT NUMBER (14) LG79ER0177-V8L-1	
9. PERFORMING ORGANIZATION NAME AND ADDRESS Lockheed-Georgia Company Marietta, Georgia 30063		8. CONTRACT OR GRANT NUMBER(s) (15) F33615-79-C-3029	
11. CONTROLLING OFFICE NAME AND ADDRESS Air Force Flight Dynamics Laboratory (FXB) Air Force Wright Aeronautical Laboratories (AFSC) Wright-Patterson AFB, Ohio 45433		10. PROGRAM ELEMENT, PROJECT, TASK AREA & WORK UNIT NUMBERS Project 2404 Task 01 Work Unit 56	
12. REPORT DATE (11) December 1979		13. NUMBER OF PAGES	
14. MONITORING AGENCY NAME & ADDRESS (if different from Controlling Office) (12) 154		15. SECURITY CLASS. (of this report) Unclassified	
16. DISTRIBUTION STATEMENT (of this Report) Approved for public release; distribution unlimited (16) 2404 / (17) 01		15a. DECLASSIFICATION/DOWNGRADING SCHEDULE	
17. DISTRIBUTION STATEMENT (of the abstract entered in Block 20, if different from Report)			
18. SUPPLEMENTARY NOTES			
19. KEY WORDS (Continue on reverse side if necessary and identify by block number)			
<ul style="list-style-type: none"> <li>o Peripheral Jet</li> <li>o Air Cushion Landing System</li> <li>o Spanloader</li> <li>o Military Aircraft</li> <li>o Cargo Aircraft</li> <li>o Advanced Technology</li> </ul>			
20. ABSTRACT (Continue on reverse side if necessary and identify by block number) Inherent in the design optimization of wing span-distributed load (spanloader) aircraft is the lack of ground operational down bending load reaction capability of the wing structure. It is necessary to provide a means to react these down bending loads if the wing structural weight is minimized. Recent studies have provided wide tread landing gears as a means to react these down bending loads, limiting the operational capability			

210065 Lau

## 20. (Cont'd)

of the aircraft where the tread width exceeds most existing airport taxiway or runway widths. This study examines the feasibility of replacing the wide tread gear with a peripheral jet air cushion landing system (PJ-ACLS) in combination with a minimum tread (75 feet) width gear. The PJ-ACLS is located adjacent to the wing tip and is used primarily as wing-down bending load reaction device. The minimum tread width gear is retained to simplify takeoff and landing procedures and to reduce the magnitude of the lift required from the PJ-ACLS.

## FOREWORD

The data contained herein are furnished in response to Air Force Flight Dynamics Laboratory, Air Force Aeronautical Systems Division Contract F33615-79-C-3029, "Peripheral Jet Air Cushion Landing System (PJ-ACLS) - Spanloader Aircraft," Project 2404, Task 01, July thru December 1979. The technical response is contained within two volumes. Volume I was prepared in direct response to the required contractual effort and contains the basic PJ-ACLS sizing and performance evaluation. Appendix B data of Volume I are directed to the expansion of the available PJ-ACLS stability and control data base and it is noted that these data were prepared under current Lockheed in-house technology development activities. Volume II data are the output of a computerized peripheral jet air cushion landing system performance program.

The Air Force program manager of the PJ-ACLS study was Dr. Squire Brown (AFFDL/FXB). The Lockheed effort was under the direction of J. W. Moore. Those persons directly responsible for the analysis and results contained within Volumes I and II are L. Barnett, B. T. Farmer, E. E. McBride, B. I. Reynolds, and R. E. Stephens.

Program management of the PJ-ACLS study resides in the Advanced Concepts Department, R. H. Lange, Manager, of the Lockheed-Georgia Advanced Design Division, Marietta, Georgia.

Approved for Release	
By	
Date	
Remarks	
A	

**PRECEDING PAGE BLANK**

## TABLE OF CONTENTS

<u>SECTION</u>	<u>PAGE</u>
1.0 INTRODUCTION	1
2.0 BASELINE SPANLOADER DEFINITION	2
3.0 PJ-ACLS CONFIGURATION CONCEPT	4
4.0 PARAMETRIC EVALUATION	12
5.0 SELECTED CUSHION CONFIGURATION	35
6.0 STABILITY AND CONTROL	38
7.0 FORWARD SPEED EFFECTS	53
8.0 CONCLUSIONS AND RECOMMENDATIONS	55
 APPENDIX A. PARAMETRIC EQUATIONS	 61
 APPENDIX B. STABILITY & CONTROL	 85
 APPENDIX C. CUSHION AIRSUPPLY COMPONENT SIZING, PERFORMANCE AND WEIGHTS	 130
 REFERENCES	 142



## LIST OF ILLUSTRATIONS

<u>NO.</u>	<u>TITLE</u>	<u>PAGE</u>
1	NASA Spanloader	3
2	PJ-ACLS Baseline Spanloader	5
3	Landing Gear Schematic - Baseline	6
4	Container Arrangement - Baseline Spanloader	7
5	Wing Sections and Ordinates	8
6	Fuselage and Wing Structural Sections	9
7	Peripheral Jet - ACLS Installation	11
8	PJ-ACLS Cushion Characteristics	13
9	PJ-ACLS Basic Dimensions	15
10	Evaluation Matrix	16
11	Air Cushion Configuration Selection Procedure	17
12	Configuration Selection Procedure - Step 1	19
13	Configuration Selection Procedure - Step 2	20
14	Configuration Selection Procedure - Step 3	21
15	Configuration Selection Procedure - Step 4	22
16	Wing Deflection vs Span and Cushion Load ( $l = 10\% b/2$ )	23
17	Wing Deflection vs Span and Cushion Load ( $l = 20\% b/2$ )	24
18	Wing Deflection vs Span and Cushion Load ( $l = 30\% b/2$ )	25
19	Wing Deflection vs Span and Cushion Load ( $l = 40\% b/2$ )	26
20	Wing Deflection vs Span and Cushion Load ( $l = 50\% b/2$ )	27
21	Wing Weight vs Cushion Span and Load	28
22	Landing Gear Weight	29
23	Baseline PJ-ACLS Cushion Height	30
24	Baseline PJ-ACLS Landing Gear Height	31
25	Centrifugal Fan Performance	33

## LIST OF ILLUSTRATIONS

<u>NO.</u>	<u>TITLE</u>	<u>PAGE</u>
26	Turboshaft Engine Size	34
27	Gearbox Weight	36
28	Tip Gear Weight vs Cushion Load	37
29	Selected Cushion Configurations	39
30	Cushion Lift vs Delta Aircraft Weight	40
31	Cushion Length vs Delta Aircraft Weight	41
32	Cushion Lift vs Fan Tip Speed and $\theta$	42
33	Cushion Lift vs Fan Tip Speed and $t$	43
34	Cushion Lift vs Number Fan Segments	44
35	Cushion Lift vs Jet and Cushion Pressure	45
36	Cushion Lift vs Cushion Airflow	46
37	Cushion Lift vs Shaft Horsepower	47
38	Cushion Lift vs Augmentation Ratio	48
39	Cushion Lift vs Total System Weight	49
40	Cushion Lift vs Total Structural Weight	50
41	Cushion Operating Height/Lift Envelope	51
42	Spanloader Configuration Comparison Summary	56
43	Recommended PJ-ACLS Spanloader Improvements	58
44	Transverse Fan Peripheral Jet Cushion	59
1A thru 18A	Carpet Plots Illustrating Parametric Sizing	67 thru 84

# LIST OF ILLUSTRATIONS (CONCLUDED)

<u>Figure No.</u>	<u>Title</u>	<u>Page</u>
1B	Baseline Spanloader - Peripheral Jet ACLS	86
2B	Rectangular Peripheral Jet	88
3B	Asymmetric Peripheral Jet Control (Vehicle Unconstrained)	89
4B	Asymmetric Peripheral Jet Control (Vehicle Constrained)	91
5B	Multi-Cushion Geometry	94
6B	Control Effectiveness of Peripheral Jet, Z/W	97
7B	Control Effectiveness of Peripheral Jet, X/W	98
8B	Control Effectiveness of Peripheral Jet, ZX/W	99
9B	Control Effectiveness of Peripheral Jet, Y/W	100
10B	Control Effectiveness of Peripheral Jet, ZY/W	101
11B	Control Effectiveness of Peripheral Jet, M/WC	102
12B	Control Effectiveness of Peripheral Jet, L/WB	103
13B	Control Effectiveness of Peripheral Jet, N/WB	104
14B	Longitudinal Data ( $\theta = 30^\circ$ , 100% Support )	107
15B	Lateral Data ( $\theta = 30^\circ$ , 100% Support )	108
16B	Longitudinal Data ( $\theta = 30^\circ$ , Variable Support )	111
17B	Lateral Data ( $\theta = 30^\circ$ , Variable Support )	112
18B	Longitudinal Data ( $\theta = 20^\circ$ , 100% Support )	114
19B	Lateral Data ( $\theta = 20^\circ$ , 100% Support )	115
20B	Longitudinal Data ( $\theta = 20^\circ$ , Variable Support )	116
21B	Lateral Data ( $\theta = 20^\circ$ , Variable Support )	117
22B	Longitudinal Data ( $\theta = 40^\circ$ , 100% Support )	118
23B	Lateral Data ( $\theta = 40^\circ$ , 100% Support )	119
24B	Longitudinal Data ( $\theta = 40^\circ$ , Variable Support )	120
25B	Lateral Data ( $\theta = 40^\circ$ , Variable Support )	121
1C	Cushion Fan Space Limit	138
2C	Delta Aircraft Weight vs Jet Thickness & Angle	140

# LIST OF SYMBOLS

$t$	=	jet thickness, ft
$\theta$	=	jet toe-in angle, positive into cushion-degrees
$P_c$	=	cavity pressure, psfg
$P_j$	=	jet pressure, psfg
$P_F$	=	fan pressure, psfg
$\rho_o$	=	standard atmosphere mass density, 0.002378 slug/ft <sup>3</sup>
$\sigma$	=	atmospheric density ratio $\rho/\rho_o$
$L$	=	rolling moment, ft. lb. (Appendix B only)
$L$	=	total cushion lift or load, lb.
$A_c$	=	cushion area, ft <sup>2</sup>
$J$	=	jet momentum flux, lb.
$\dot{P}$	=	air horsepower
$A$	=	thrust augmentation ratio ( $L/J$ )
$Q_J$	=	jet air flow required per semispan, ft <sup>3</sup> /sec
$Q_F$	=	fan airflow per fan, ft <sup>3</sup> /min.
$S$	=	peripheral length of jet, ft.
$N_F$	=	fan tip speed - rpm
$W$ or $GW$	=	gross weight - lb.
$\Lambda$	=	wing sweep angle - degrees
$l$	=	cushion length - ft.

### LIST OF SYMBOLS

$h_o$	=	main gear height - ft.
$h_c$	=	cushion height @ mid span - ft.
$h_d$	=	jet plane height @ 90% semispan - ft.
$h_t$	=	jet plane height @ wing tip - ft.
$b, B$	=	wing span, feet
$c$	=	wing chord, feet
$d$	=	height of cushion above ground, feet
$F_c$	=	cushion support force, lb.
$J^i$	=	total jet reaction, lb.
$J_F^i$	=	forward or aft jet reaction, lb.
$\eta$	=	jet thickness factor
$M$	=	pitching moment, ft. lb.
$N$	=	yawing moment, ft. lb.
$S_x$	=	x dimension of cushion, feet
$S_y$	=	y dimension of cushion, feet
$X$	=	axial or forward force along x axis, lb.
$Y$	=	side force, lb.
$Z_i$	=	initial vertical cushion force, lb.
$\Delta Z$	=	incremental vertical cushion force, lb.
$\delta\theta$	=	incremental change in jet inclination angle, degree

### LIST OF SYMBOLS

$\phi$	=	roll angle of cushion vehicle, degree
		subscripts
		L left
		R right
w	=	cushion width - ft.
SHP	=	shaft horsepower
$W_{TG}$	=	wing tip gear weight - lb.
$W_{LG}$	=	main landing gear weight - lb.

## 1.0 INTRODUCTION

Recently completed AFFDL New Strategic Airlift Concept (NSAC) studies have indicated that military transports of the span-distributed load type gave lowest life cycle costs among a number of other advanced-technology transports performing the same mission. However, a problem area in the operation of these span-distributed load transports is the requirement for a wide-tread landing gear which exceeds the width of runways and taxiways at most airports. As the originator of the Spanloader design concept in 1969, the Lockheed-Georgia Company attempted to solve the airport problem by use of a pressurized, trunk-type, air-cushion landing system (ACLS) on its aircraft employing ACLS technology of that time period. The recent results of the NSAC studies favoring the use of span-distributed load transports provide justification for the re-evaluation of these aircraft with new approaches for a peripheral-jet, air-cushion landing system (PJ-ACLS).

This report presents the results of a feasibility study of the application of a PJ-ACLS to a spanloader aircraft. A single spanloader configuration defined by a previous Lockheed/NASA study (Reference 1) is used as the baseline aircraft to which the PJ-ACLS is applied. The scope of the study does not allow for the reoptimization of spanloader characteristics for improved compatibility with the use of the PJ-ACLS. However, where it is determined that overall system integration can possibly be improved by spanloader characteristic changes, recommendations are made for future analysis.

The study includes the development of theoretical methods required to define static hover performance in terms of parametric relationships; integration of the PJ-ACLS into the baseline spanloader aircraft with the PJ-ACLS configuration being selected on the basis of minimum total aircraft weight, and a limited dynamic analysis of the PJ-ACLS spanloader aircraft while operating on the air cushion. Stability and control analyses are also performed both from a theoretical viewpoint, see Appendix B, and for the point design aircraft which incorporates the selected cushion configuration.

## 2.0 SPANLOADER AIRCRAFT

The Spanloader aircraft from which the PJ-ACLS baseline configuration is derived is shown on Figure 1. This aircraft was developed by Lockheed for the NASA and is defined by Reference 1. The gross weight given by Reference 1 for the final Spanloader configuration is 1,543,266 pounds. Its gross weight as used by this study is redefined as 1,498,000 pounds. This improvement results from replacing the STF429 engine with the STF477 engine which has a lower fuel consumption rate. Those weight items significant to PJ-ACLS study for this Spanloader configuration are as follows:

### WEIGHT SUMMARY - LB NASA SPANLOADER

<u>Item</u>		<u>Weight</u>
Structure		405,096
Wing	241,599	
Landing Gear	58,111	
Other	105,386	
Propulsion System		72,060
Systems & Equipment		47,510
Weight Empty		524,666
Operating Weight		540,204
Payload		600,000
Zero Fuel Weight		1,140,204
Fuel		358,045
Gross Weight		1,498,249

Inherent in the design optimization of a wing span distributed load (spanloader) aircraft is the lack of ground operation down bending load reaction capability of the wing structure. Cruise flight up bending load relief is provided by the payload being distributed over the wing span. When the wing structure is optimized for this condition the structure becomes down bending critical during ground operations unless auxiliary support is provided by a landing gear with reactions distributed over a large portion of the wing span. This wide



SPEED	0.75 MACH
PAYLOAD	600,000 LB
RANGE	3,000 NM
OPERATING WT.	540,204 LB
ZERO FUEL WT.	1,140,204 LB
FUEL	358,045 LB
GROSS WT.	1,498,000 LB
ENGINE THRUST	59,500 LB
ASPECT RATIO	5.90
SWEEP ANGLE	40°
WING AREA	18,560 SQ. FT.

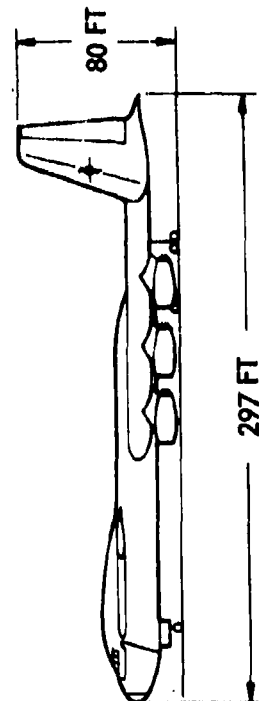
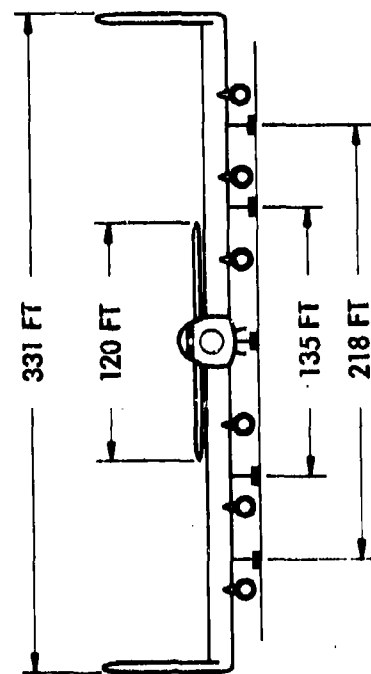
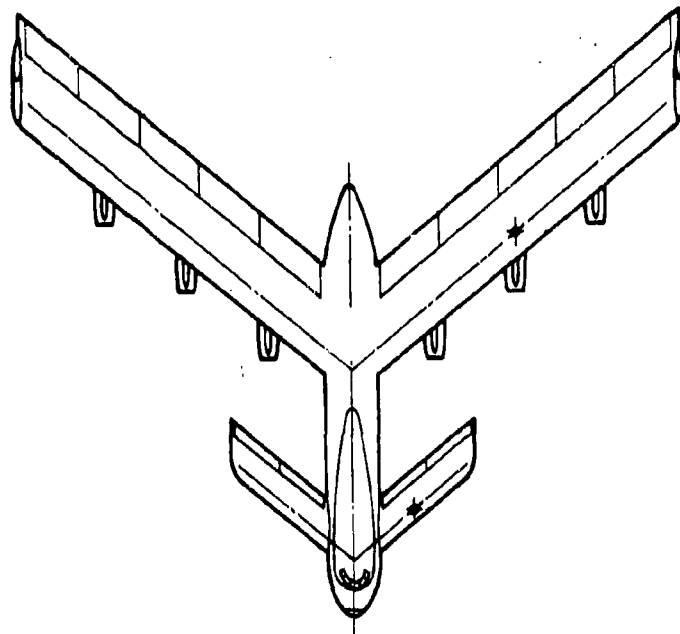


Figure 1. NASA Spanloader

tread landing gear limits the operational capability of the aircraft as the tread width exceeds the runway or taxiway widths at most airports.

The wing weight given is based on having a main landing gear consisting of four bogies distributed across the wing span. The tread width of the outer two bogies is 218 feet. This wide tread gear reacts the negative loads realized during ground operations, thus allowing the wing weight to be optimized for the cruise flight condition.

In order to satisfy the installation requirements of the PJ-ACLS, a number of additional modifications to the Spanloader are required. These modifications are described in the following report section, however, it is noted that aircraft characteristics such as wing sweep, aspect ratio, or airfoil shape are not reoptimized to meet PJ-ACLS needs.

### 3.0 PJ-ACLS SPANLOADER CONFIGURATION CONCEPT

The objective of the PJ-ACLS Spanloader aircraft is to provide a configuration concept which is compatible with existing runways and taxiways but retain the advantage of the lower wing weights which result from span-distributed load type aircraft. To accomplish this objective the following study steps are performed:

- 1) A revised Spanloader configuration, identified as the PJ-ACLS baseline Spanloader, is defined. Modifications to the NASA Spanloader include relocating the prime propulsive engines to the wing upper surface, reducing landing gear height to a minimum installation height, redesigning the canard surface for improved lift characteristics, reducing the main gear tread width to 75 feet, and increasing the wing structural weight to provide structural capability to react 2g negative loads. This configuration is illustrated on Figure 2. Additional configuration details are shown on Figures 3 through 6. Zero fuel weight and gross weight are held constant with the increase in wing weight reducing design payload by a corresponding value as shown in the following weight summary:

SPEED 0.75 MACH  
 PAYLOAD 548,327 LB  
 RANGE 3,000 NM  
 OPERATING WT. 591,877 LB  
 ZERO FUEL WT. 1,140,204 LB  
 FUEL 358,045 LB  
 GROSS WT. 1,498,000 LB  
 ENGINE THRUST 59,500 LB  
 ASPECT RATIO 5.90  
 SWEEP ANGLE 40°  
 WING AREA 18,560 SQ. FT.

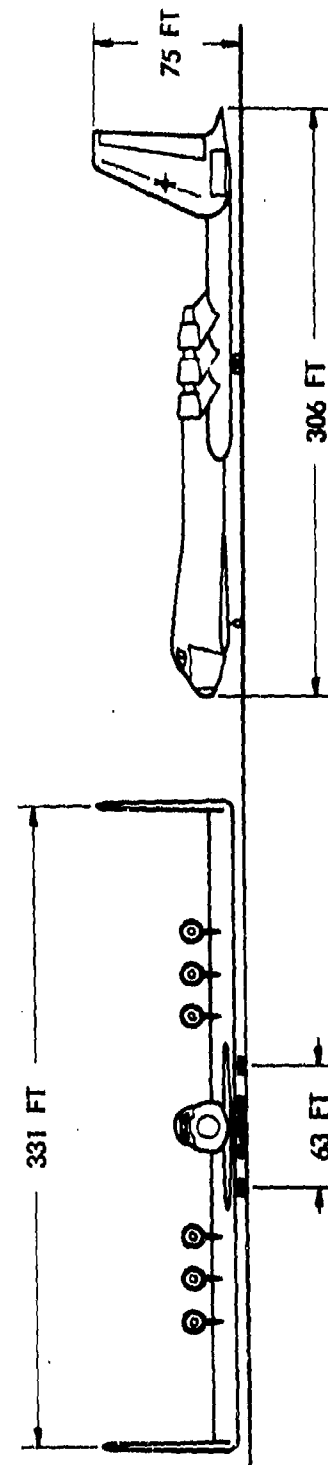
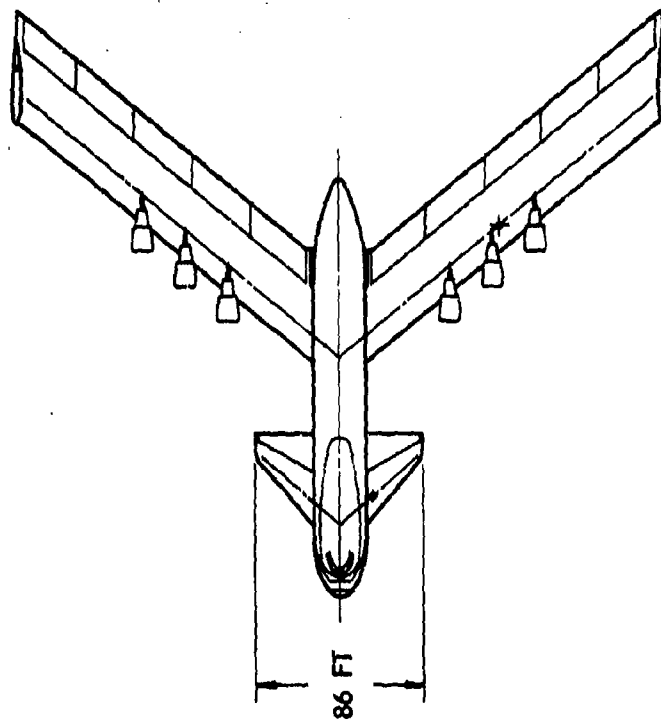


Figure 2. PJ-ACLS Baseline Spanloader

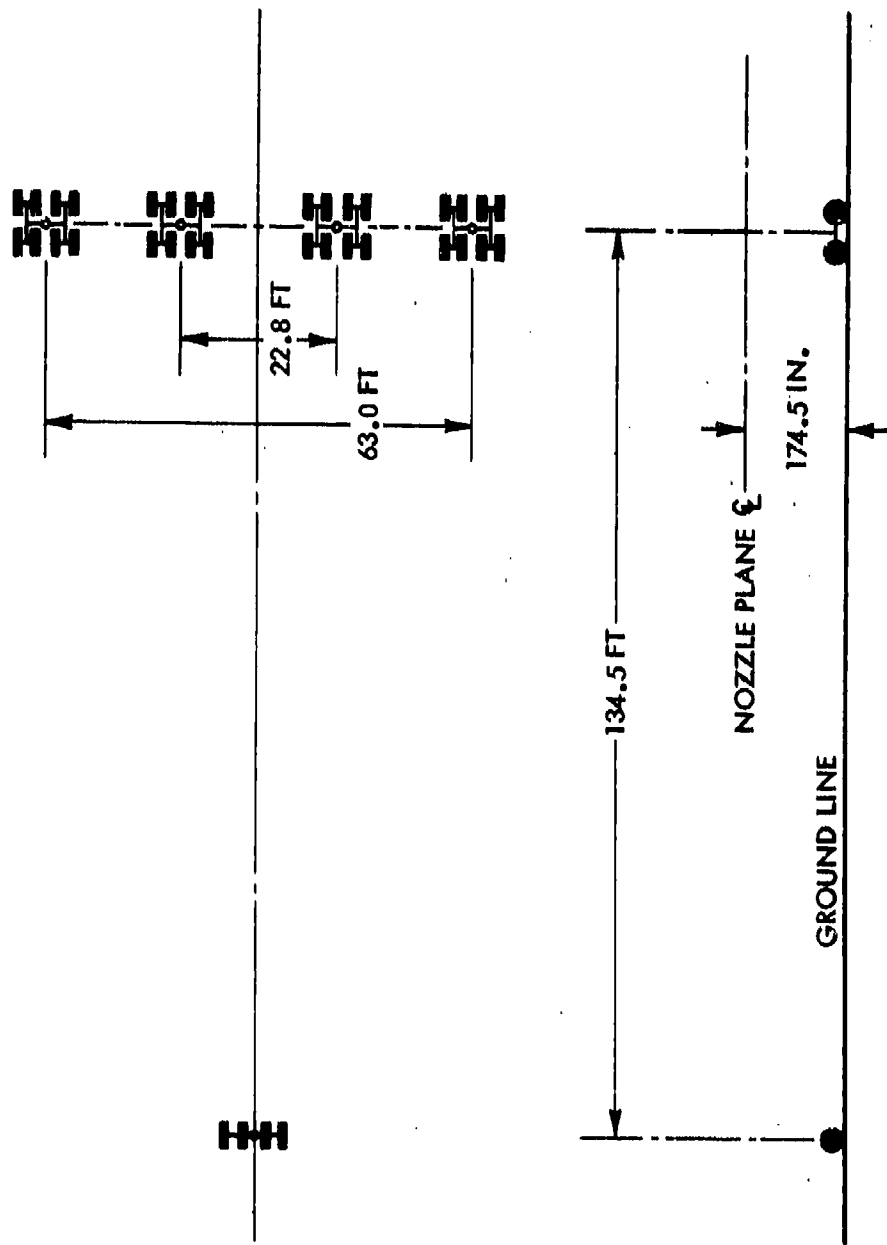
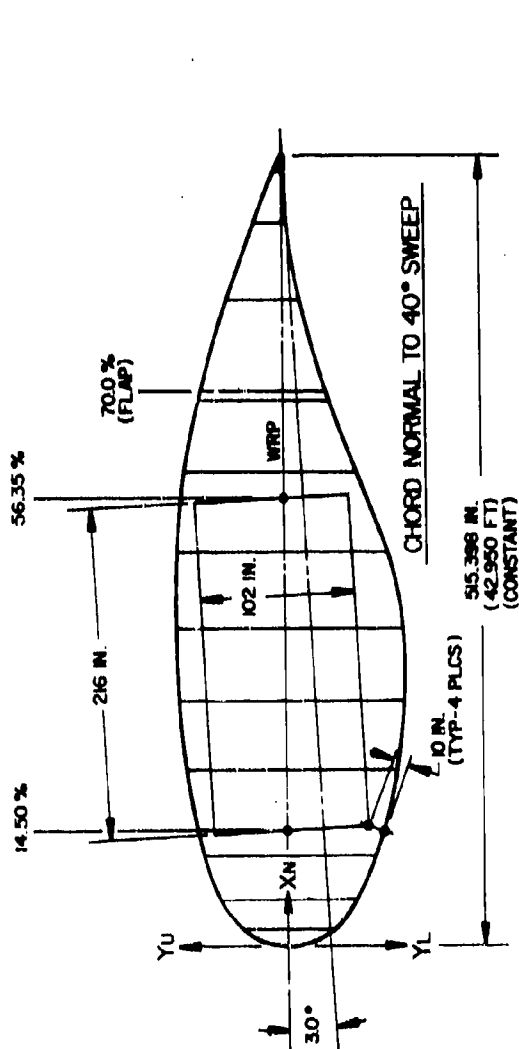


Figure 3. Landing Gear Schematic - Baseline





X <sub>N</sub> (IN.)
0.0
11.081
30.408
58.498
114.418
159.258
207.190
257.889
308.208
356.140
421.080
472.105
505.080
515.398

LG5-621 SUPERCRITICAL AIRFOIL SCALED TO 21.892 % T/C			
X (%)	X (IN.)	Y <sub>U</sub> (IN.)	Y <sub>L</sub> (IN.)
0.0	0.0	0.0	0.0
2.15	14.485	28.195	28.095
5.90	39.895	42.794	43.488
11.35	76.353	52.094	57.443
22.30	149.382	63.895	72.242
50.90	337.895	68.735	77.192
40.80	270.487	70.840	75.749
50.00	338.402	70.198	65.229
58.80	402.357	63.890	48.983
68.10	464.908	58.111	33.177
81.70	548.888	35.472	10.390
91.80	638.398	18.957	1.884
98.00	672.348	6.032	0.421
100.00	672.804	1.048	1.048

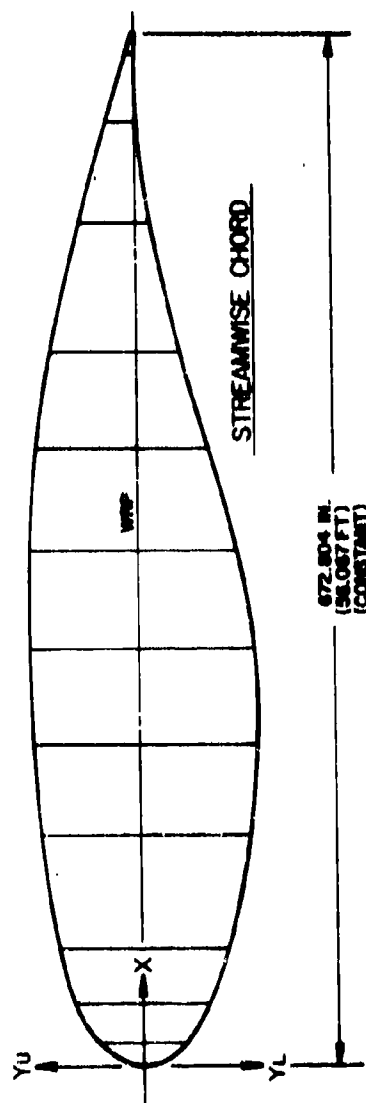
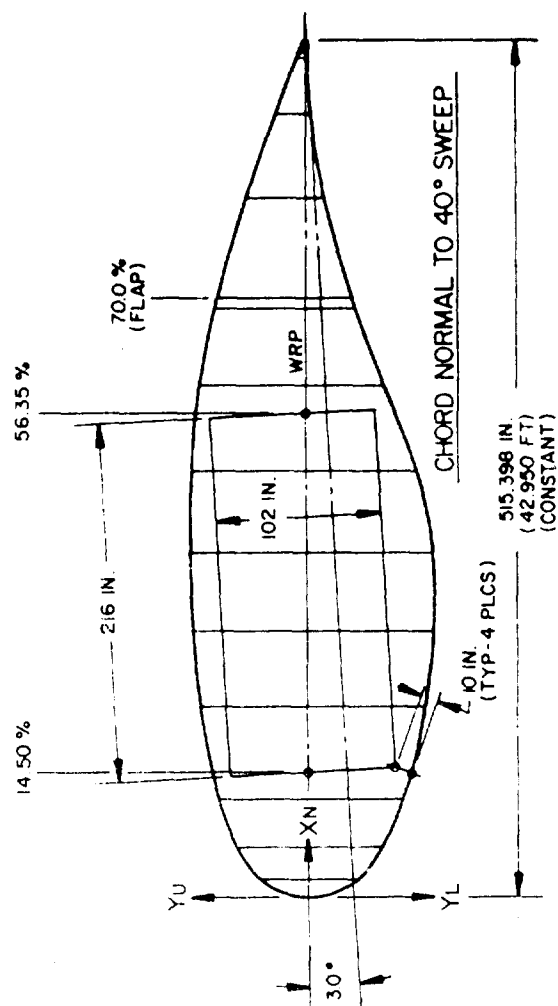


Figure 5. Wing Sections and Ordinates



XN(IN.)
0.0
11.081
30.408
58.498
114.418
159.258
207.190
257.699
308.208
356.140
421.080
472.105
505.090
515.398

LG5-621 SUPERCRITICAL AIRFOIL SCALED TO 21.892 % T/C				
X(%)	X(IN.)	YU(IN.)	YL(IN.)	
0.0	0.0	0.0	0.0	
2.15	14.465	28.196	28.055	
5.50	39.695	42.784	43.486	
11.35	76.363	52.024	51.443	
22.20	143.562	63.626	72.242	
30.90	207.896	68.735	77.152	
40.20	270.447	70.840	75.749	
50.00	336.402	70.138	65.229	
59.80	406.337	65.950	46.993	
68.10	464.808	56.111	29.177	
81.70	548.681	34.472	10.340	
91.80	646.288	18.937	1.894	
98.00	659.348	6.032	0.421	
100.00	672.804	1.045	1.045	

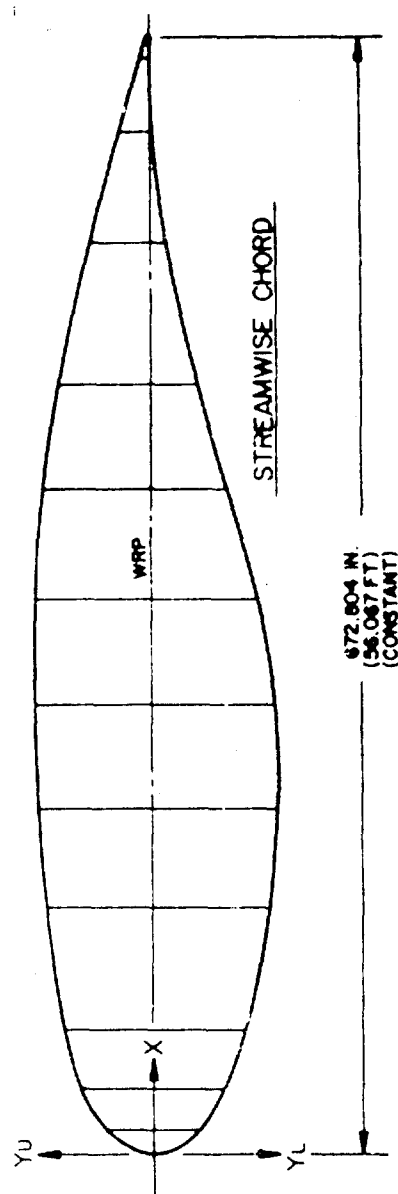
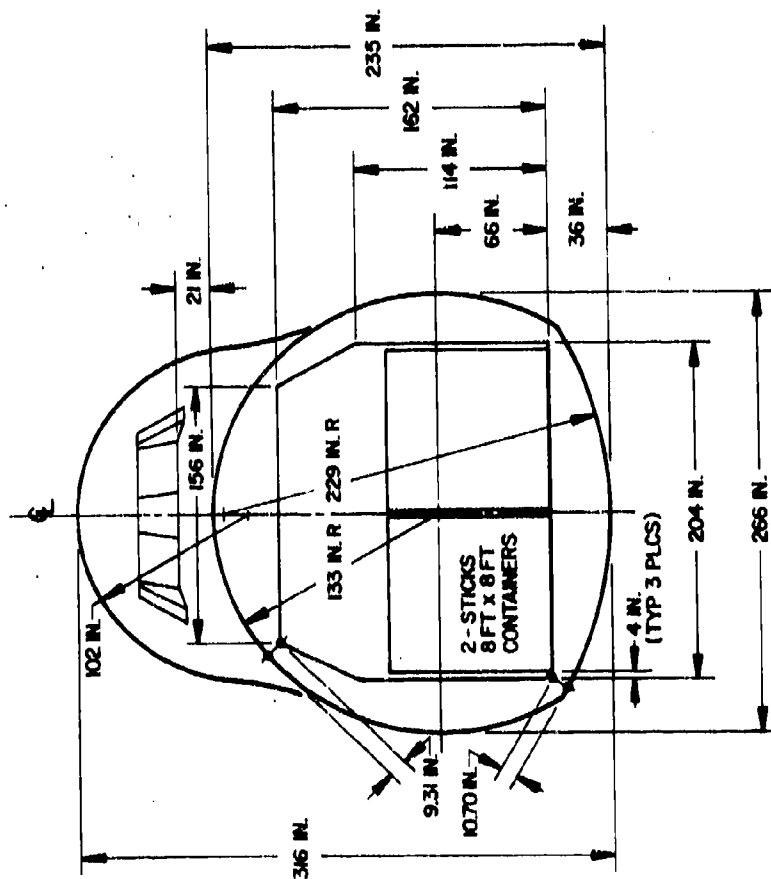
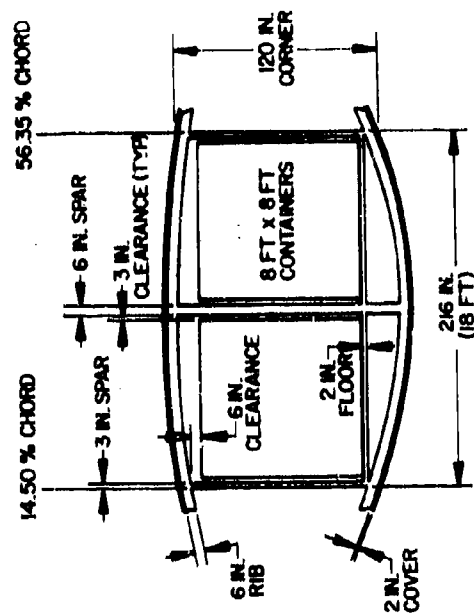


Figure 5. Wing Sections and Ordinates



### FUSELAGE CONSTANT SECTION

X-SECT. AREA = 351.00 SQ. FT  
EQ. DIA. = 21.14 FT  
PERIMETER = 805 IN. (67.08 FT)



### WING CARGO COMPARTMENT PROFILE WITH STRUCTURAL ALLOWANCES

Figure 6. Fuselage and Wing Structural Sections



**WEIGHT SUMMARY - LB**  
**PJ-ACLS BASELINE SPANLOADER**

<u>Item</u>		<u>Weight</u>
Structure		456,769
Wing	293,272	
Landing Gear	58,111	
Other	105,386	
Propulsion System		72,060
Systems & Equipment		47,510
Weight Empty		576,339
Operating Weight		591,877
Payload		548,327
Zero Fuel Weight		1,140,204
Fuel		358,045
Gross Weight		1,498,249

- 2) Various PJ-cushion lift and configuration combinations are incorporated into the baseline to provide wing down bending relief and thereby reduce wing structural weight. The removal of this structural weight requires the addition of a wing tip gear to provide wing support for the static (cushion power off) condition. The identifiable tradeoff then becomes one of added PJ-cushion system weight vs reduced wing weight. The parametric procedure used to perform this tradeoff is described in report section 4.0.

**3.1 CUSHION AIR SUPPLY SYSTEM DESCRIPTION**

The peripheral jet airflow required to pressurize the air cushions is provided by centrifugal fans located within the wing leading and trailing edge cavities just fore and aft of each cushion as shown on Figure 7. Within each cavity the fan installations occupy a space which extends over the length of the respective cushion. Also, as required, one additional fan is located beyond the corner of each cushion, outside the cushion periphery. Because of fan duct space constraints, any other additional fans outside the cushion periphery do



not appear feasible, and thus the number of fans possible for each cushion is space limited - the effects of which are addressed in Appendix C. The fan arrangement provides each cushion with two gangs of fans, one for each cushion "segment." Within each fan gang, the fans are shafted together, with universal joints provided as required to compensate for wing deflections. The fans are driven by turboshaft engines, one at each end of each gang of fans, with the power being transmitted to the fans through speed reduction gearboxes. The chosen aircraft study configuration, incorporating one single cushion per wing semi-span, therefore requires a total of four gangs of fans, eight turboshaft engines, and eight gearboxes. The turboshaft engines and gearboxes are oversized to allow for system failure. For the purposes of this study the remainder of the air supply system is assumed 100 percent reliable.

#### 4.0 PARAMETRIC EVALUATION

The sizing and selection of the PJ-ACLS require the evaluation of numerous variables. The primary independent or sizing variables are cushion width, span and spanwise placement, jet thickness, jet toe-in angle, and height above the ground plane. For a free flying surface effect vehicle, the cushion lift is a specified quantity, however, for the vehicle studies here the main landing gear is retained and only partial lift is provided such that free flight on cushion lift is not obtained. With this type system, cushion lift magnitude also becomes an input variable with cushion power, airflow, jet pressure, and jet thrust being dependent parameters for each combination of cushion lift and sizing variables evaluated.

The cushion sizing variables are illustrated on Figure 8. The cushion area is located adjacent to the wing tip to provide the maximum moment or wing down bending relief. For all cases evaluated the outboard end of the cushion is located at 90 percent semispan. This ten percent semispan outboard of the cushion is maintained to house the wing tip outrigger gear and the turboshaft engine installation.

The essential requirement to be met by all PJ-ACLS configurations considered is that under all ground operation conditions no portion of the wing shall contact the ground surface.

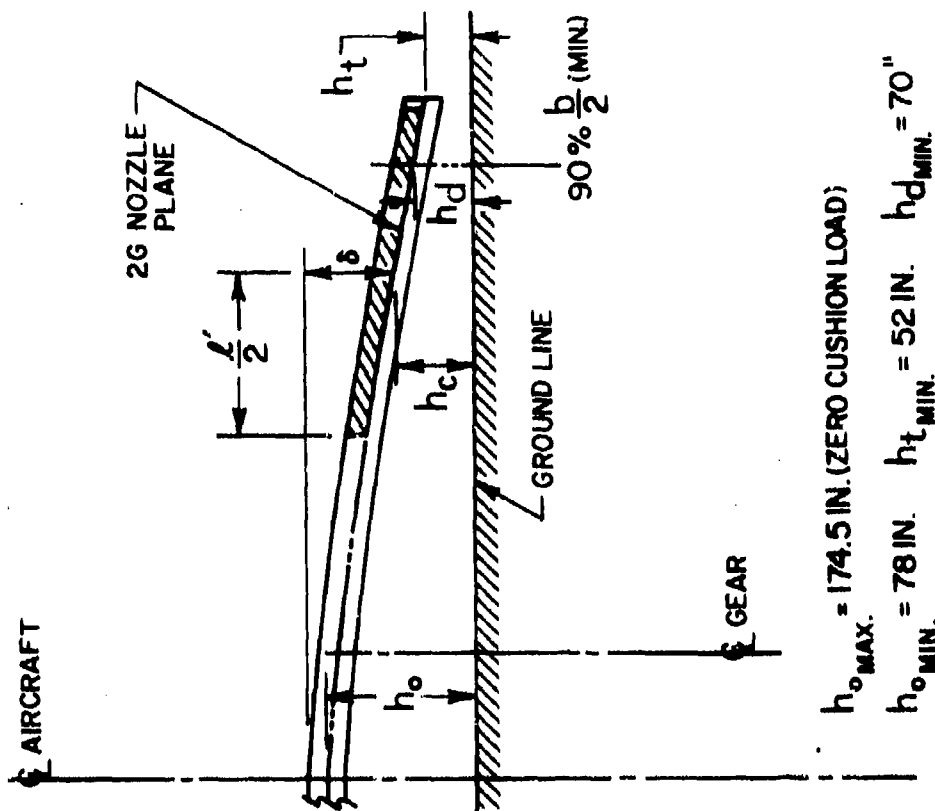
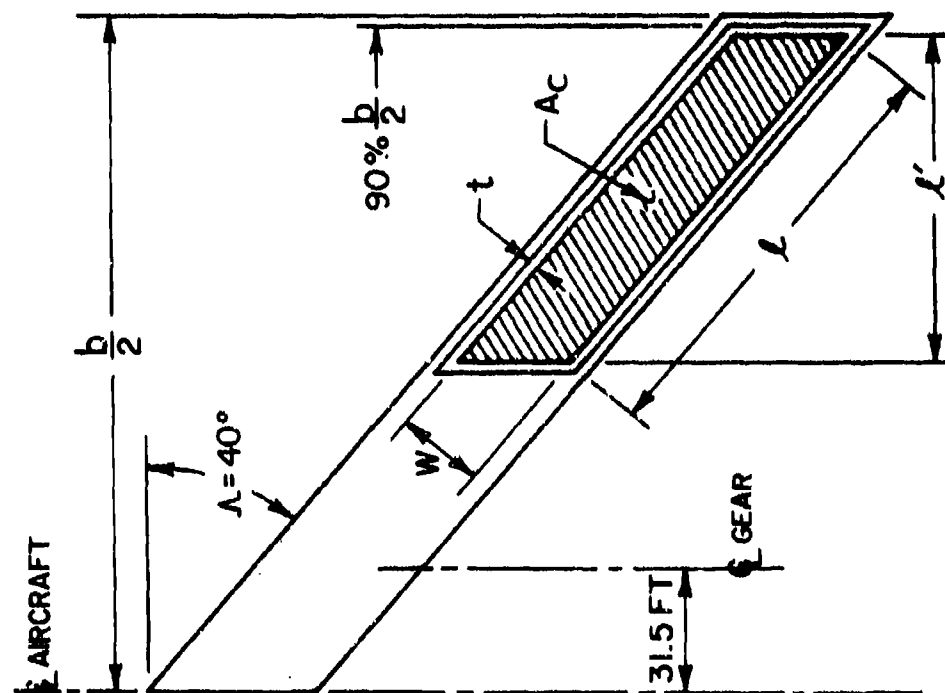


Figure 8. PJ-ACLS Cushion Characteristics

The cushions are thus sized to a ground clearance requirement resulting from the most severe down bending condition. For this purpose, a 2g negative loading is assumed to be critical in lieu of a more refined dynamic taxi analysis. At this condition a 12 inch ground clearance is imposed. The air cushion is sized to provide the corresponding lift requirement. This is not a fixed design situation, since wing flexibility allows the ground clearance requirement to be met by various combinations of cushion lift and main landing gear height.

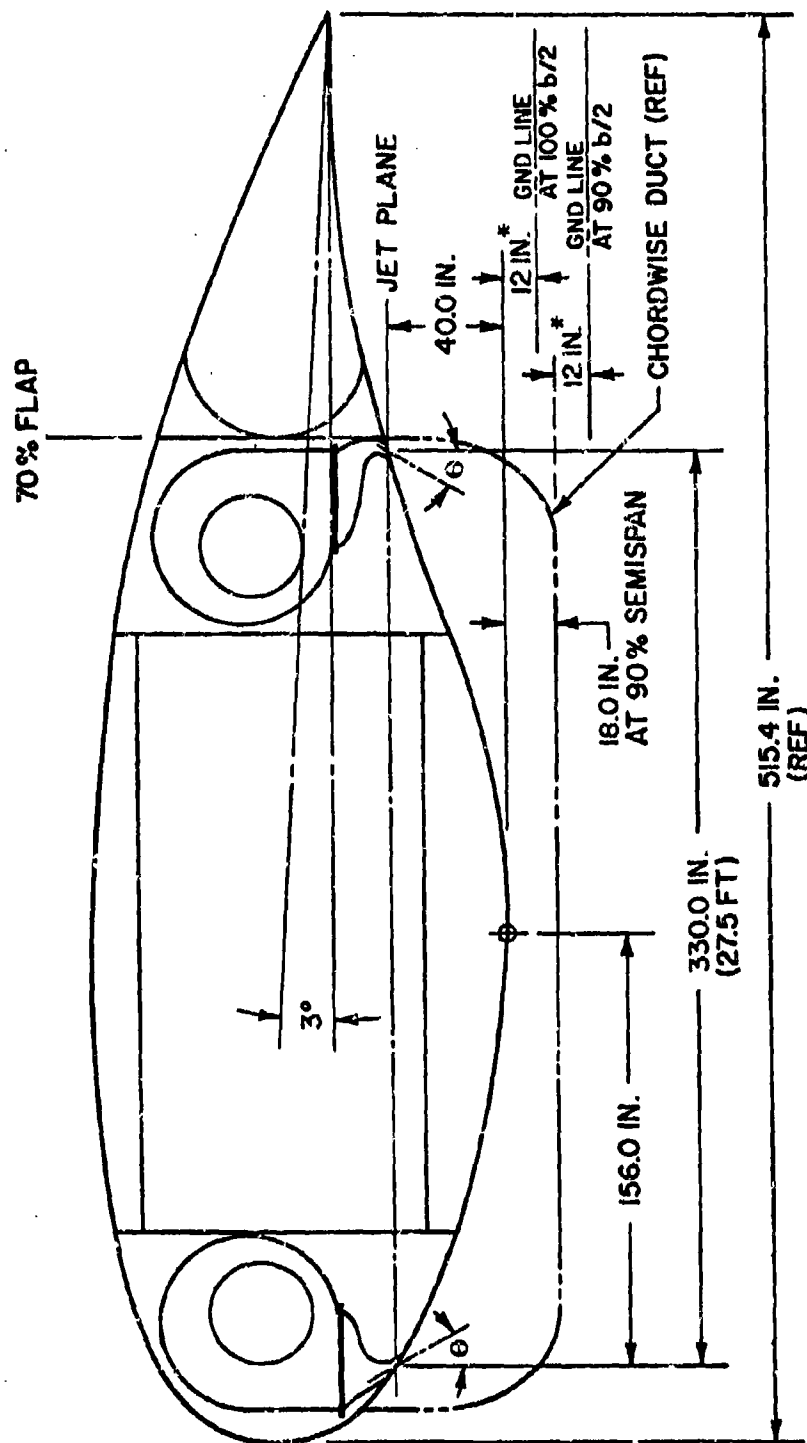
As shown on Figure 8, there are three critical height dimensions that must be met by all cushion configurations. To maintain the 12 inch ground clearance, the cushion jet plane must be at least 52 and 70 inches above the ground at the wing tip and at 90 percent semi-span, respectively. The 90 percent location is critical as the cushion chordwise outboard supply duct occurs at this wing station. The minimum main landing gear height required for installation is 78 inches. Cushion height is a fallout when these three controlling heights are met. These height constraints are also illustrated on Figure 9. This figure defines the maximum cushion width dimension, which is a function of the required cargo compartment width, flap chord, and wing leading edge length, as 27.5 feet.

#### 4.1 EVALUATION MATRIX

The matrix of cushion sizing parameters evaluated are given on Figure 10. As shown, these sizing parameters are evaluated as a function of cushion lift provided. Five values of cushion length, jet thickness, and load are evaluated in combination with 4 values of jet toe-in angle resulting in 500 data points for the baseline cushion heights. To provide a sensitivity to cushion height, which is a critical parameter in the design of the PJ-ACLS, the baseline cushion heights are reduced by 40 inches resulting in an additional 500 data points.

#### 4.2 EVALUATION PROCEDURE

The procedure by which the parameter matrix is evaluated is shown on Figure 11. This parametric procedure requires the formulation of three major blocks of data and the sequential processing of these data into cushion system weight, structural weight, and aircraft delta weight using the baseline Spanloader as a comparison base. In order of use,



MAX. NOZZLE WIDTH = 8.0 IN. (27.5 FT. SEPARATION)

\* MINIMUM MINUS 2g LOAD GROUND CLEARANCE

Figure 9. PJ-ACLS Basic Dimensions

CUSHION LENGTH (L) % b/2	CUSHION LOAD (L) % G.W.	JET ANGLE (θ) DEGREES	JET THICKNESS (t) INCHES
10	2.5		2
20	5.0	15	4
30	7.5	30	6
40	10.0	45	8
50	15.0	60	10
(5)	(5)	(4)	(5) > 500

• CUSHION WIDTH (W) = 27.5 FT

•  $\frac{b}{2} = 216$  FT

• GROSS WEIGHT (G.W.) = 1,498,000 LB

$$\left[ \begin{array}{c} \text{BASELINE } h_c \\ \text{AND} \\ \text{BASELINE } h_c - 40 \end{array} \right] - 1000$$

Figure 10. Evaluation Matrix



### Figure 11. Air Cushion Configuration Selection Procedure



these data blocks to be described in detail by the following paragraphs are:

- 1) Wing deflection as a function of cushion lift and cushion span. (See Figure 12)
- 2) Cushion aerodynamic performance as a function of cushion length, width, height, jet toe-in angle, jet thickness, and lift. (See Figure 13)
- 3) Centrifugal fan system performance as a function of cushion airflow and jet pressure requirements. (See Figure 14)
- 4) Aircraft structural and cushion system weights data as a function of cushion lift and configuration. Structural weights include both wing and main landing gear effects. The cushion system weight includes the required fans, the fan power source, the fuel to operate the fan power source, and the wing tip gear installation. (See Figure 15)

**4.2.1 WING DEFLECTION & STRUCTURAL WEIGHTS DATA** - Wing deflection data are given on Figures 16 through 20 for each matrix value of cushion load (lift) and cushion length defined in terms of percent wing semispan. Cushion width is held constant at a value of 27.5 feet. Wing and landing gear weights data for each cushion lift and length combination are given on Figures 21 and 22. Cushion height ( $h_c$ ) and landing gear height ( $h_g$ ), as shown on Figure 8, are determined as previously described from the wing deflection curves. These heights are given on Figures 23 and 24 as a function of cushion length and lift. With these data, cushion geometric relationships ( $h_c/w$ ,  $l/w$ ,  $t/w$ , and  $L/A_c$ ) are defined as a function of cushion load (lift), as shown on Figure 12, for use as input to the cushion performance data block.

**4.2.2 CUSHION AERODYNAMIC PERFORMANCE** - The cushion aerodynamic performance procedure is illustrated on Figure 13. For each matrix combination of cushion geometry and lift, cushion airhorsepower, airflow, jet pressure, and augmentation ratio are determined. Cushion performance is based entirely upon the Barratt theory as reported in Reference 2. The derivation of the relationships required to perform this procedure are defined in Appendix A.

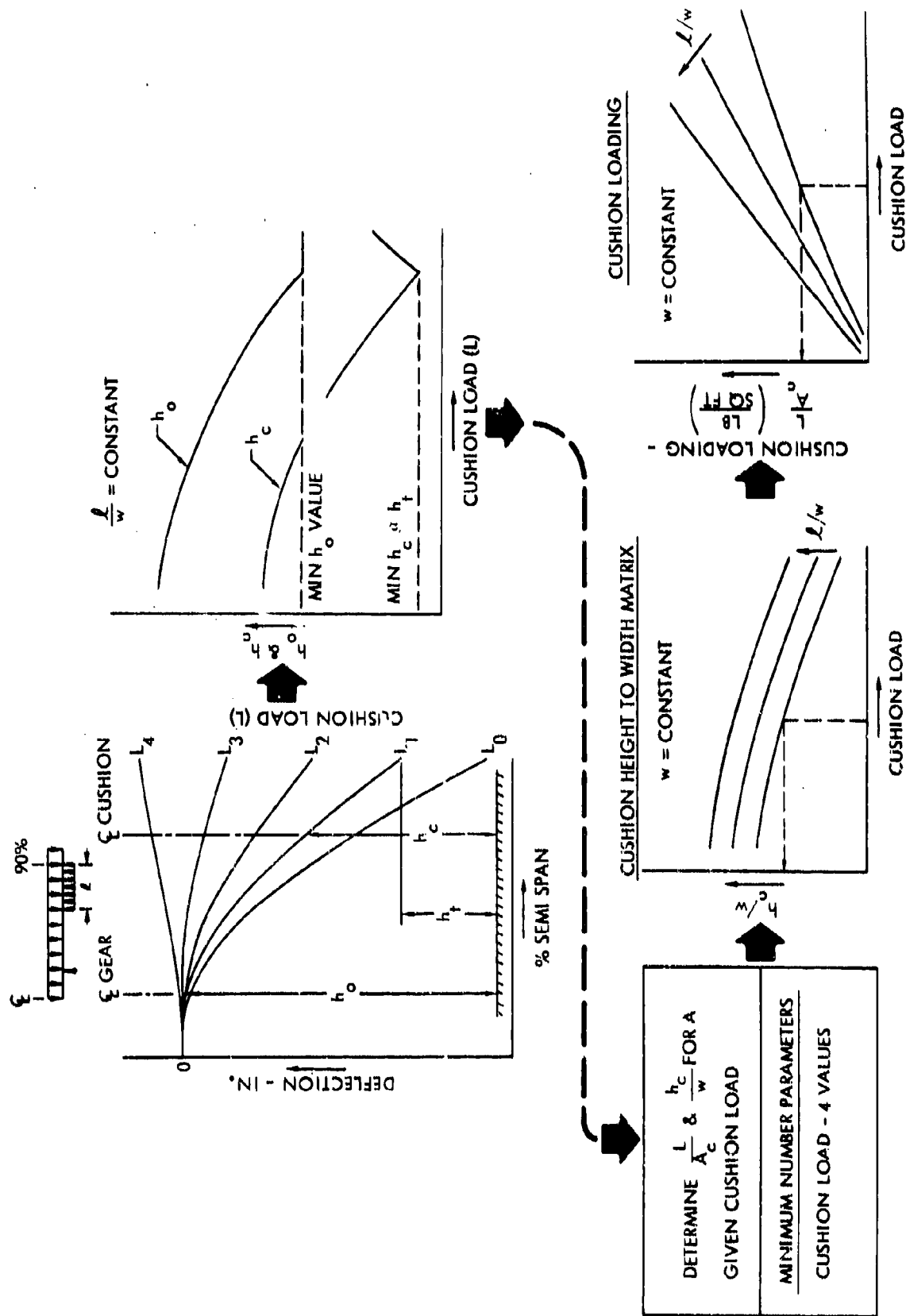


Figure 12. Configuration Selection Procedure - Step 1

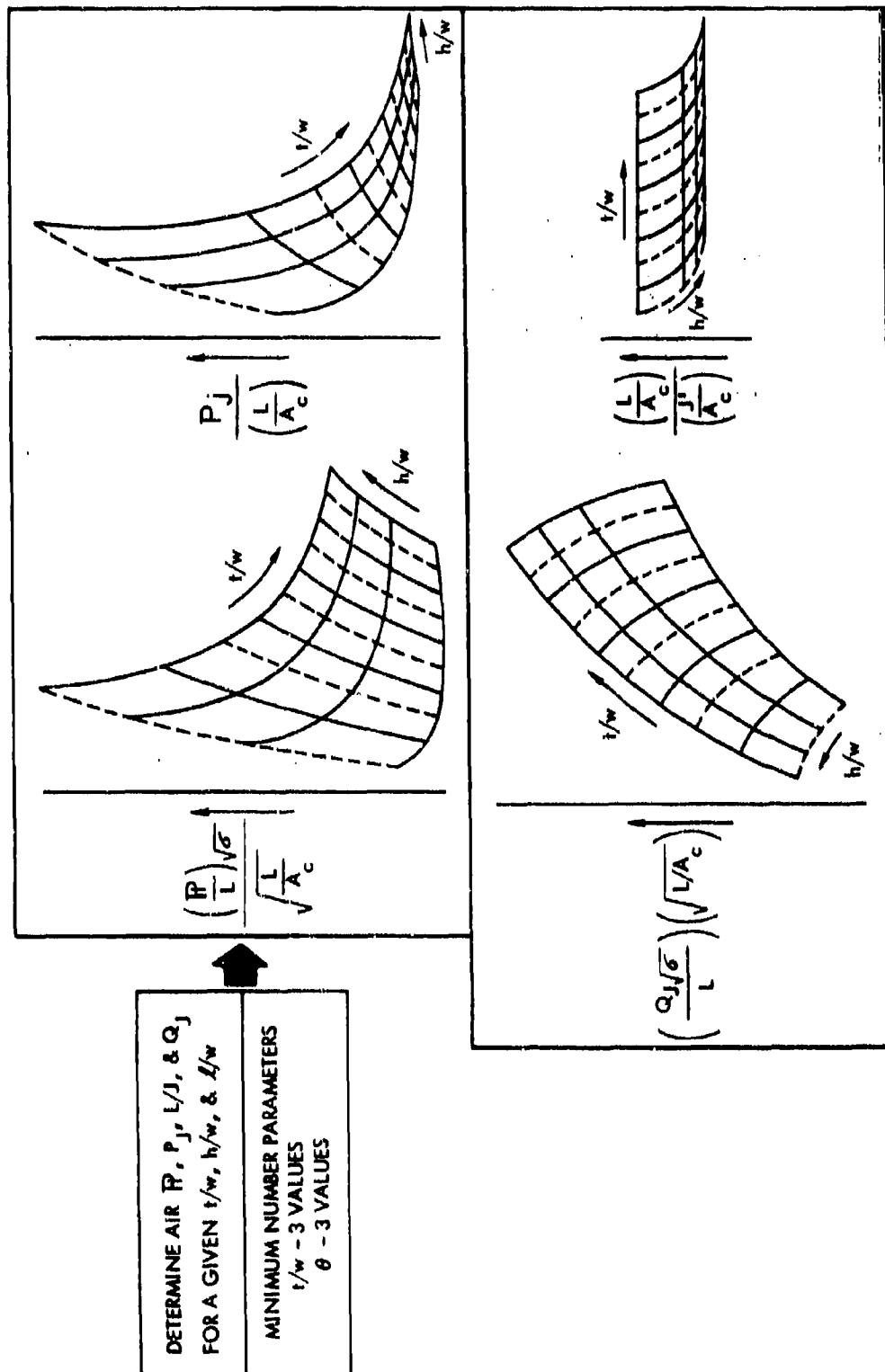


Figure 13. Configuration Selection Procedure - Step 2

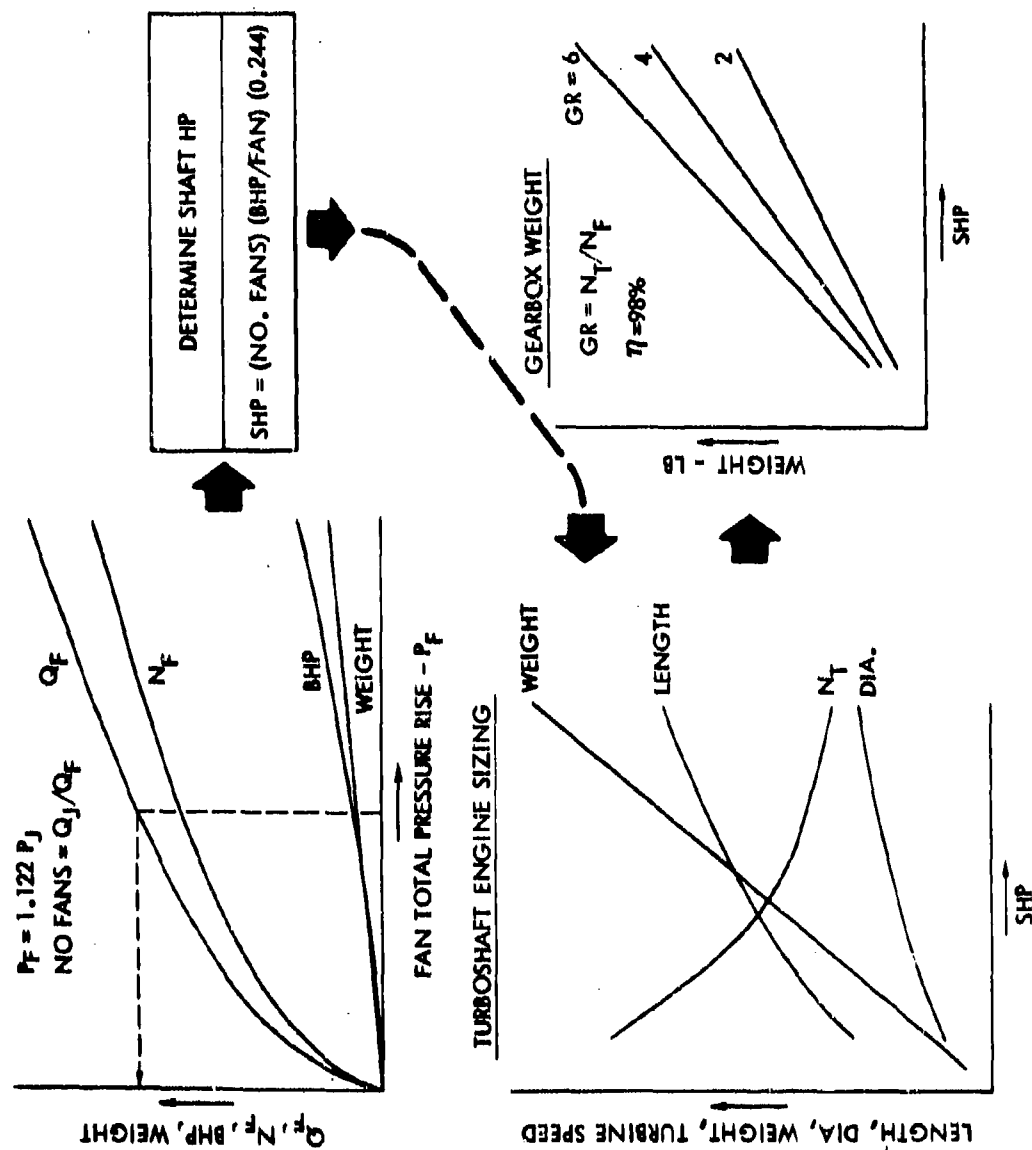


Figure 14. Configuration Selection Procedure - Step 3

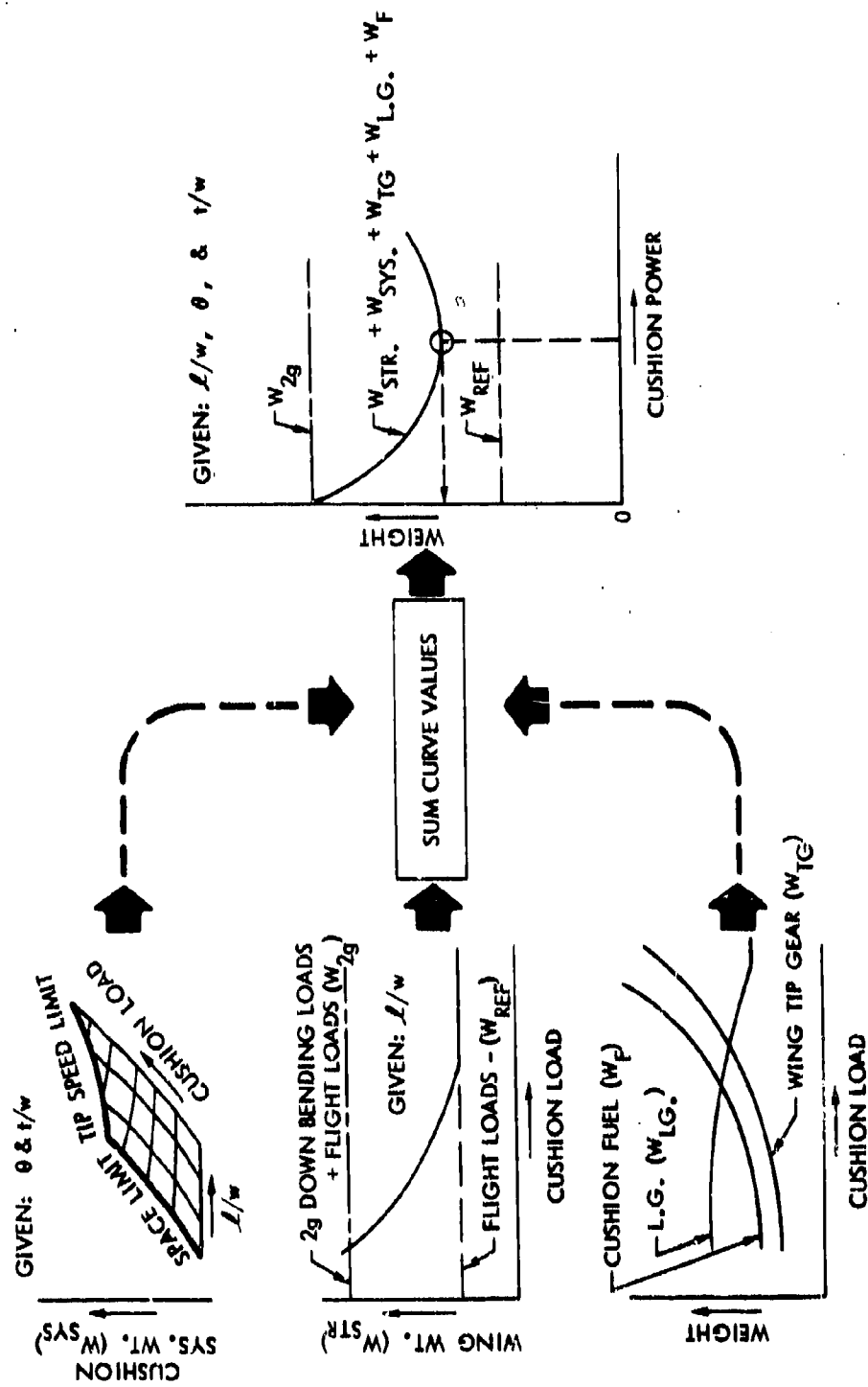


Figure 15. Configuration Selection Procedure - Step 4

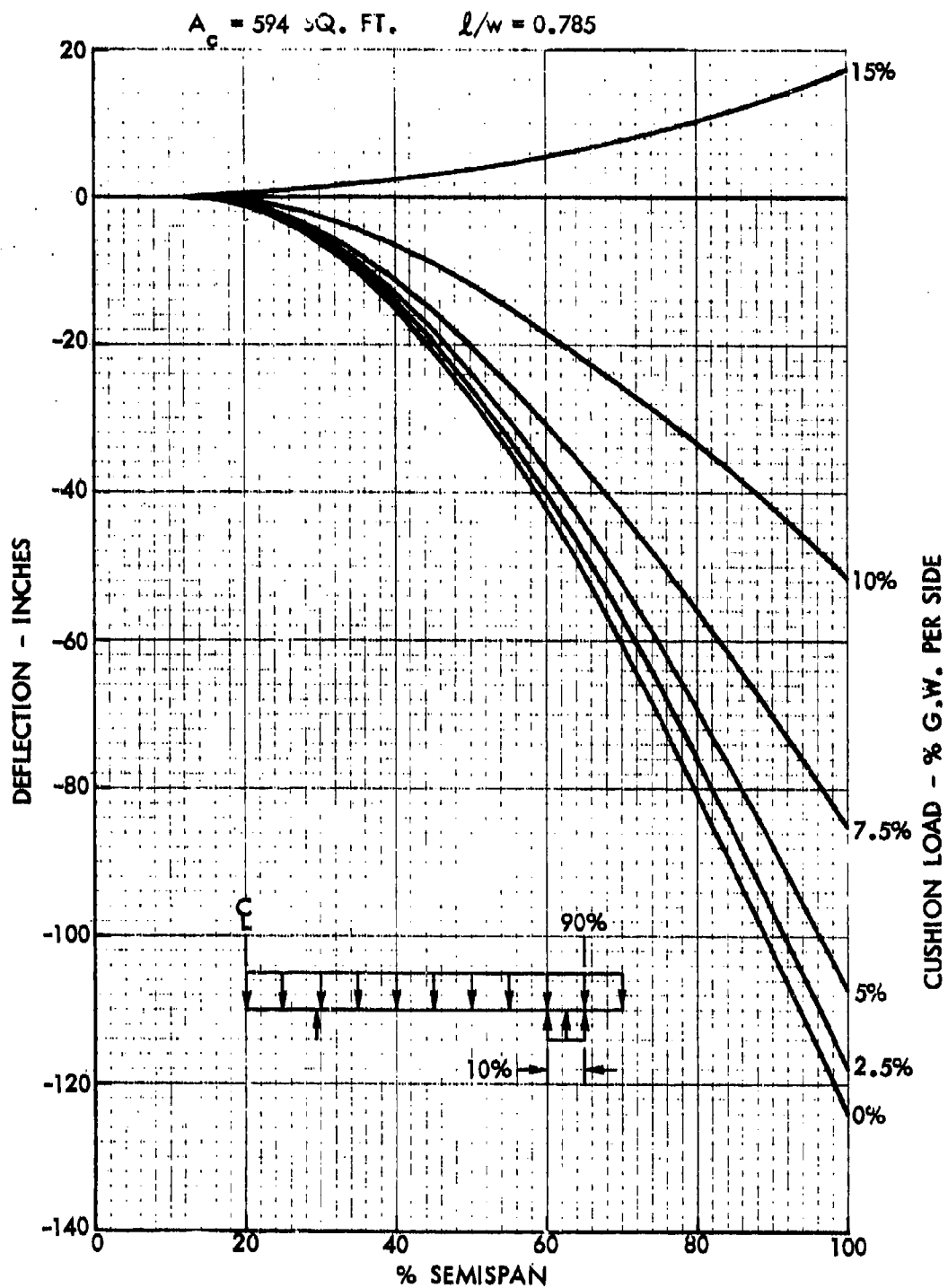


Figure 16. Wing Deflection vs Span and Cushion Load ( $l = 10\% b/2$ )

$A_c = 1188 \text{ SQ. FT.}$      $l/w = 1.57$

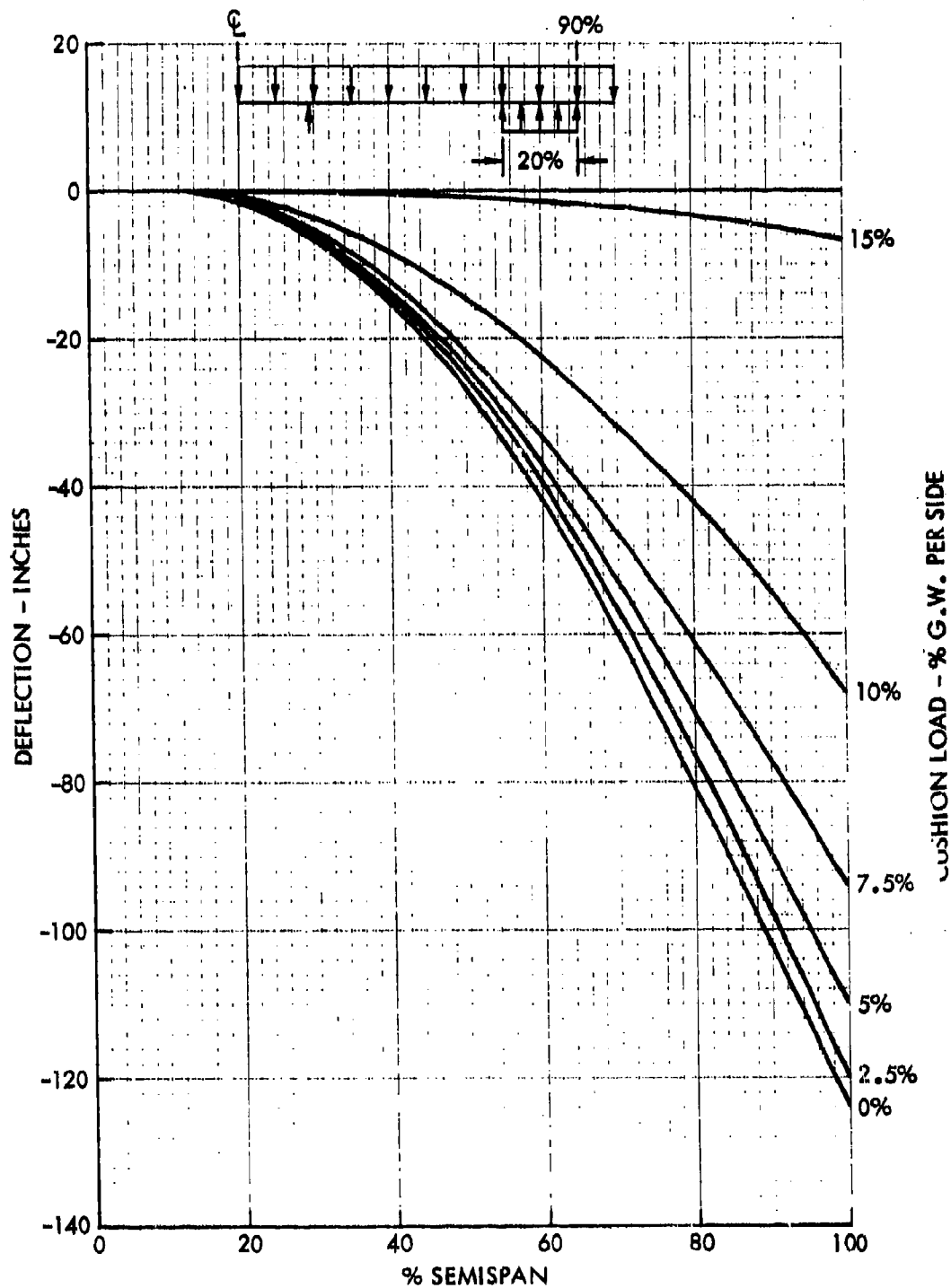


Figure 17. Wing Deflection vs Span and Cushion Load ( $l = 20\% b/2$ )

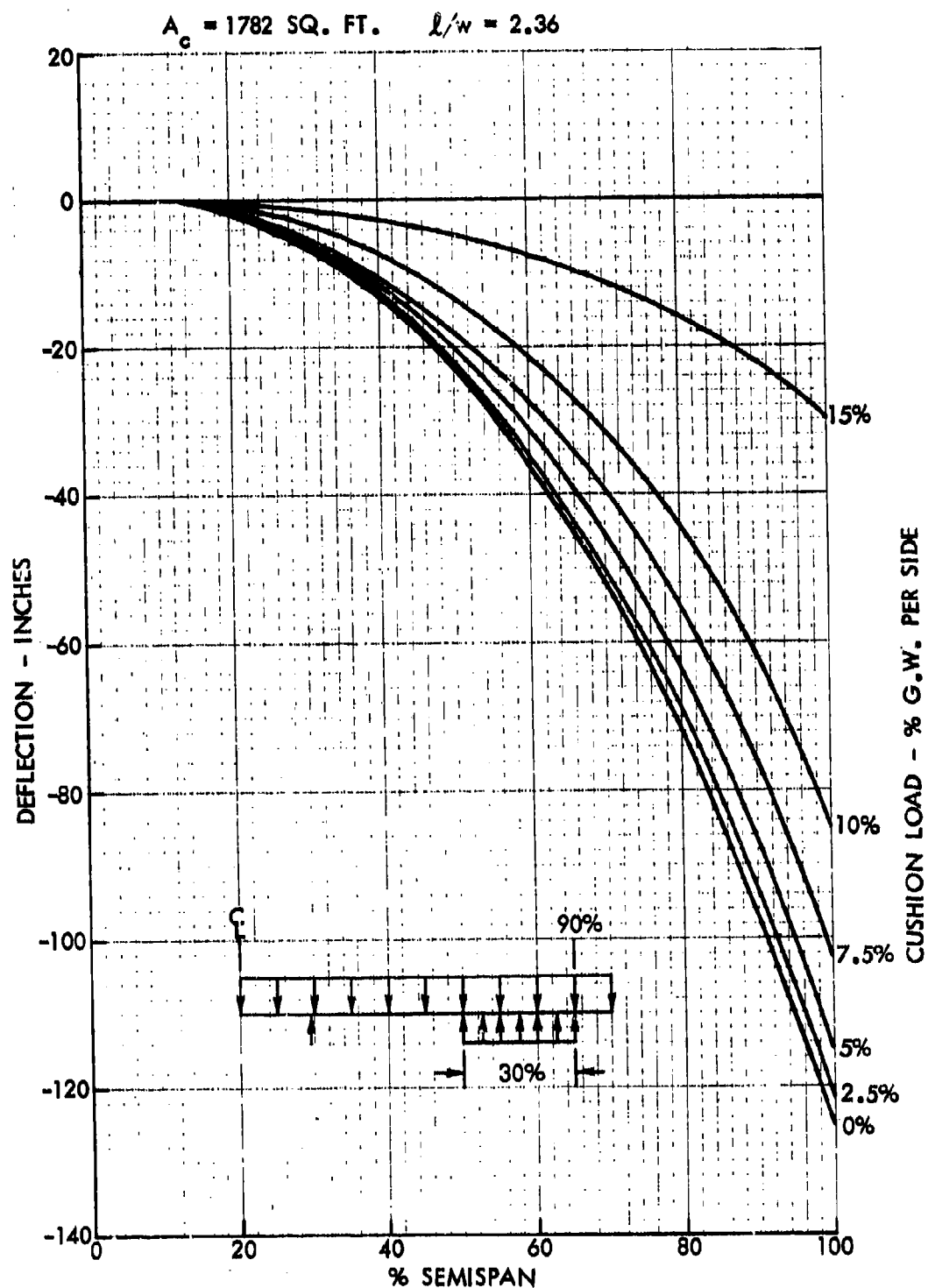


Figure 18. Wing Deflection vs Span and Cushion Load ( $l = 30\% b/2$ )



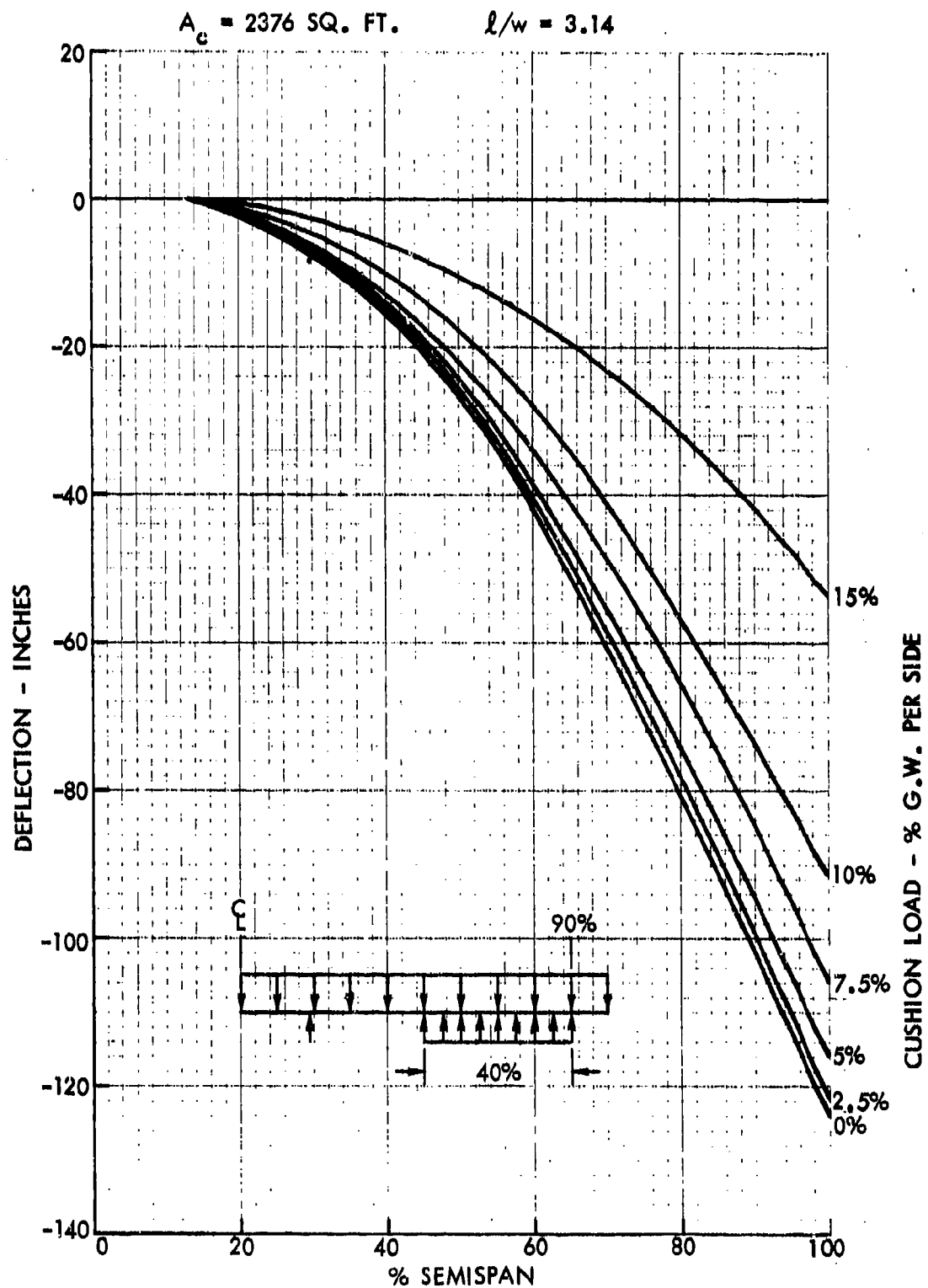


Figure 19. Wing Deflection vs Span and Cushion Load ( $\ell = 40\% b/2$ )

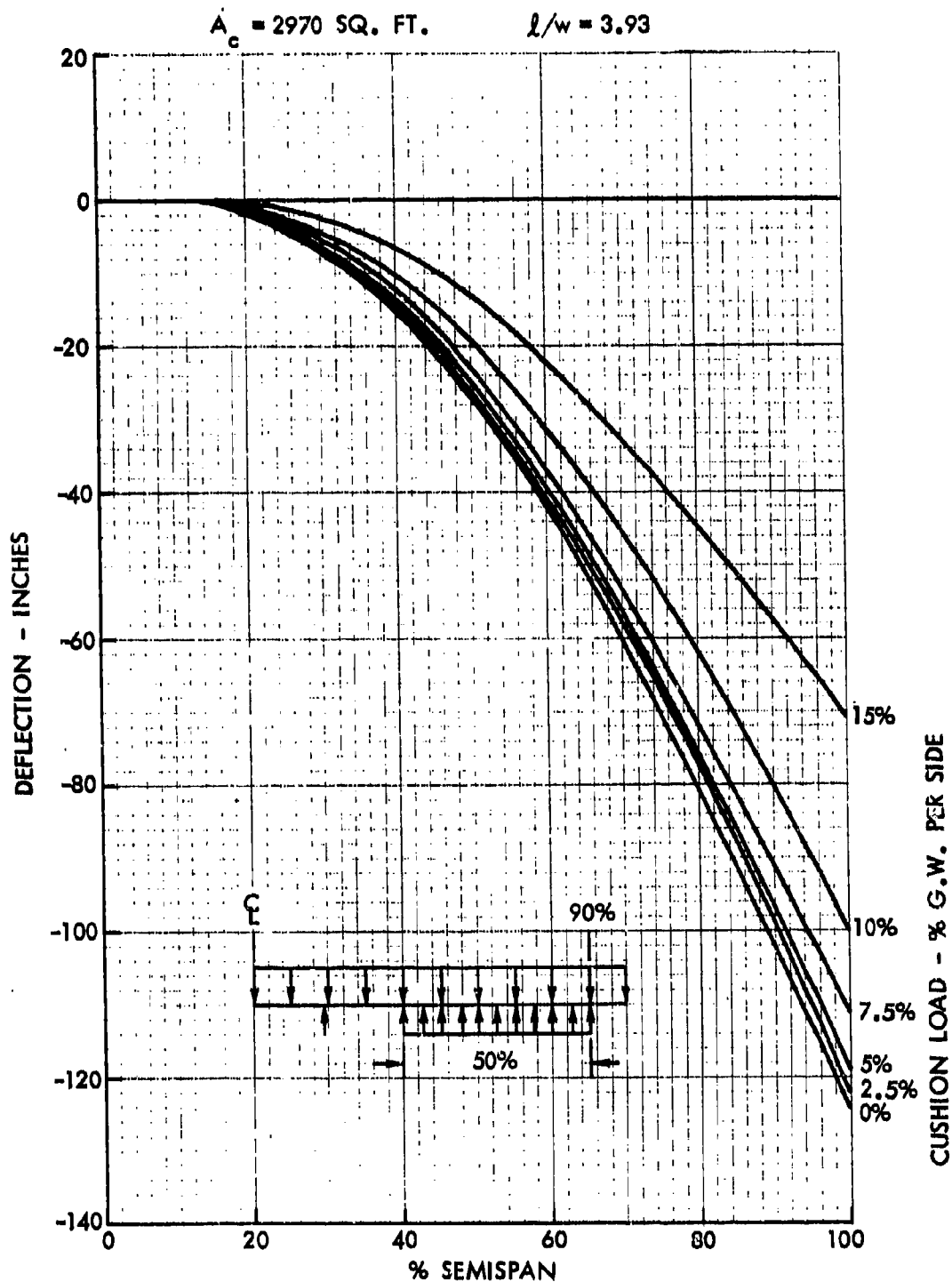


Figure 20. Wing Deflection vs Span and Cushion Load ( $l = 50\% b/2$ )

( $W_{REF} = 241,819 \text{ LB}$ )

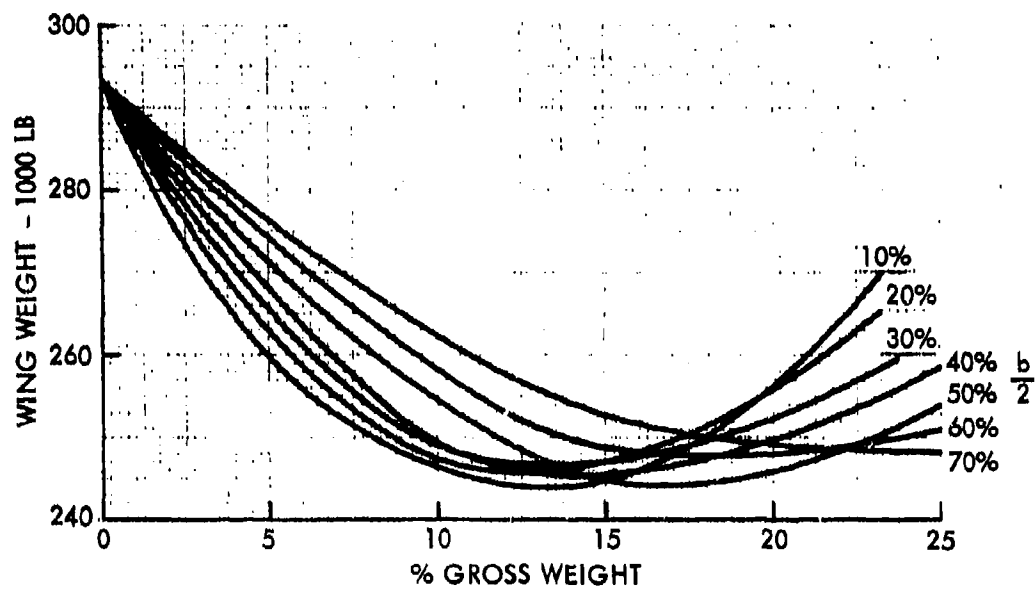


Figure 21. Wing Weight vs Cushion Span and Load

$$W_{LG} = \left[ 0.30 \left( \frac{h_o}{178} \right)^2 + 0.7 \right] (1-L) 58111$$

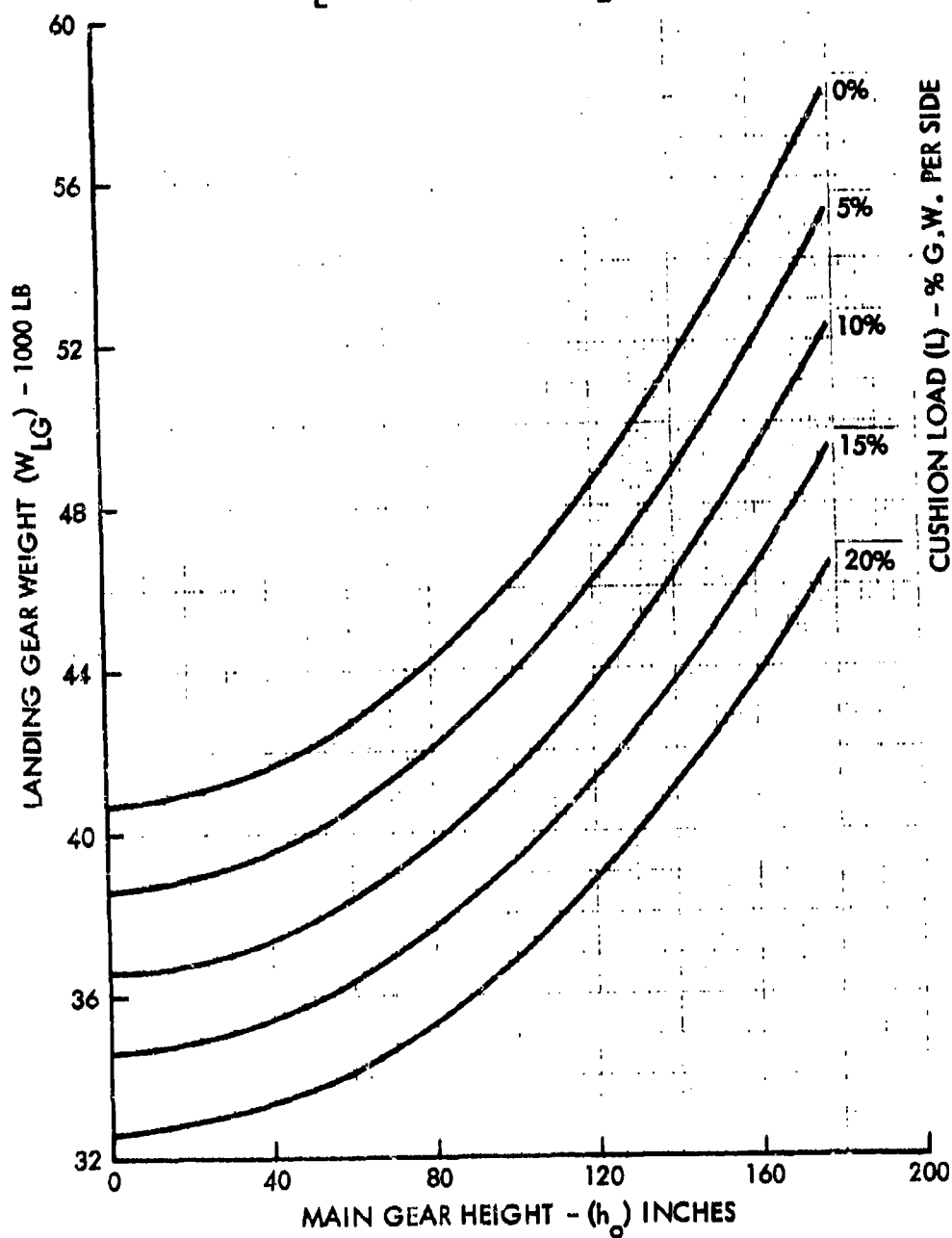


Figure 22. Landing Gear Weight

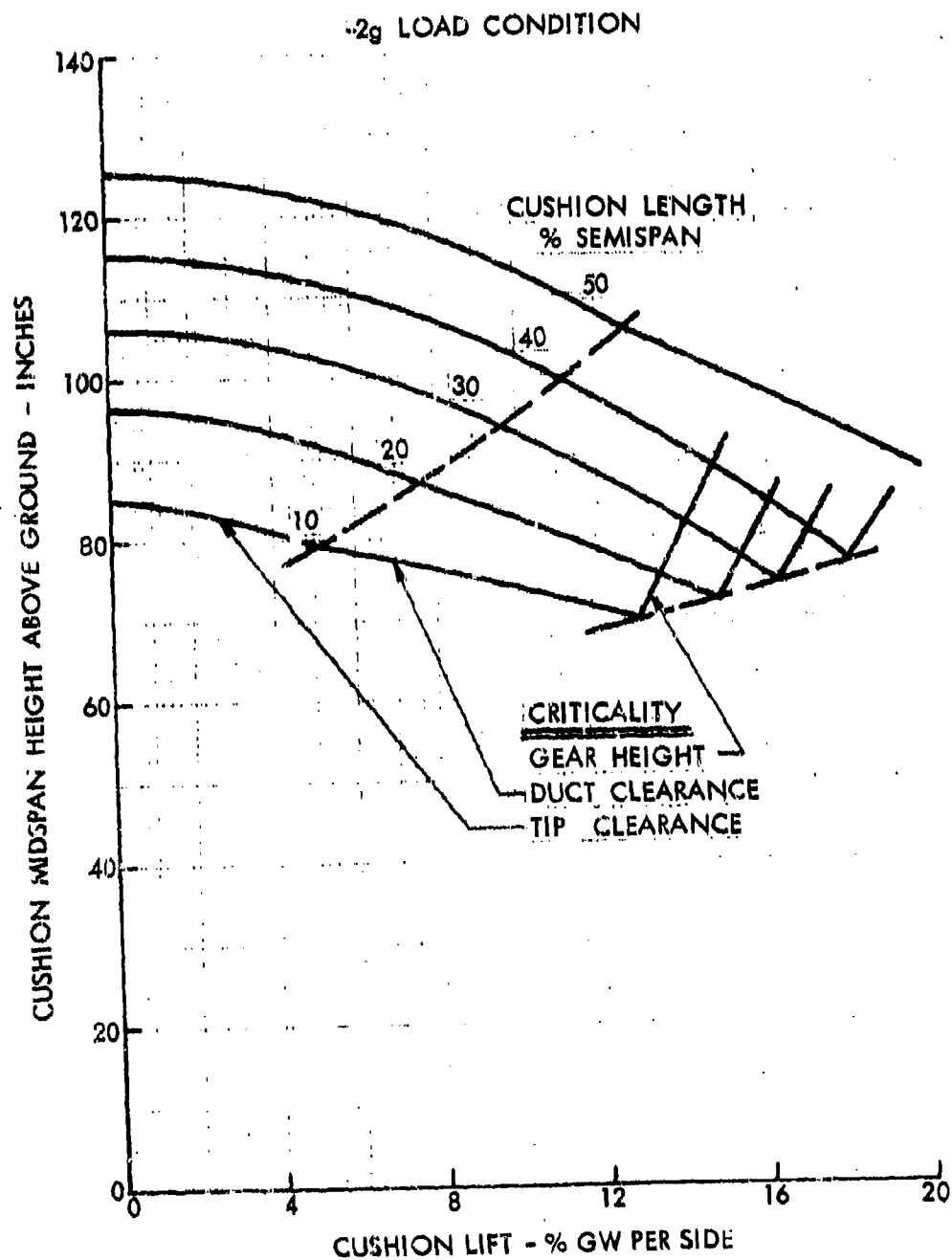


Figure 23. Baseline PJ-ACLS Cushion Height

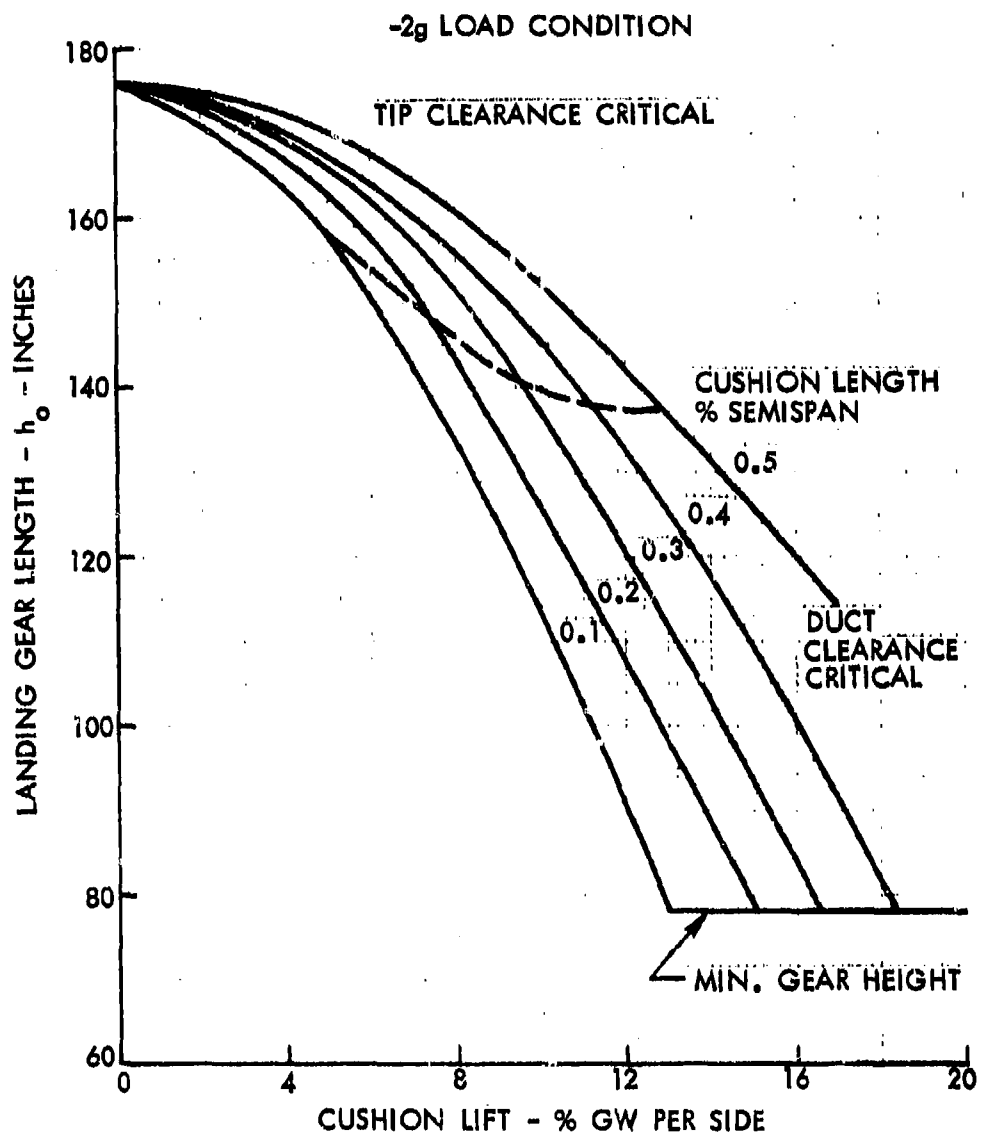


Figure 24. Baseline PJ-ACIS Landing Gear Height

**4.2.3 CUSHION PERFORMANCE AND COMPONENT SELECTION** - The characteristics of the selected air supply components, i.e., the fans, turboshafts, and gearboxes, are based on component data available from component manufacturers and vendors. The data, as required, have been scaled by conventional methods to the sizes applicable to the subject PJ-ACLS requirements. The steps defining the required fan performance, system power, and system weight, as shown on Figure 14, are summarized in Appendix C.

Centrifugal Fans - The fan performance characteristics, which are shown on Figure 25, were estimated by scaling an off-the-shelf industrial type fan in accordance with fan laws, assuming constant fan efficiency and specific speed. The data are based on a fixed geometric size, scaled to the maximum fixed size possible within the installation space available within the wing leading and trailing edge compartments. Since for a given fan pressure, fan volumetric flow is proportional to the square of the fan dimensions, utilization of the largest possible fans provides the highest flow per unit installation space, and thus the lightest-weight fan installation. The estimated fan dimensions are also shown on Figure 25.

The fan weight characteristics shown on Figure 25 are based on an assumed fan thrust-to-weight ratio ( $T/W$ ) of 5. For light-weight centrifugal fans, the literature (References 3 and 4) indicate a feasible  $T/W$  range from approximately 3 to 5. The present study assumes the optimistic extreme of this range.

The particular off-the-shelf fan upon which the fan data are based utilizes a backward-curved type fan impeller design. Several fan manufacturers were contacted for information on more efficient centrifugal fan designs. Little interest was shown, however, due primarily to the combined requirements of light weight and large size.

Turboshaft Engines - The turboshaft engine characteristics are shown on Figure 26. These characteristics are based on the P&W STS 487 turboshaft study engine (Reference 5), the commonality companion of the P&W STF 477 turbofan engine (Reference 6), which is used as the primary propulsive





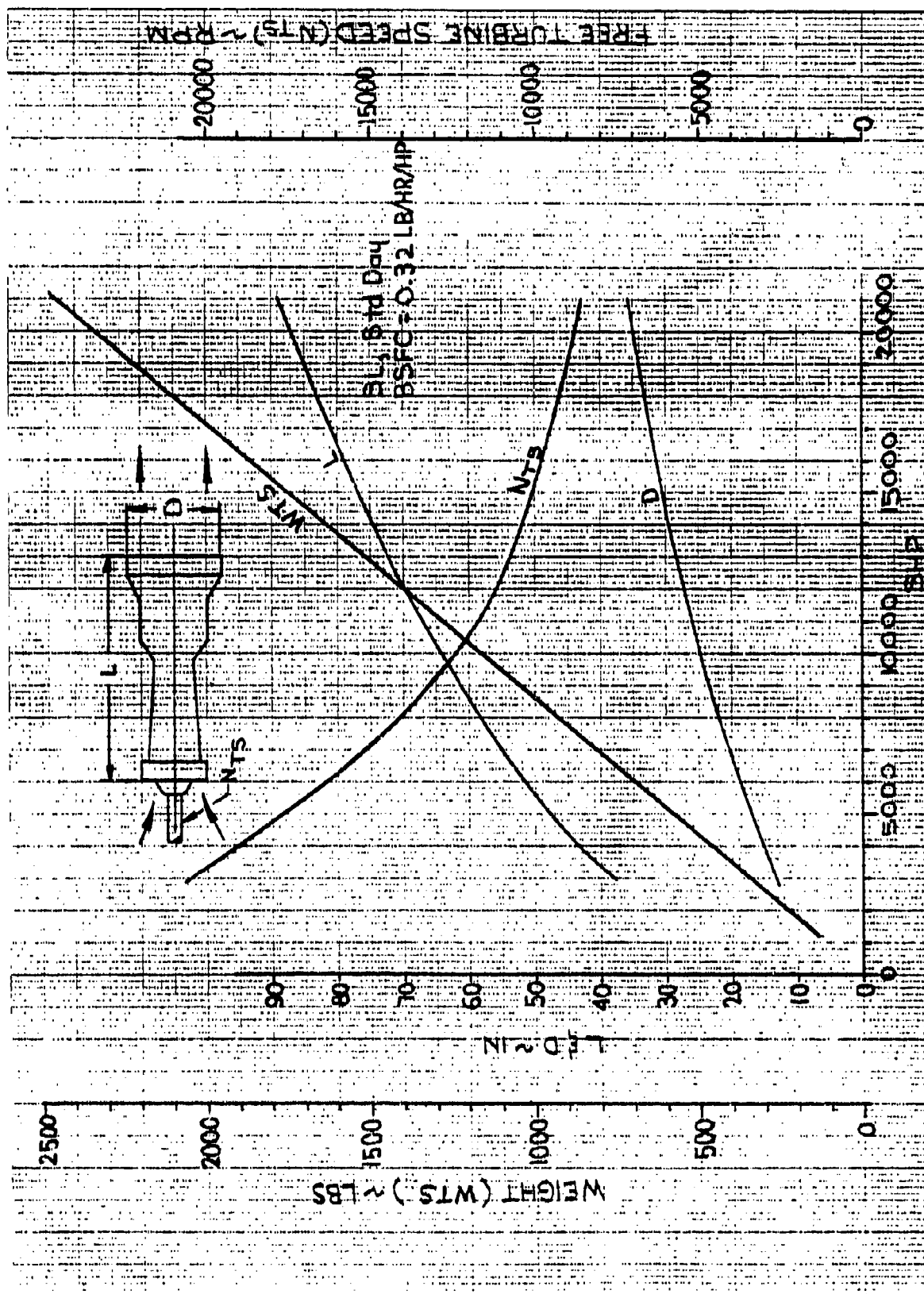


Figure 26. Turboshaft Engine Size

engine on the spanloader aircraft. The STS 487 is considered representative of the typical state-of-the-art expected of operational turboshaft engines in the 1990's time-frame.

Power Transfer Gearbox - The estimated weight characteristics of the speed reduction gearboxes are shown on Figure 27. These data are based on gearbox characteristics as provided by Detroit Diesel Allison in Reference 7. The power transfer efficiency is assumed to be 98%.

Wing Tip Gear - The addition of the PJ-ACLS reduces wing strength required to react downbending loads, therefore, cushion off, one g static wing deflection increases in direct proportion to increased cushion lift. To provide wing tip support during cushion off conditions a wing tip gear is used as a component of the PJ-ACLS. Wing tip gear weight as a function of cushion load is given on Figure 28.

4.2.4 STRUCTURAL AND SYSTEM WEIGHT COMPARISON - The PJ-ACLS baseline spanloader (-2g wing capability) is used as the comparison base for this weight comparison. The structural weight (wing weight + main gear weight) and cushion system weight (cushion component weights + cushion fuel weight + wing tip gear weight) are determined for each evaluation matrix data point given on Figure 10. The structural weight and system weight are summed and compared to the baseline PJ-ACLS spanloader wing weight plus main gear weight to determine the delta aircraft weight.

### 5.0 SELECTED CUSHION CONFIGURATION

Selection of the minimum weight cushion configuration requires the analysis of 1000 data points; 500 for the baseline spanloader and 500 for the baseline spanloader minus 40 inches in cushion height. As previously explained, the baseline minus 40 inches is provided to illustrate cushion performance sensitivity to cushion height. The analysis of these 1000 data points was performed by a computerized cushion performance and weights program with the results provided in Volume II.

REF ID: A6331

WE 135E

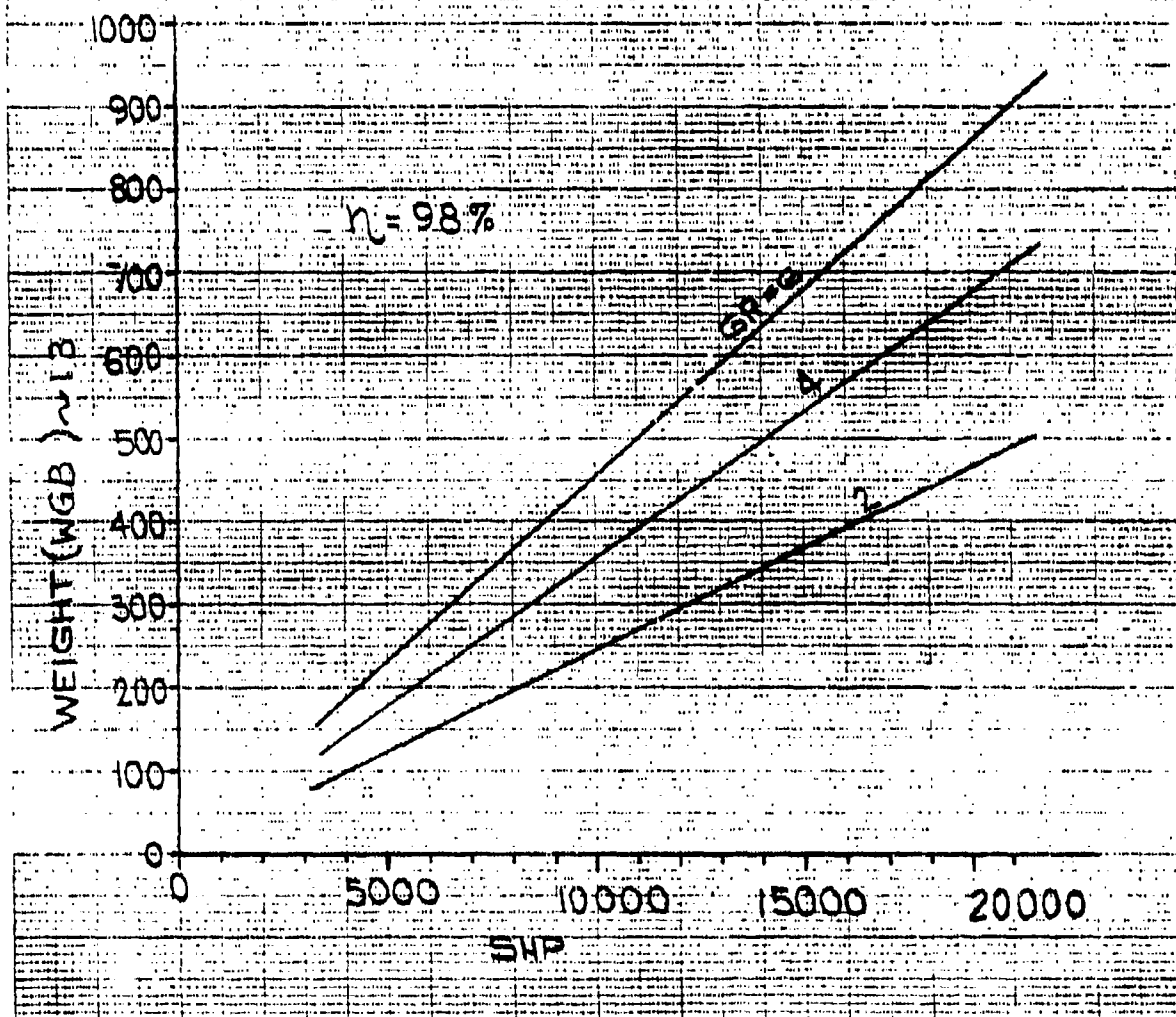


Figure 27. Gearbox Weight  
36

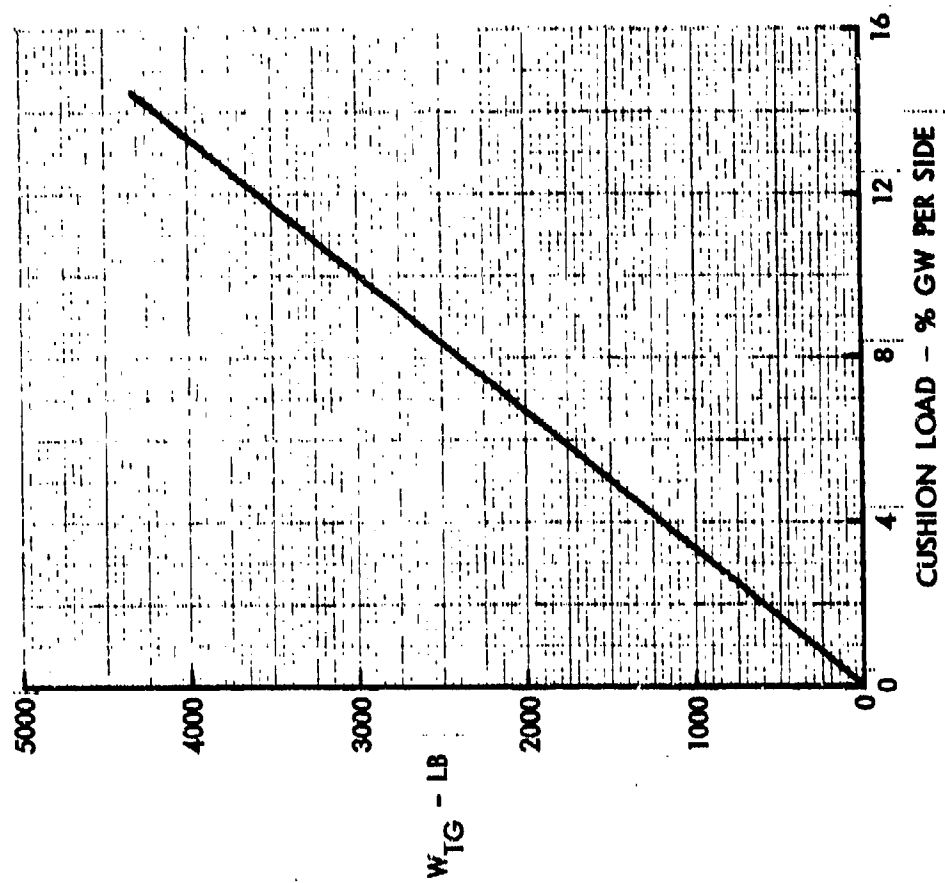


Figure 28. Tip Gear Weight vs Cushion Load

A review of the data contained in Volume II shows that all cushion configurations for the baseline spanloader result in a weight penalty. The selected configuration has a minimum weight penalty of 625 pounds which occurs for a cushion lift of 2.5 percent gross weight, length of 20 percent wing semispan, jet toe-in angle of 45 degrees and jet thickness of 4 inches. Other characteristics data for this cushion are given on Figure 29.

The data given in Appendix B for the baseline minus 40 inches indicate a weight savings can be achieved with reduced cushion heights. The maximum weight savings, within the limits of fan installation space and fan tip speed, is 16,629 pounds. Basic cushion characteristics are a lift of 7.5 percent gross weight, a length of 20 percent wing semispan, a jet toe-in angle of 60 degrees, and a jet thickness of 4 inches. Other characteristics of this cushion are also summarized on Figure 29. Various parametric curves for this cushion selection are given on Figures 30 through 40.

Cushion lift available as a function of cushion height is shown by the upper curve on Figure 41 for the selected cushion configuration. The lift required to operate at any given cushion height is shown for 1g negative condition by the solid line curve. This curve is obtained based upon the assumption that given a 2g negative deflection vs load curve, the 1g negative curve can be plotted using a relationship of one half 2g negative deflection vs one half 2g negative load. Therefore, from Figure 41 it is seen that the selected cushion height and load of 47 inches and 7.5 percent gross weight at 2g negative conditions adjusts to a height of 83 inches and a load of 4.5 percent gross weight for the 1g negative condition. Typically, forward speed augments the available lift with an increase in cushion height above the static value as shown schematically on Figure 41.

## 6.0 STABILITY AND CONTROL

### 6.1 TAKEOFF

The selected cushion configuration for the baseline minus 40 inches results in 85 percent of the aircraft gross weight being supported by the conventional landing gear. The ground

**BASELINE**

LENGTH (L)	43.2 FT (20% b/2)
WIDTH (w)	27.5 FT
AREA ( $A_C$ )	1188 SQ. FT.
JET THICKNESS (t)	4 INCHES
JET ANGLE ( $\theta$ )	45 DEGREES
CUSHION HEIGHT ( $h_c$ )	95.3 INCHES
LIFT/CUSHION (L)	37,450 LB. (0.025% GW)
SHAFT HORSEPOWER (HP)	31,601 (3950/ENGINE)
CUSHION PRESSURE ( $P_c$ )	21.20 psf
JET PRESSURE ( $P_j$ )	164.32 psf
AIRFLOW/CUSHION ( $Q_j$ )	18,910 cfs
AUGMENTATION RATIO ( $A_i$ )	2.321
MAIN GEAR HEIGHT ( $h_o$ )	171.6 INCHES
DELTA AIRCRAFT WEIGHT	+625 LB.

**BASELINE MINUS 40 INCHES**

LENGTH (L)	43.2 FT (20% b/2)
WIDTH (w)	27.5 FT
AREA ( $A_C$ )	1188 SQ. FT
JET THICKNESS (t)	4 INCHES
JET ANGLE ( $\theta$ )	60 DEGREES
CUSHION HEIGHT ( $h_c$ )	46.8 INCHES
LIFT/CUSHION (L)	112,350 LB (0.075% GW)
SHAFT HORSEPOWER:	76,459 (9557/ENGINE)
CUSHION PRESSURE ( $P_c$ )	80.99 psf
JET PRESSURE ( $P_j$ )	305.1 psf
AIRFLOW/CUSHION ( $Q_j$ )	24,644 cfs
AUGMENTATION RATIO ( $A_i$ )	4.093
MAIN GEAR HEIGHT ( $h_o$ )	107.5 INCHES
DELTA AIRCRAFT WEIGHT	- 16,629 LB

Figure 29. Selected Cushion Configurations

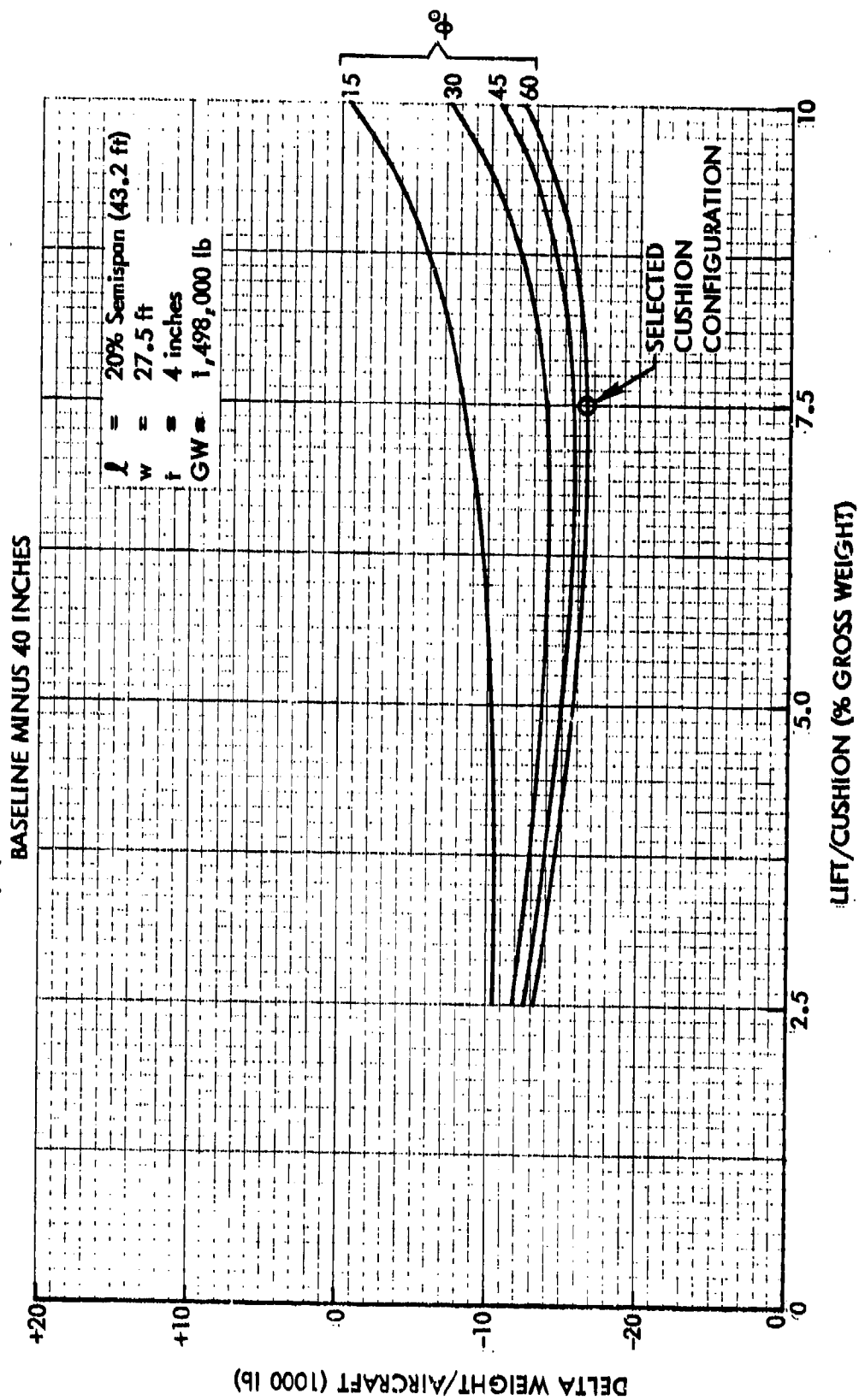


Figure 30. Cushion Lift vs Delta Aircraft Weight

BASELINE MINUS 40 INCHES

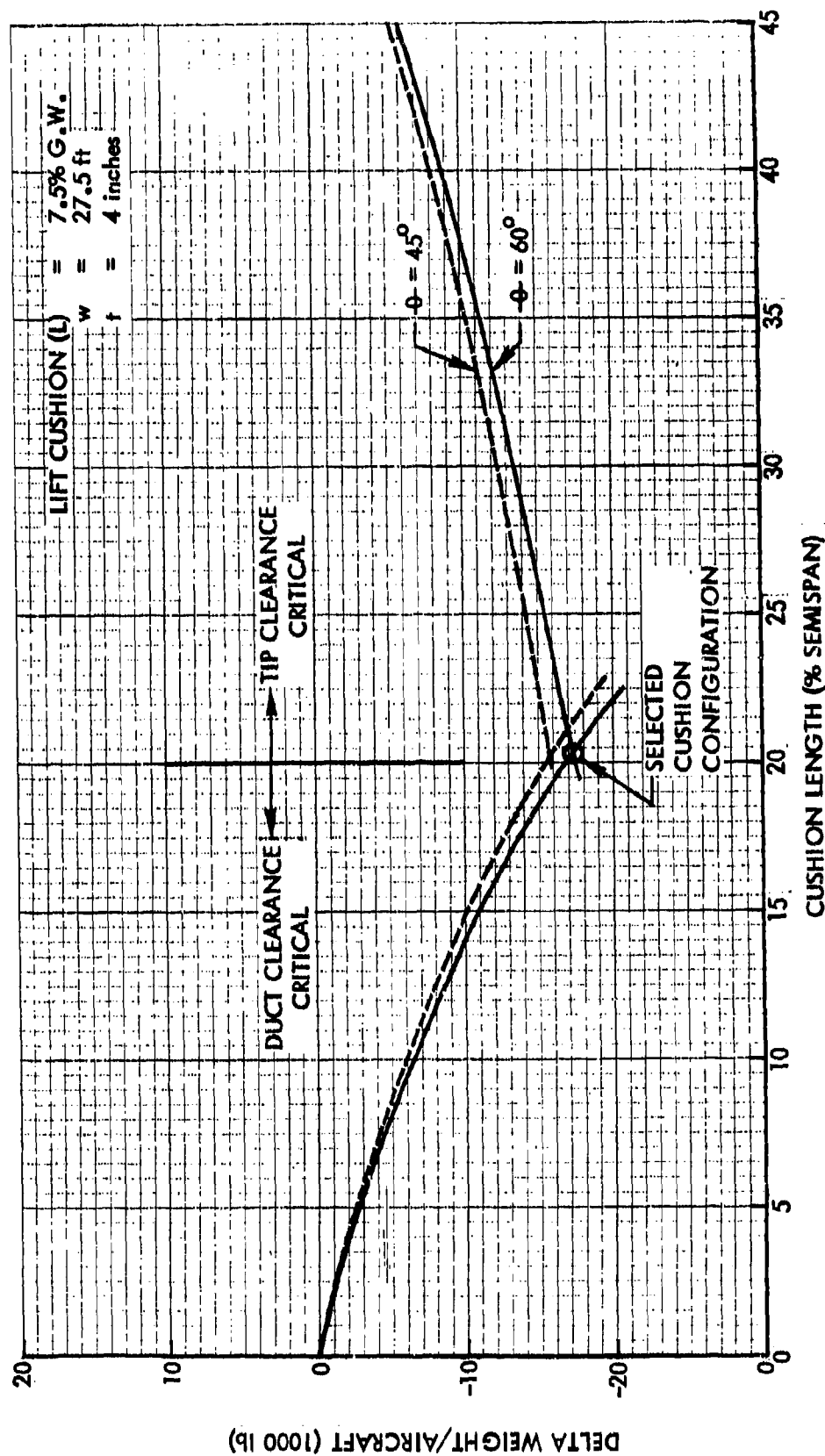


Figure 31. Cushion Length vs Delta Aircraft Weight



BASELINE MINUS 40 INCHES

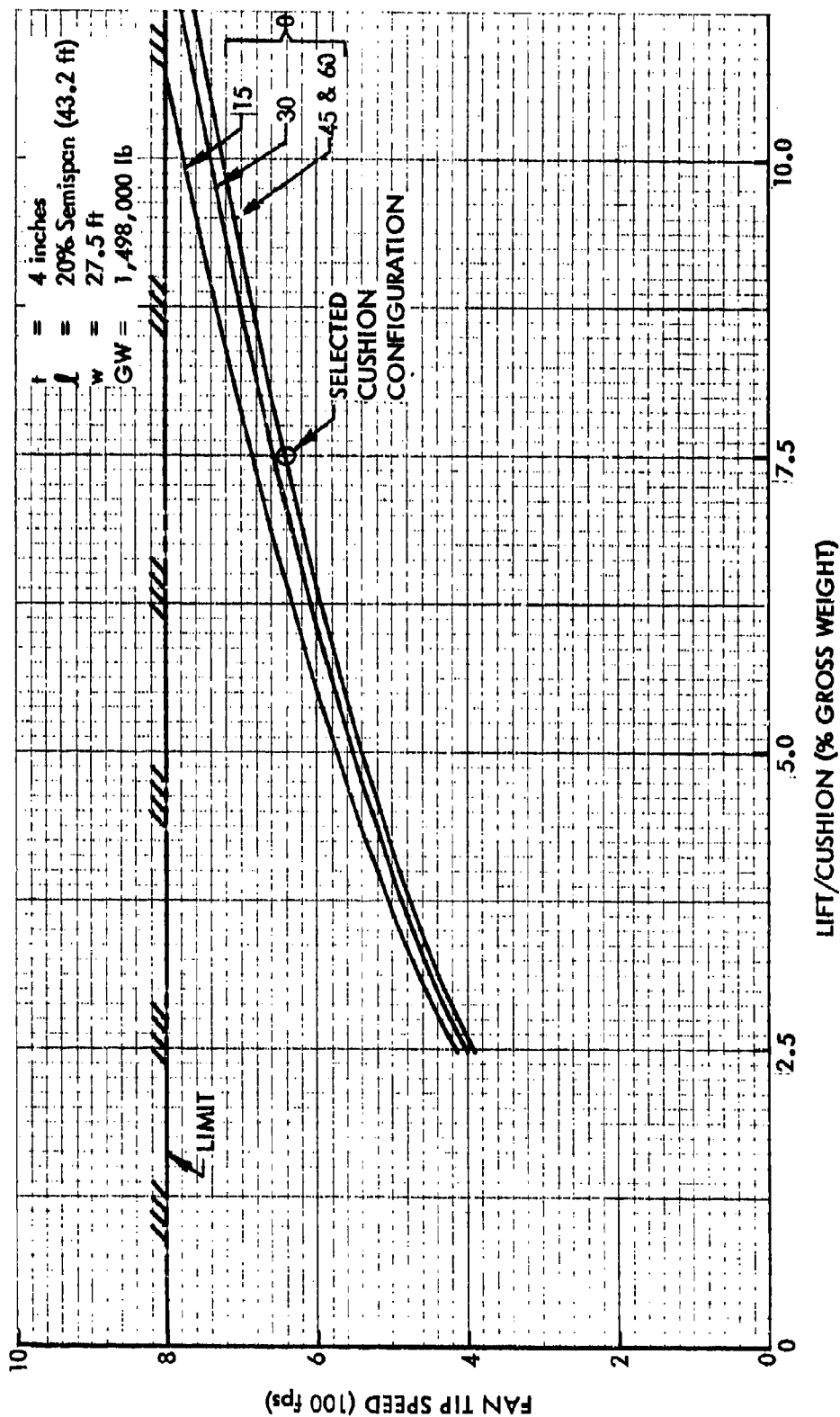


Figure 32. Cushion Lift vs Fan Tip Speed and  $\theta$

# BASELINE MINUS 40 INCHES

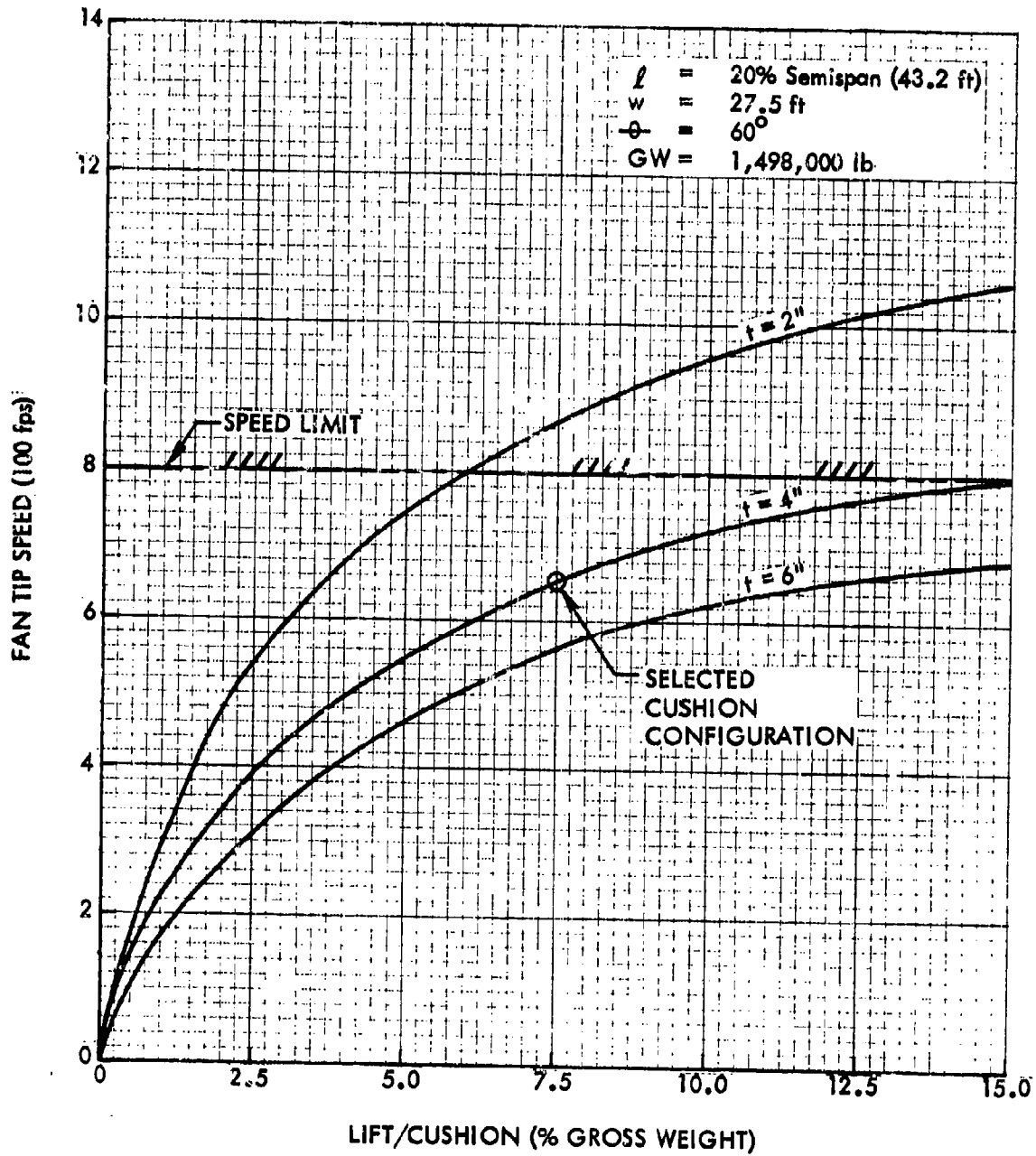


Figure 33. Cushion Lift vs Fan Tip Speed and  $t$

# BASELINE MINUS 40 INCHES

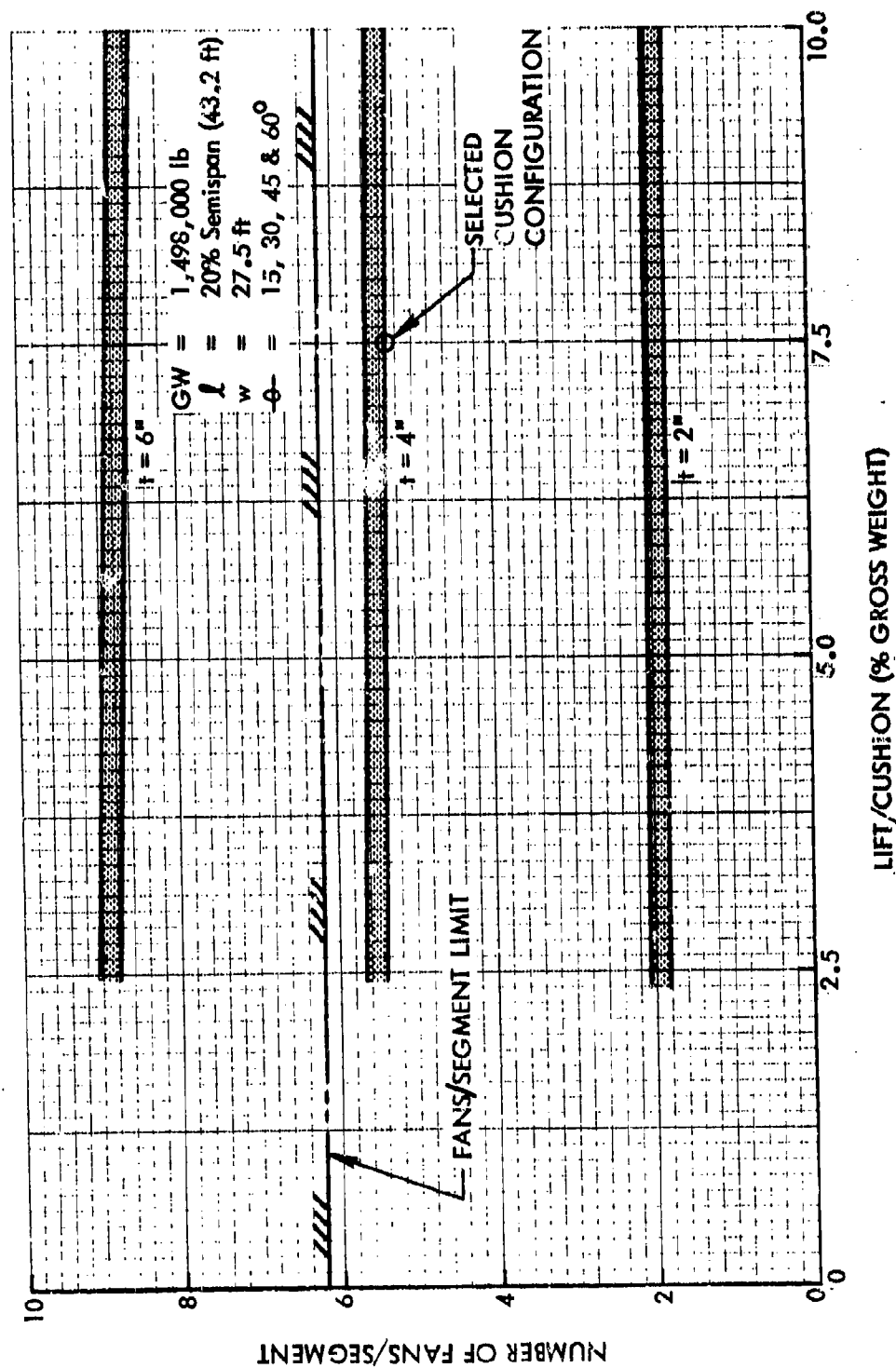


Figure 34. Cushion Lift vs Number Fan Segments

# BASELINE MINUS 40 INCHES

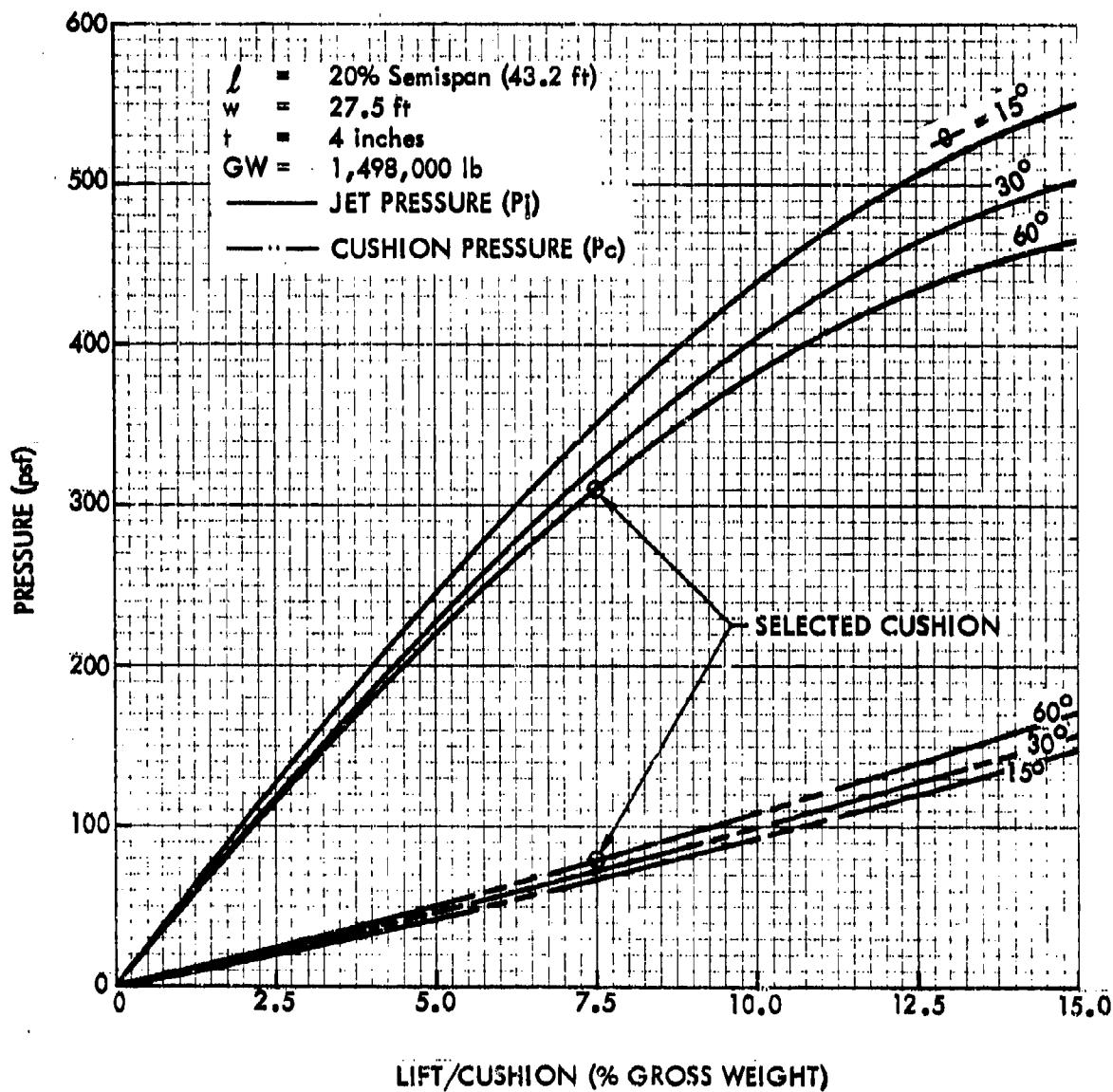


Figure 35. Cushion Lift vs Jet and Cushion Pressure

# BASELINE MINUS 40 INCHES

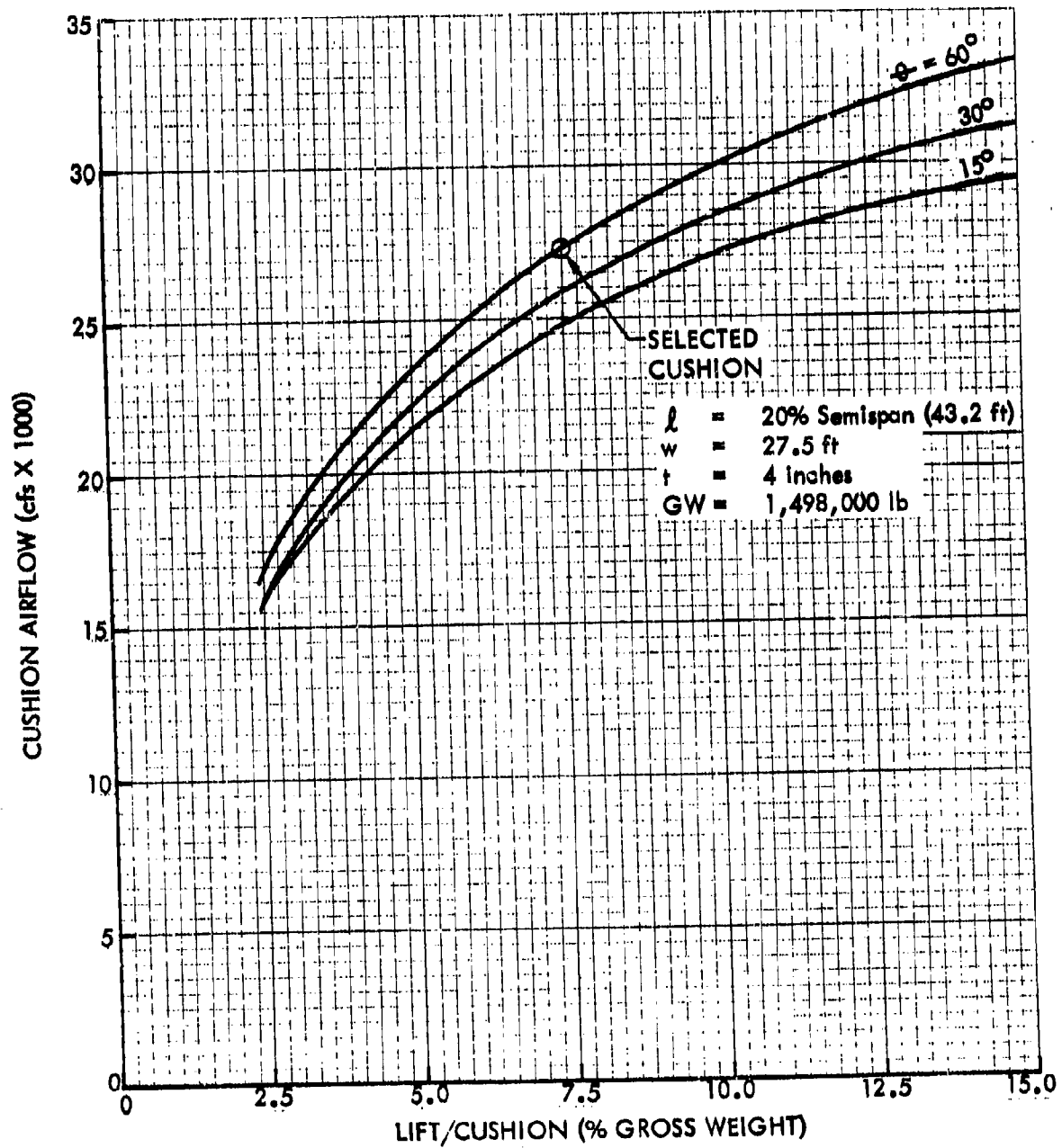


Figure 36. Cushion Lift vs Cushion Airflow

BASELINE MINUS 40 INCHES

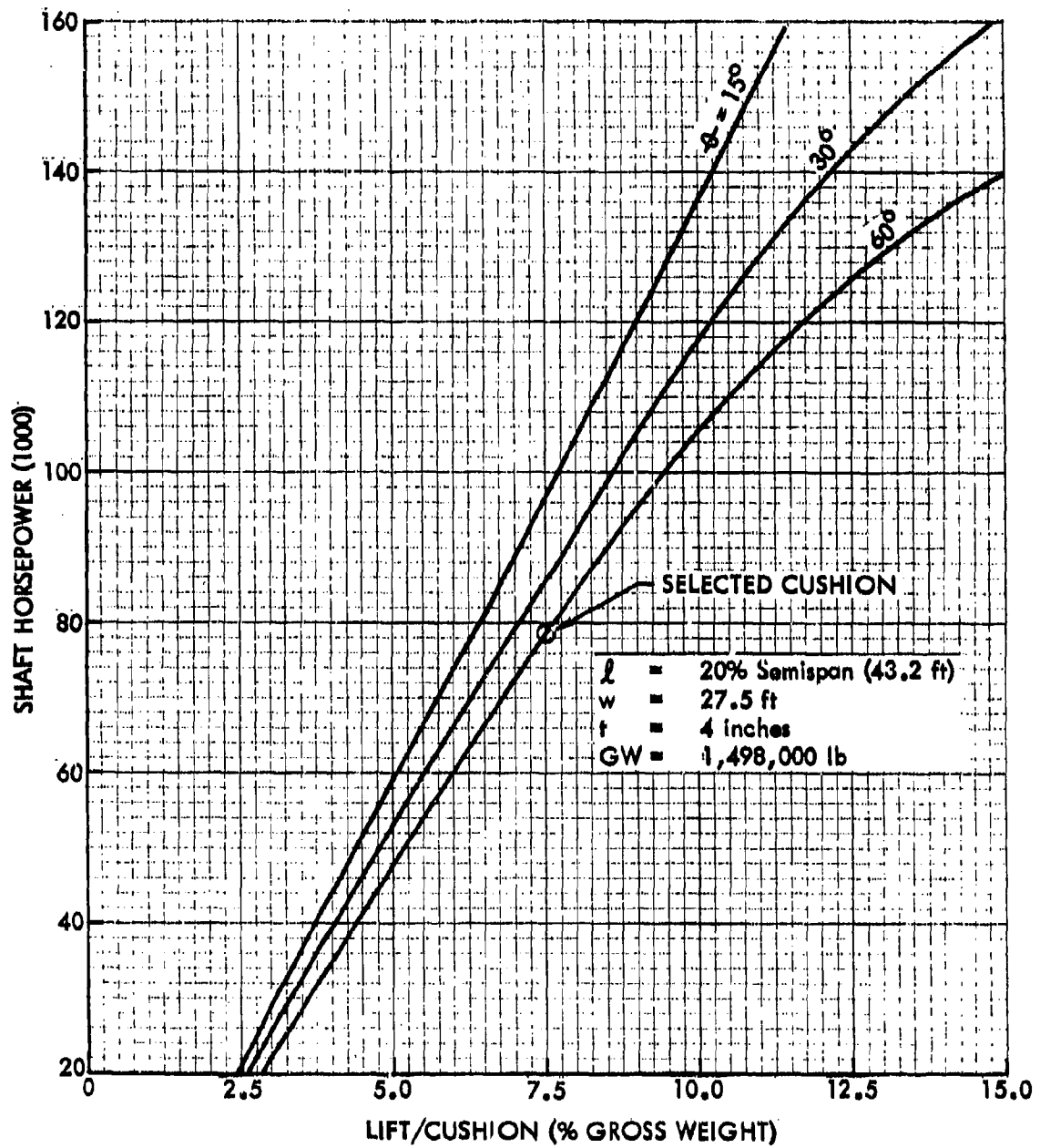


Figure 37. Cushion Lift vs Shaft Horsepower

# BASELINE MINUS 40 INCHES

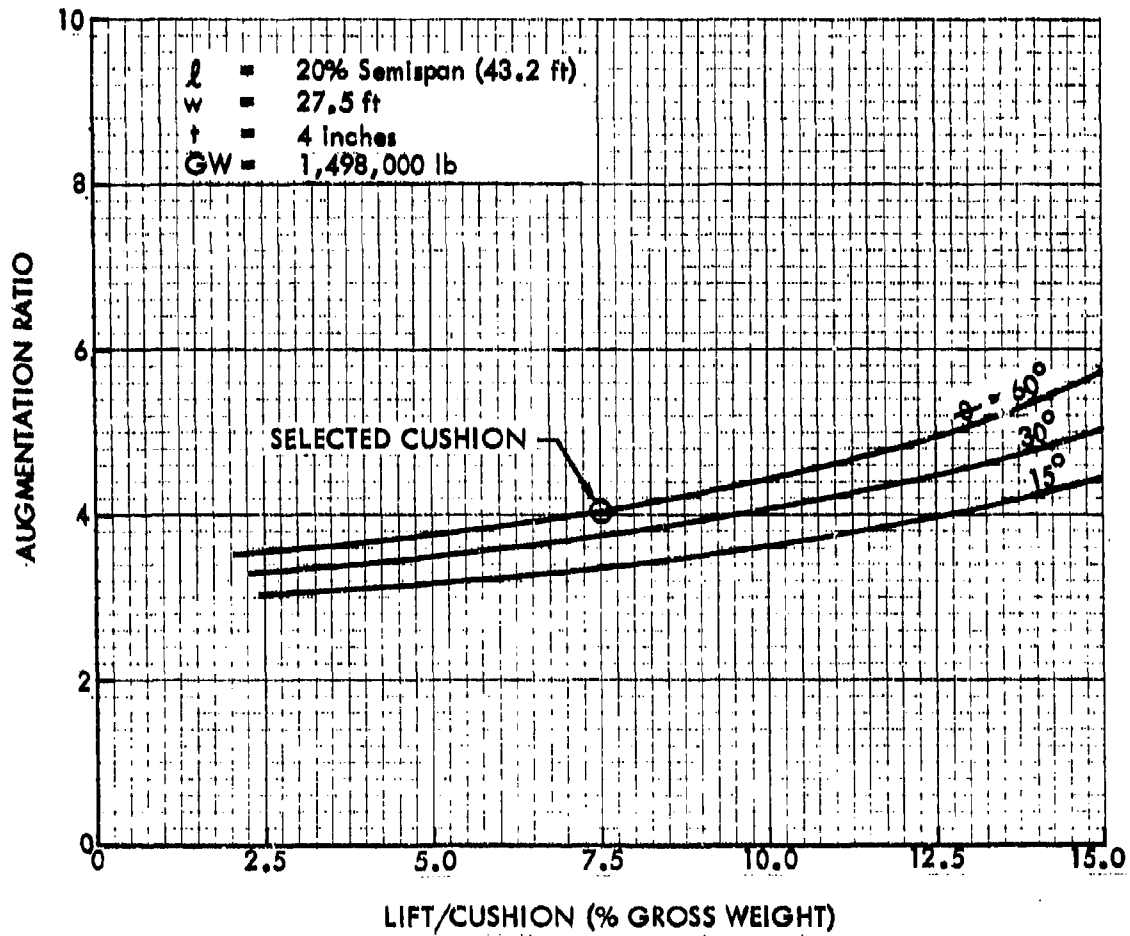


Figure 38. Cushion Lift vs Augmentation Ratio

# BASELINE MINUS 40 INCHES

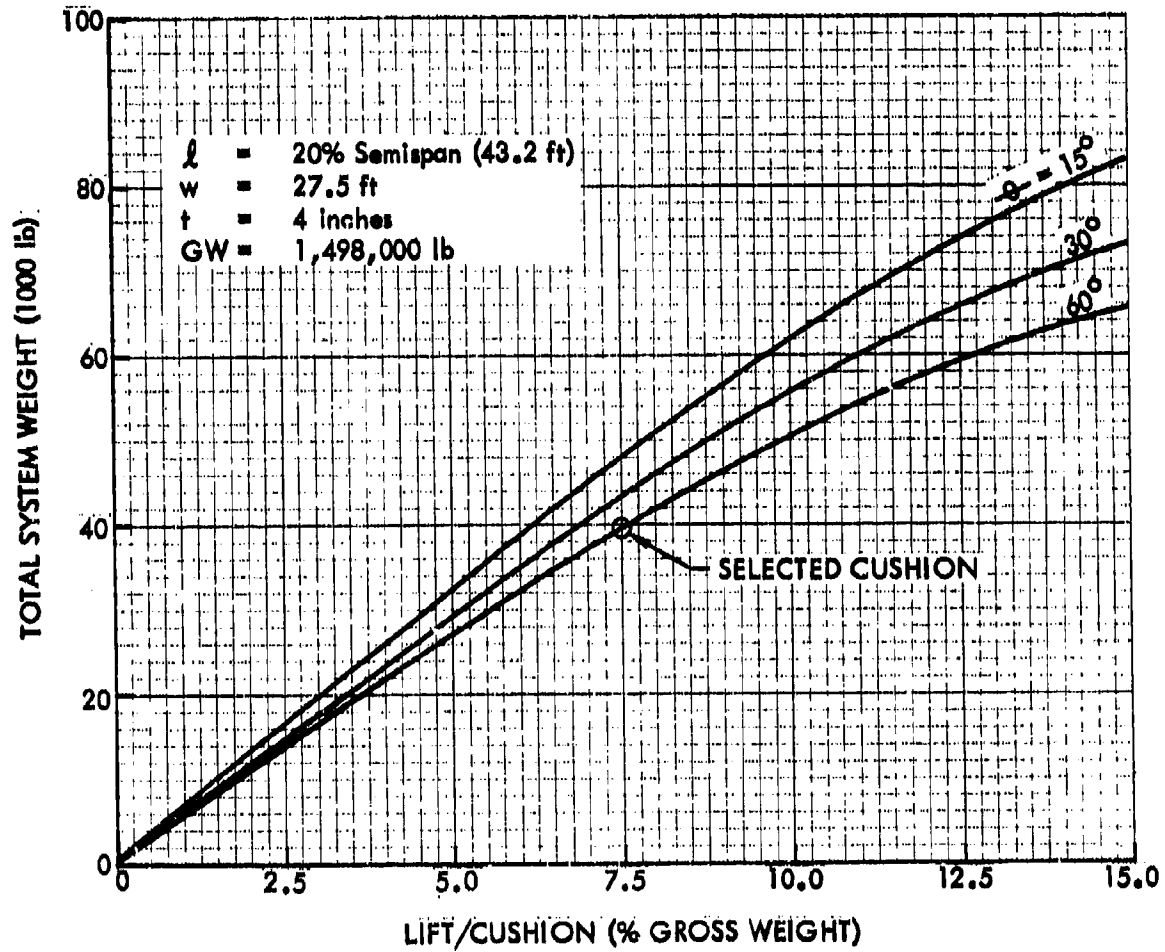


Figure 39. Cushion Lift vs Total System Weight



BASELINE MINUS 40 INCHES

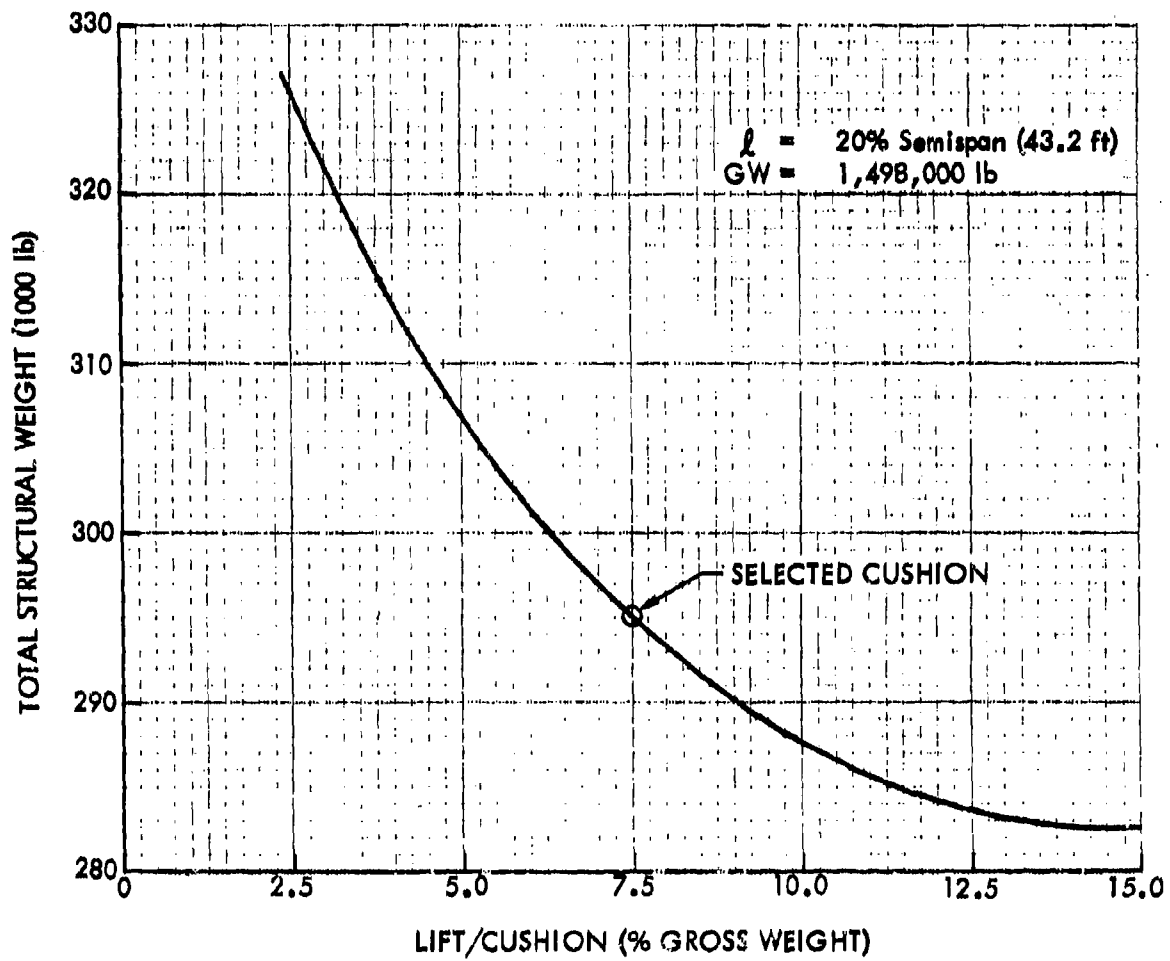


Figure 40. Cushion Lift vs Total Structural Weight

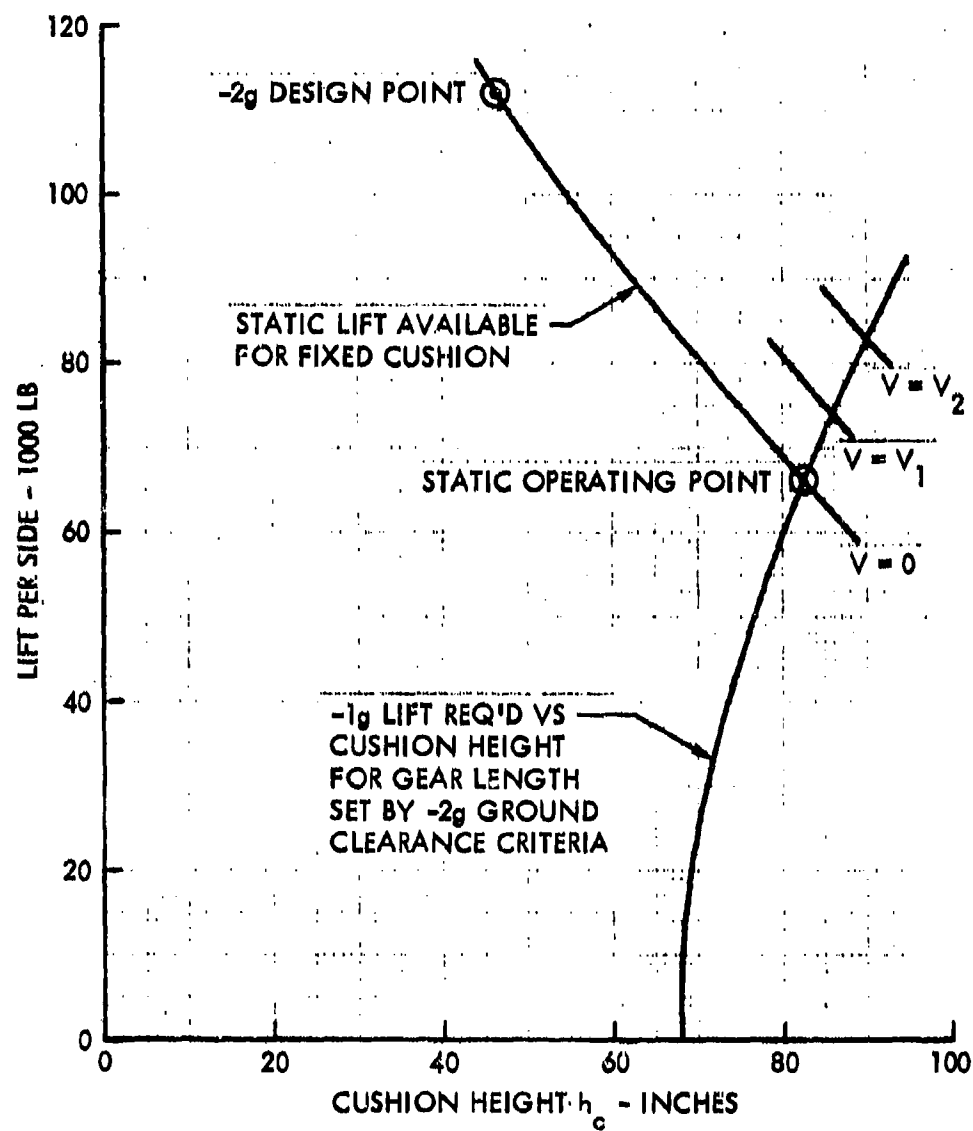


Figure 41. Cushion Operating Height/Lift Envelope

run portion of the takeoff phase is essentially like that of the original baseline spanloader aircraft. The consideration of engine out control, crosswind capability and lateral and directional control will essentially be unaltered by the addition of the peripheral jet cushion.

The primary impact of the addition of the cushions is on longitudinal trim. As the main landing gear is moved inboard on the  $40^\circ$  swept wing configuration to provide the required 75 foot track width, it is by necessity also moved forward. This resulted in a gear location which is forward of the aircraft center of gravity and at zero forward speed, with propulsive engines off, cushion lift or wing tip gear extension is necessary to provide nose gear contact.

The wind tunnel data of AFFDL-TR-65-59 shows that the cushion at the aircraft minimum flying speeds will provide approximately the same additional wing lift as it does at zero velocity. The same result is obtained if that portion of the wing encompassing the cushion is treated as a jet flap, at minimum flying speed. If lift off is attempted with the cushion operating, the moment produced by the cushion must be balanced by the canard surface. The  $40^\circ$  swept wing results in a cushion location approximately one mean aerodynamic chord length aft of the center of gravity. This procedure would increase the required canard lift by 75 percent. Lift off could be achieved by turning off the cushion system at the lift off speed.

## 6.2 LANDING

The cushion must be operating on final approach. At approximately 200 feet altitude the contribution of the system would be only the jet thrust component which, even with the highly swept wing, is small and within the capability of the baseline canard surface. As the ground is approached, the lift and consequently the nose down moment produced by the cushion would increase rapidly. The ability to hold the nose wheel clear of the runway at touchdown will require a 75 percent increase in the available canard lift.

In summary, the only stability and control problems associated with this application of a peripheral jet landing system are those associated with the baseline configuration selected. A configuration which aligns the cushion lift with the center of gravity of the aircraft would be much better. Such a configuration would exhibit a stronger than normal cushioning effect due to coming into the ground proximity, and perhaps, some flying qualities improvements on approach can be obtained by the direct lift control associated with varying the jet tilt angle. (See Appendix B Analysis)

## 7.0 FORWARD SPEED EFFECTS AND AIRPORT PERFORMANCE

The emphasis of this study has been directed at the feasibility of the peripheral jet air cushion as a supportive device in low speed operation. Based on present knowledge, there is no reason to expect any significant problem at low speeds. However, the cushion must be operative up to approximately lift off speed and takeoff, and must be fully operative from landing approach speed to a full stop. There is no firm requirement for operation at significantly higher speeds.

It is beyond the scope of this study to establish the effect of a particular selected cushion on airport performance. Nevertheless there will be significant effects which are very dependent upon the details of the cushion geometry, its size relative to the wing, the load carried by the cushion and the local momentum coefficient  $J/qS_c$ .

The greatest ACLS military potential is the enhancement of operation from battle-damaged runways. For whatever number of gear tracks, the probability of executing landing or takeoff is seriously degraded by long runway requirements coupled with battle damage. Therefore, every effort must be made to minimize adverse effects on landing and takeoff distances. With ingenuity and good design, it may be possible to suffer no airport performance penalty. The following discussion addresses the primary problems as they relate to each other and to the achievement of satisfactory airport performance.

### 7.1 INTERACTING FACTORS

7.1.1 CUSHION INTERACTION WITH MECHANICAL FLAP DESIGN - Typical span-loader wing loadings and good airport performance require fairly good high lift performance.

A baseline spanloader with its wing stiffened to accommodate a reduced landing gear width would use full span mechanical flaps. On the other hand, if reconfigured to accommodate an air cushion, the vehicle may not be able to utilize mechanical flaps over the span covered by the air cushion, particularly as cushion operating height is reduced to minimize system weights. Operating height reduction achieved by flattening the airfoil lower surface complicates this further. In addition, the aerodynamic interaction between a mechanical flap on an air cushioned section of wing is not known.

In any event, a careful matching of the air cushion and mechanical flap system is required. The development problems center primarily on the development of a suitable combination of air cushion, airfoil shape, and high lift system. The low-deflection, very large extension flap is therefore a candidate for further development.

7.1.2 CUSHION AERODYNAMICS AT FORWARD SPEED - Aside from interaction with the mechanical flap design, the basic aerodynamic characteristics of the air cushion must be considered. At low forward speeds, the freestream constitutes a small perturbation to the basic cushion flow field. At high speeds, the jet cushion is a small interaction to the freestream. Neither of these speed ranges, where analysis is simplified, is of real concern. Typical liftoff and approach speeds are in the range where freestream and jet effects are comparable and have maximum interaction. It is also severely compounded by ground effects. The entire picture is analagous to a powered lift STOL system operating between normal STOL and VTOL speed regimes. Thus, no simple flow model is possible, and a strong reliance must be placed on experimental data for specific configurations.

The major feature of jet-freestream interaction is a characteristic switch from cushion behavior to a jet flap type behavior above certain speeds. This is characterized by the forward jet tucking under the wing and a strong increase in lift augmentation accompanied by a drag increase and moment shift. The abruptness of this shift in flow regime is strongly attenuated by 3-D effects. All these effects are highly dependent upon configuration, angle of attack, and height above ground. There is reason to believe that with appropriate nozzle vectoring and flap deflection, a highly effective jet flap can be achieved at higher speeds, with beneficial effects on both landing and takeoff distances.

Some data has been acquired for an aspect ratio 4 peripheral jet cushion using an unflapped NACA 0015 symmetrical section (References 8, 9, 10, and 11). The air cushion is full chord and a number of jet toe-in angles were tested. The range of variables is inadequate for use as a generalized prediction base. Such data must be supplemented by a broad-based experimental program designed to fully explore the combined effects of airfoil shape, mechanical flaps, relative cushion chord, jet toe-in angles, and modulated toe-in angles, effect of sweep, etc.

7.1.3 OTHER CUSHION SELECTION CRITERIA - In the present study the air cushion is selected on the basis of lowest operating weight. However, in a real design process the system weight must be traded against factors which impact airport performance. Some of these factors are (1) large ram drag, which can be minimized by higher fan pressure ratios, which is affected by the geometric parameters and load carried, (2) the aforementioned interaction with the mechanical flap design, (3) the range of cushion momentum coefficient  $J/qS_{\text{cushion}}$  which governs the freestream interaction for each specific configuration, and (4) some impact on minimum control speeds and associated tail volumes.

## 7.2 AIRPORT PERFORMANCE

The impact of the preceding factors on airport performance can vary from nominal to significant depending upon the airport performance required and upon the details of both cushion and overall configuration. These details, while not considered here, should form the basis for airport performance studies after an adequate data base is established. A general area of concern is the attitude constraints due to ground proximity and its impact on takeoff rotation and landing flare. In this regard, it is noted that additional cushion augmentation due to forward speed can lift the wing tips high enough to alleviate this problem, particularly at low wing sweep.

## 8.0 CONCLUSIONS AND RECOMMENDATIONS

The results of this study as summarized on Figure 42 show that for an operating weight penalty of less than 10 percent the NASA/Lockheed Spanloader, Configuration 1, can be configured

CONFIG. IDENT. →	NASA/LOCKHEED SPANLOADER	BASELINE PJ-ACLS SPANLOADER		
		WITHOUT CUSHION	WITH CUSHION	WITH CUSHION -40 INCHES
	1	2	3	4
GEAR TREAD - FT	218.0	75	75	75
CUSHION LIFT - LB	ZERO	ZERO	74,900	224,700
WING WEIGHT - LB	241,599	293,272	276,900	251,351
LANDING GEAR WT - LB	58,111	58,111	55,458	43,509
PJ-ACLS WEIGHT - LB	ZERO	ZERO	19,650	39,894
OPERATING WT - LB	540,204	591,877	592,502	575,248
PAYLOAD - LB	600,000	548,327	547,702	564,956
ZERO FUEL WT - LB	1,140,204	1,140,204	1,140,204	1,140,204
FUEL WT - LB	358,045	358,045	358,045	358,045
GROSS WT - LB	1,498,249	1,498,249	1,498,249	1,498,249

Figure 42. Spanloader Configuration Comparison Summary

with a landing gear tread width of 75 feet, Configuration 2. This is accomplished by strengthening the basic wing structure to react the increased wing down bending loads realized under negative 2g ground operations in combination with the 75 foot gear tread. As shown by the data given for Configuration 3, approximately the same weight penalty is incurred with the use of a PJ-ACLS. However, if it is assumed that the cushion heights required for the baseline PJ-ACLS Spanloader are reduced by 40 inches by some configuration design change such as the use of a "flat bottom" airfoil, then Configuration 4 incurs less of an operating weight penalty than does Configuration 2. The operating weight penalty of Configuration 4 compared to Configuration 1 is less than 7 percent.

As the addition of the PJ-ACLS to the Spanloader aircraft has a direct impact on its operational capability and versatility, the merits of the system should not be judged solely on aircraft weight impact. The use of a wide tread gear such as the 218 feet of Configuration 1 would severely limit the number of compatible airports. Configuration 2 meets runway width requirement needs, however, the total gross weight of the aircraft must be reacted by the closely spaced bogie arrangement. Whereas gear loads for Configurations 3 and 4 which utilize the same closely spaced gear arrangement, are reduced by a magnitude equivalent to the cushion lift, providing increased gear flotation.

The results of this study are compromised to the degree that the basic Spanloader configuration was not reoptimized to benefit cushion installation or performance. Given this freedom of reconfiguring the Spanloader, it is felt improved cushion weight and performance can be obtained. Tradeoff studies between cruise performance and cushion performance are required. Cushion improvements can be obtained by the Spanloader configuration changes as summarized on Figure 43.

Although the transverse fan is not included in the present PJ-ACLS system analyses, a cursory qualitative assessment was made to identify possible advantages of a transverse fan system. One conceivable scheme for utilizing this concept is shown on Figure 44. The following briefly lists possible advantages of this transverse fan system as related to the centrifugal fan system:



**REDUCE WING ASPECT RATIO (5-90)**

- IMPROVES AUGMENTATION RATIO BY REDUCING CUSHION HEIGHT TO WIDTH RATIO
- REDUCES MAXIMUM WING DEFLECTIONS ALLOWING A REDUCTION IN CUSHION HEIGHT

**TRANSPORT TOTAL PAYLOAD WITHIN WING CONTOUR (20-80)**

- INCREASED POTENTIAL WEIGHT SAVING AS WEIGHT INCREMENT BETWEEN  $W_{REF}$  &  $W_{2G}$  INCREASES

**USE MODIFIED SUPERCRITICAL OR CLARK Y AIRFOIL SHAPE**

- REDUCES CUSHION HEIGHT & IMPROVES AUGMENTATION RATIO

**USE TWIN BOOM AFT EMPENNAGE CONFIGURATION**

- IMPROVED STABILITY AND CONTROL CAPABILITY

**REDUCE WING SWEEP (40 DEGREES)**

- REDUCES CONTROL FORCES REQUIRED TO REACT CUSHION MOMENTS
- DECREASED ALTITUDE AT WHICH NOSE-UP ATTITUDE CAN BE ACHIEVED
- INCREASES WING CHORD FOR A GIVEN CARGO CAPABILITY AND HENCE IMPROVING AUGMENTATION BY INCREASING CUSHION WIDTH

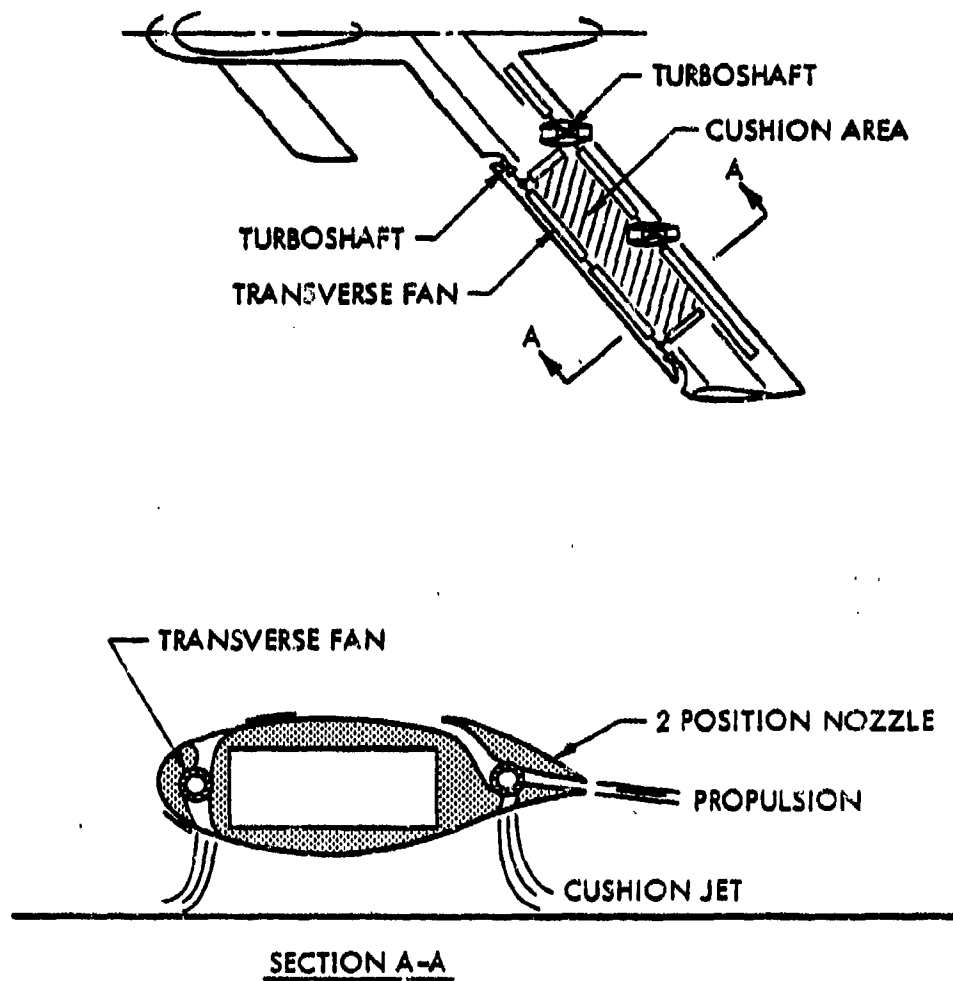


Figure 44. Transverse Fan Peripheral Jet Cushion

1. For a given required jet flow, the transverse fan would require less space than the centrifugal fans:
  - o The capability of the transverse fan to inject airflow radially into the impeller eliminates the requirement for spacing between fans to allow for inlet flow.
  - o Since there is no aerodynamic limit on the axial length of the transverse fan impeller, the number of fans may be reduced, thus reducing the space required for fan housing, and for shaft coupling between fans.
2. As indicated on Figure 44, the trailing edge fans could be used to provide both cushion and propulsion; and as applicable this concept could also include a jet flap with boundary layer control.
3. Assuming a transverse fan efficiency at least as good as for the study centrifugal fan, both the preceding effects should result in a reduced air supply system weight.

Lockheed is currently investigating a transverse-fan propulsive wing concept (References 12 and 13). It is expected that the results of this investigation may reveal additional transverse fan advantages.

Possibly the greatest military benefit to be derived from the PJ-ACLS is one of enhancement of operation from battle-damaged runways. It appears possible with a PJ-ACLS to offer a large aircraft concept which requires only a single gear track (bicycle gear arrangement). This single gear track would increase the probability of runway operation after runway battle damage.

## APPENDIX A

### PJ-ACLS PARAMETRIC EQUATIONS

The parametric equations used to define performance data as a function of various sizing parameters are derived from the Barratt theory as given by Reference 2. The essentials of this theory, with some changes in notations from Reference 2, are given by Equations 1 through 4.

$$J = 2Sp_j t \sqrt{1 - p_c/p_j} \quad (1)$$

$$Q_j = tS \sqrt{\frac{2}{\rho}} (p_j) \frac{\sqrt{1 - p_c/p_j}}{1 - \sqrt{1 - p_c/p_j}} \log_e (1 - p_c/p_j)^{-1/2} \quad (2)$$

$$p_c/p_j = 2X \left( \sqrt{X^2 + 1} - X \right) \quad (3)$$

$$\text{where: } X = t/h_c (1 + \sin \theta) \quad (4)$$

The following relationships are next defined for air horsepower and total cushion lift:

$$HP = Q_j p_j / 550 \quad (5)$$

$$L = J \cos \theta + p_c A_c \quad (6)$$

Equations 1 and 6 are rewritten as follows:

$$J/A_c p_j = (2St/A_c) \sqrt{1 - p_c/p_j} \quad (1a)$$

$$L/A_c = \left[ (J/A_c p_j) (\cos \theta) + p_c/p_j \right] p_j \quad (6a)$$

From combining Equation 1a and 6a the following is obtained:

$$p_j/(L/A_c) = 1/G \quad (7)$$

where:

$$G = \left[ (2St/A_c) \cos \theta \sqrt{1 - p_c/p_j} + p_c/p_j \right] \quad (8)$$

Using Equations 2, 6a, and 8 the following relationships are defined:

$$\begin{aligned} \left( \frac{Q_1 \sqrt{\sigma}}{L} \right) \left( \sqrt{\frac{L}{A_c}} \right) &= \frac{Q_1 \sqrt{\sigma}}{(\sqrt{L/A_c}) A_c} \\ &= \frac{\frac{tS}{A_c} \sqrt{2p_j/\rho_o} \sqrt{1 - p_c/p_j}}{\sqrt{G} \sqrt{p_j} [1 - \sqrt{1 - p_c/p_j}]} \log_e (1 - p_c/p_j)^{-1/2} \\ &= \frac{KF \sqrt{2/\rho_o}}{\sqrt{G}} \end{aligned} \quad (9)$$

where:

$$K = tS/A_c \quad (10)$$

$$F = \frac{\sqrt{1 - p_c/p_1}}{1 - \sqrt{1 - p_c/p_j}} \log_e (1 - p_c/p_j)^{-1/2} \quad (11)$$

Also from Equations 5, 7, and 9:

$$\begin{aligned} \frac{P\sqrt{\sigma}}{L\sqrt{L/A_c}} &= \frac{\left[ \frac{\sqrt{\sigma} Q_1}{L} \sqrt{\frac{L}{A_c}} \right] \left[ \frac{P_1}{L/A_c} \right]}{550} \\ &= \frac{KF \sqrt{2/\rho_o}}{550(G)^{3/2}} \end{aligned} \quad (12)$$

$$A_I = L/J = \frac{G}{2K \sqrt{1 - p_c/p_j}} \quad (13)$$

#### Summary

The parametric fan sizing relationships provided are:

$$\frac{\left[ \frac{P}{L} \right] \sqrt{\sigma}}{\sqrt{\frac{L}{A_c}}} = \frac{K}{550} \left[ \frac{F}{G^{3/2}} \right] \sqrt{\frac{2}{\rho_o}} \quad (14)$$

$$\frac{P_1}{\left[ \frac{L}{A_c} \right]} = \frac{1}{G} \quad (15)$$

$$\frac{Q_j \sqrt{\sigma}}{L} \sqrt{\frac{L}{A_c}} = \frac{KF \sqrt{\frac{2}{\rho_o}}}{\sqrt{G}} \quad (16)$$

$$A = \frac{G}{2K \sqrt{1 - p_c/p_j}} \quad (17)$$

Where:

$$F = \frac{\sqrt{1 - p_c/p_j}}{1 - \sqrt{1 - p_c/p_j}} \log_e (1 - p_c/p_j)^{-1/2}$$

$$G = 2K \cos \theta \sqrt{1 - (p_c/p_j)} + (p_c/p_j)$$

$$\frac{p_c}{p_j} = 2X \left[ \sqrt{X^2 + 1} - X \right]$$

$$X = \frac{t}{h_c} (1 + \sin \theta) = \left[ (t/w)/(h_c/w) \right] [1 + \sin \theta]$$

$$X = \frac{\text{jet area}}{\text{cushion area}} = St/A_c$$

t = jet thickness, ft.

h = height above ground, ft.

$\theta$  = jet toe-in angle, positive into cushion

$p_c$  = cavity pressure, psfg

$p_j$  = jet pressure, psfg

$\rho_o$  = standard atmosphere mass density, 0.002378 slugs/ft<sup>3</sup>

$\sigma$  = atmospheric density ratio  $\rho/\rho_0$

$L$  = total cushion lift, lb.

$A_c$  = cushion area,  $\text{ft}^2$

$J$  = jet momentum flux, lb.

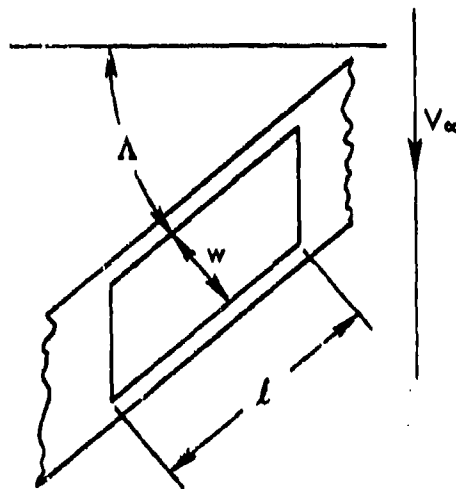
$\mathcal{P}$  = air horsepower

$A$  = thrust augmentation ratio ( $L/J$ )

$Q_j$  = jet air flow,  $\text{ft}^3/\text{sec}$ .

$S$  = peripheral length of jet, ft.

The expressions as given here are extremely useful in that horsepower per pound of lift, jet pressure, and jet volume flow per pound of lift are given by geometry ( $\theta$ ,  $t/h$ ,  $K$ ) and cushion loading. For utilization purposes, the latter two parameters are specialized to the cushion illustrated



for which  $t/h = \frac{t}{w} / \frac{h}{w}$

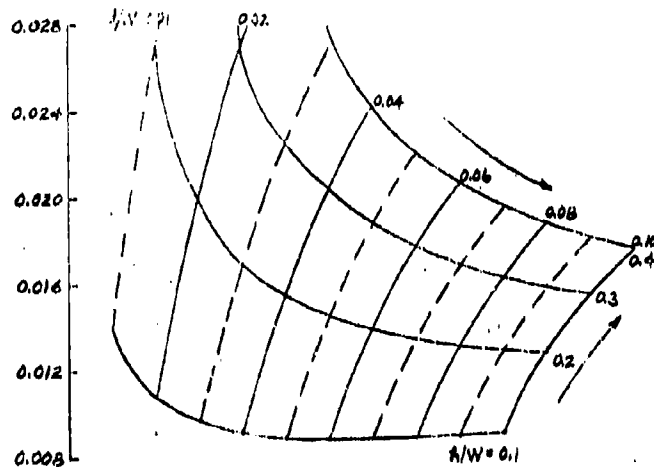


$$K = 2 \left[ 1 + \frac{w/l}{\cos \Lambda} \right] t/w$$

Carpet plots have been constructed which show the relationships of Equations 14 through 17 to  $t/w$  and  $h/w$ . These data are for  $\Lambda = 40^\circ$  only, and are shown in Figures 1A through 18A for the matrix  $\theta = 0, 10^\circ, 20^\circ, 30^\circ, 40^\circ, 50^\circ$ , and  $l/w = 2, 4, 6$ .

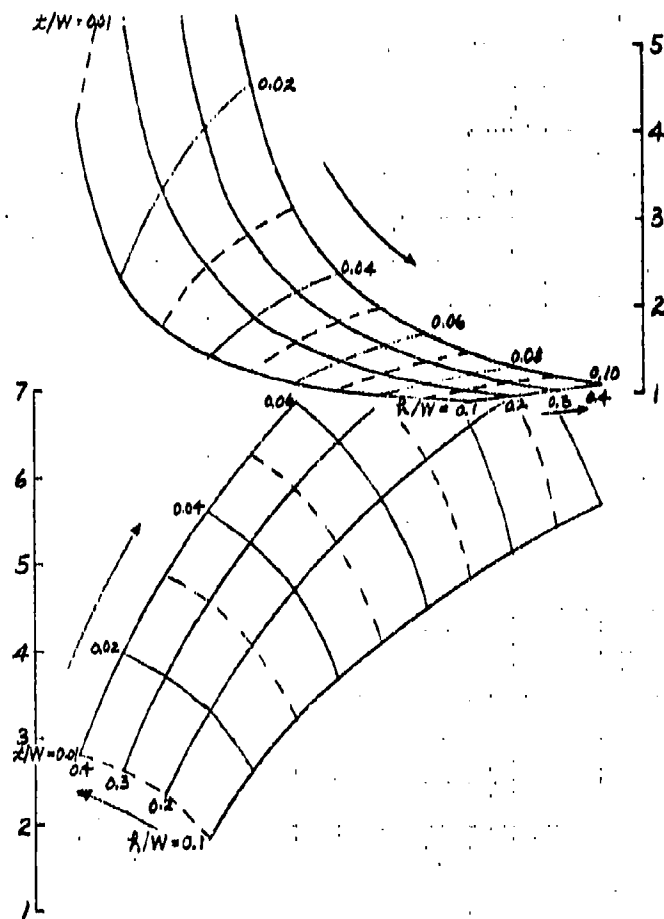
The figures shown are usable for other sweep angles at other values of  $l/w$ , that is  $\frac{l/w}{\cos \Lambda} = \left( \frac{l/w}{\cos \Lambda} \right)_{\text{Basic}}$

$$\frac{\left(\frac{P}{L}\right)\sqrt{\sigma}}{\sqrt{\frac{L}{A_c}}}$$

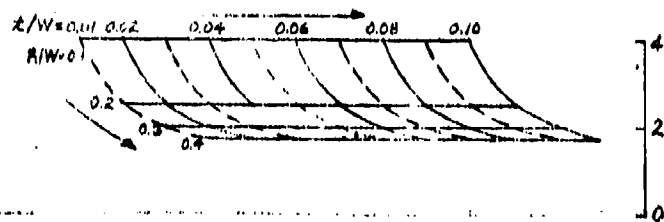


CONDITIONS  
 $\frac{L}{W} = 2$   
 $\theta = 0^\circ$   
 $\Lambda = 40^\circ$

$$\left(\frac{Q_L\sqrt{\sigma}}{L}\right)\left(\sqrt{\frac{L}{A_c}}\right)$$

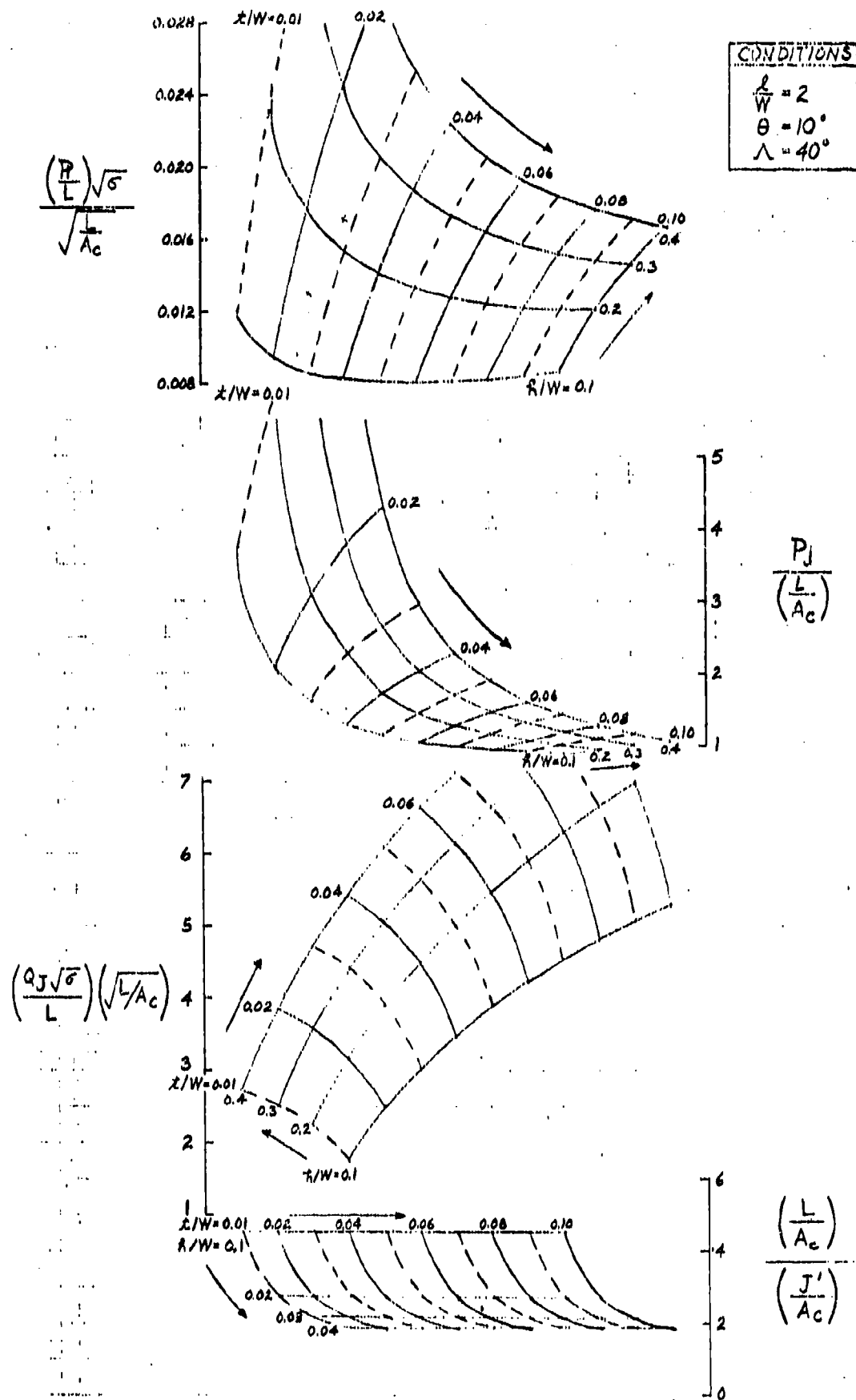


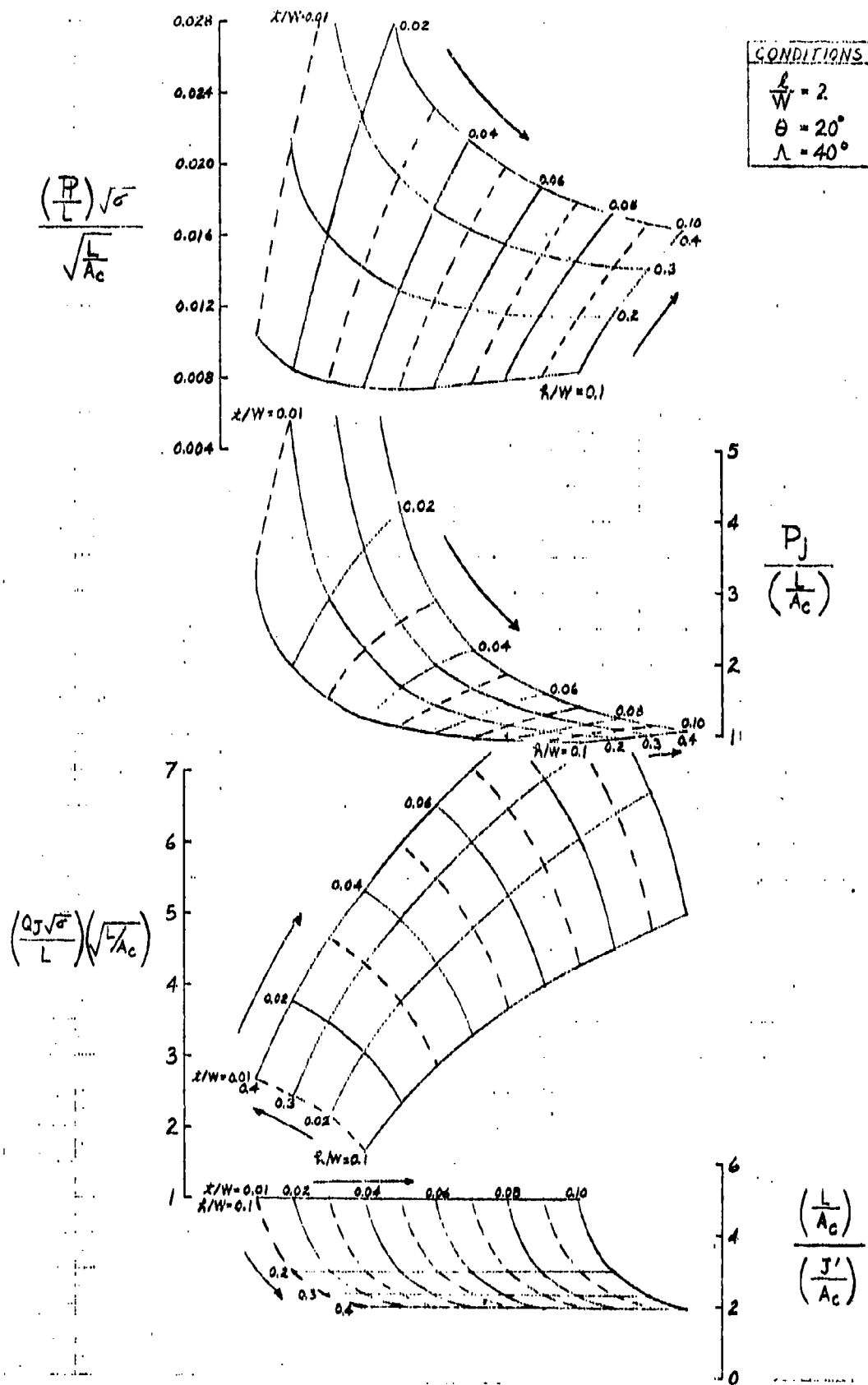
$$\frac{P_j}{\left(\frac{L}{A_c}\right)}$$

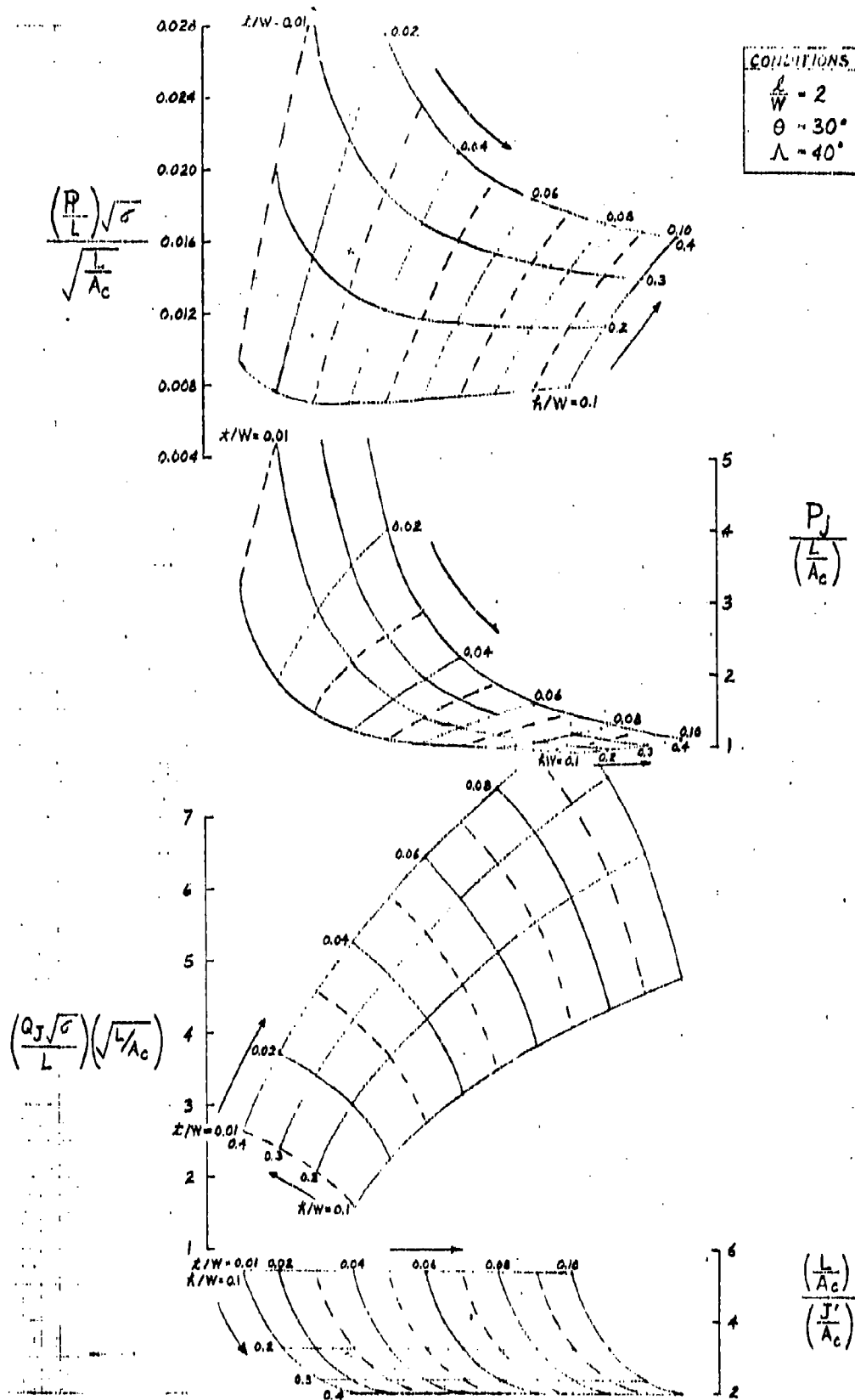


$$\frac{\left(\frac{L}{A_c}\right)}{\left(\frac{J'}{A_c}\right)}$$

FIGURE 1A







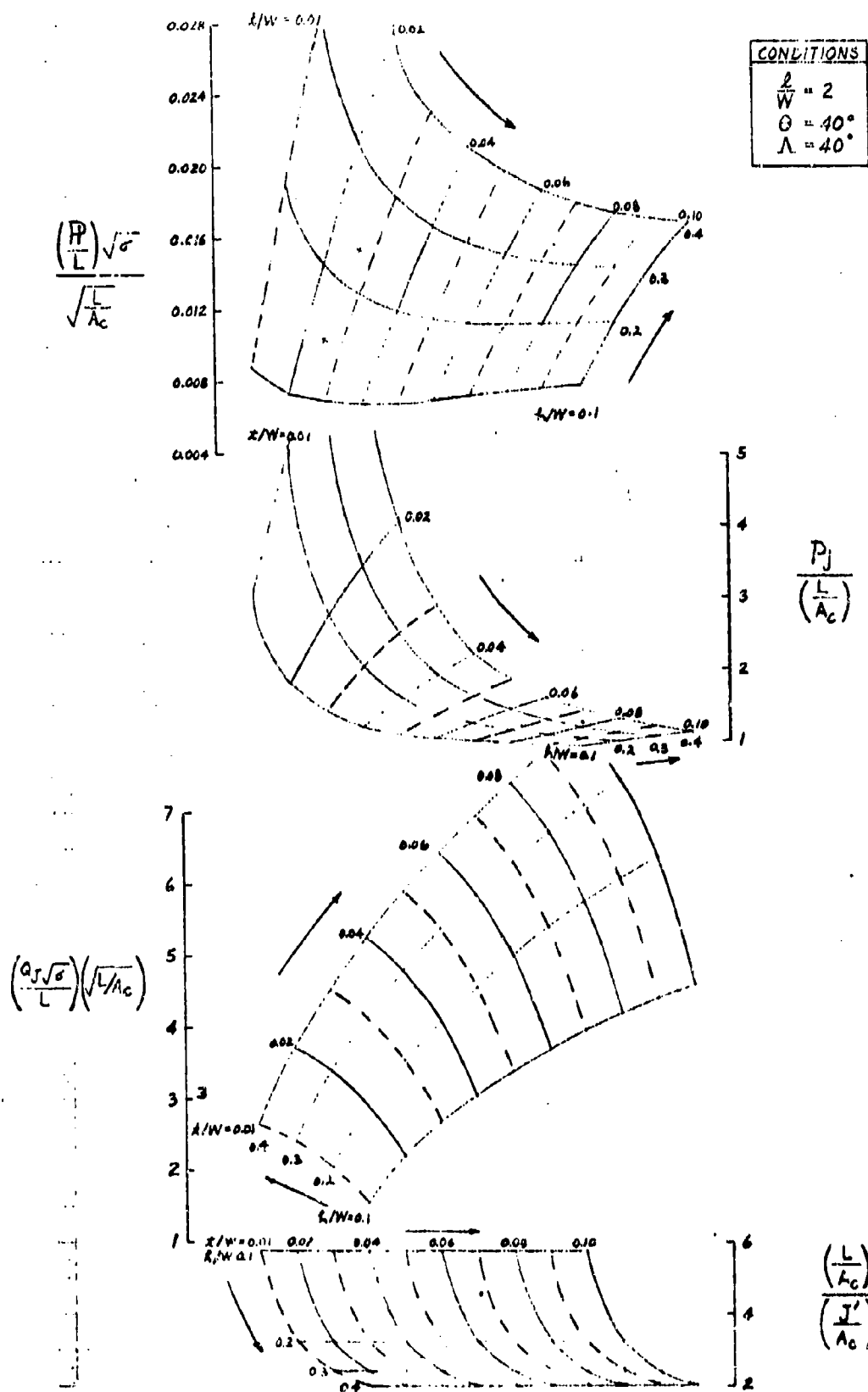
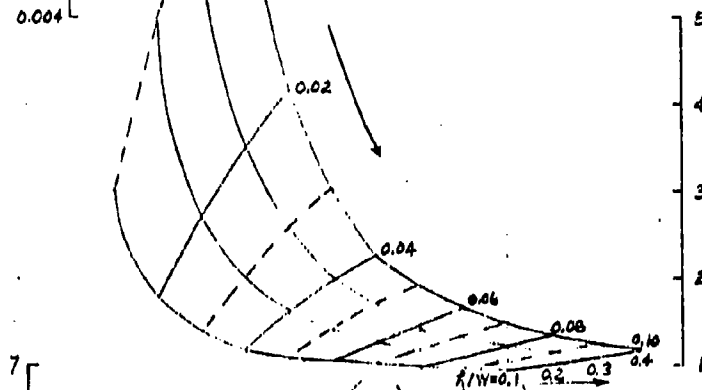
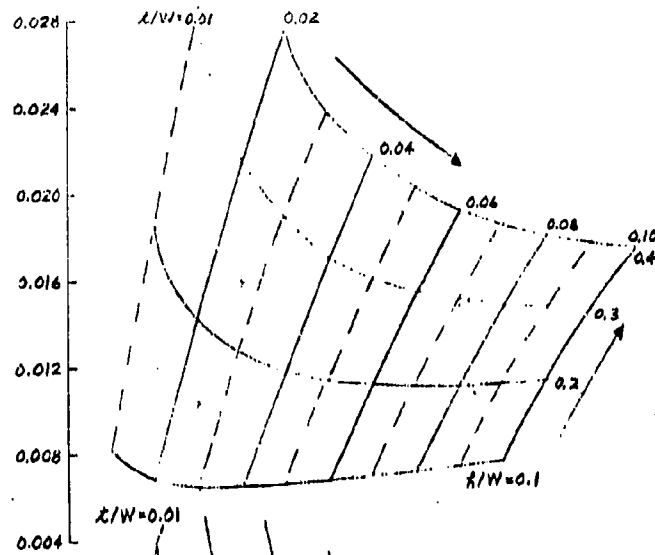
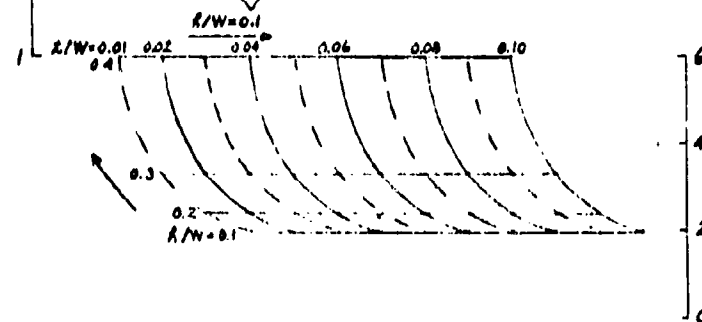
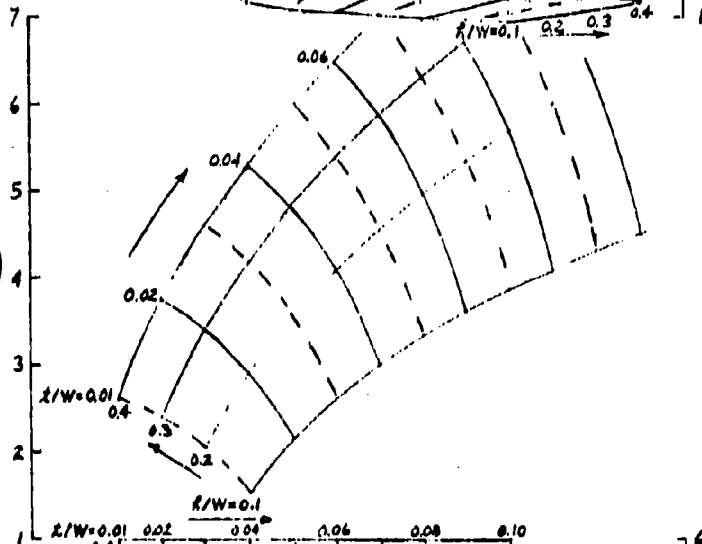


FIGURE 5A

$$\frac{\left(\frac{P}{L}\right)\sqrt{\sigma}}{\sqrt{\frac{L}{A_c}}}$$



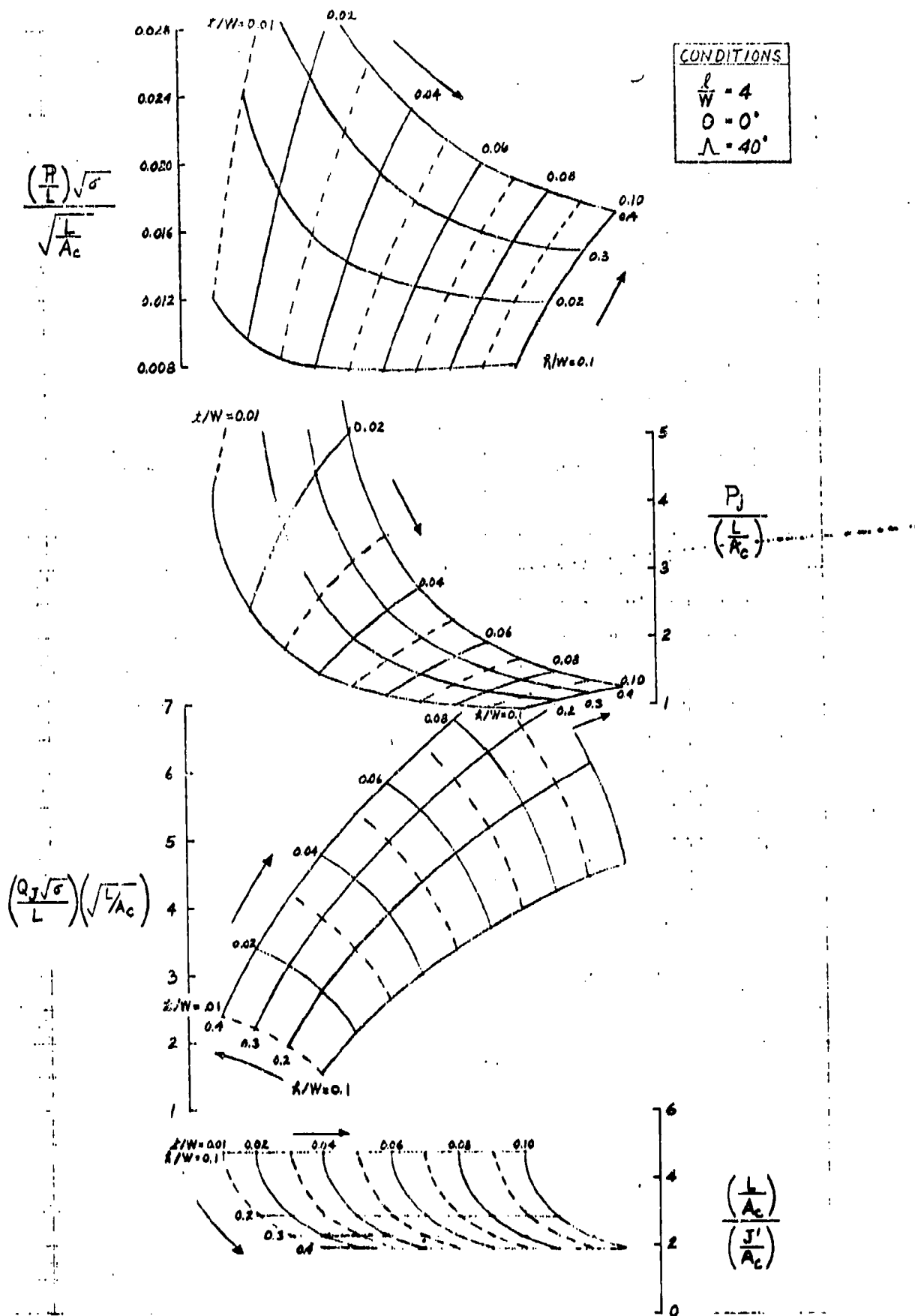
$$\left(\frac{Q_j \sqrt{\sigma}}{L}\right) \left(\sqrt{\frac{L}{A_c}}\right)$$



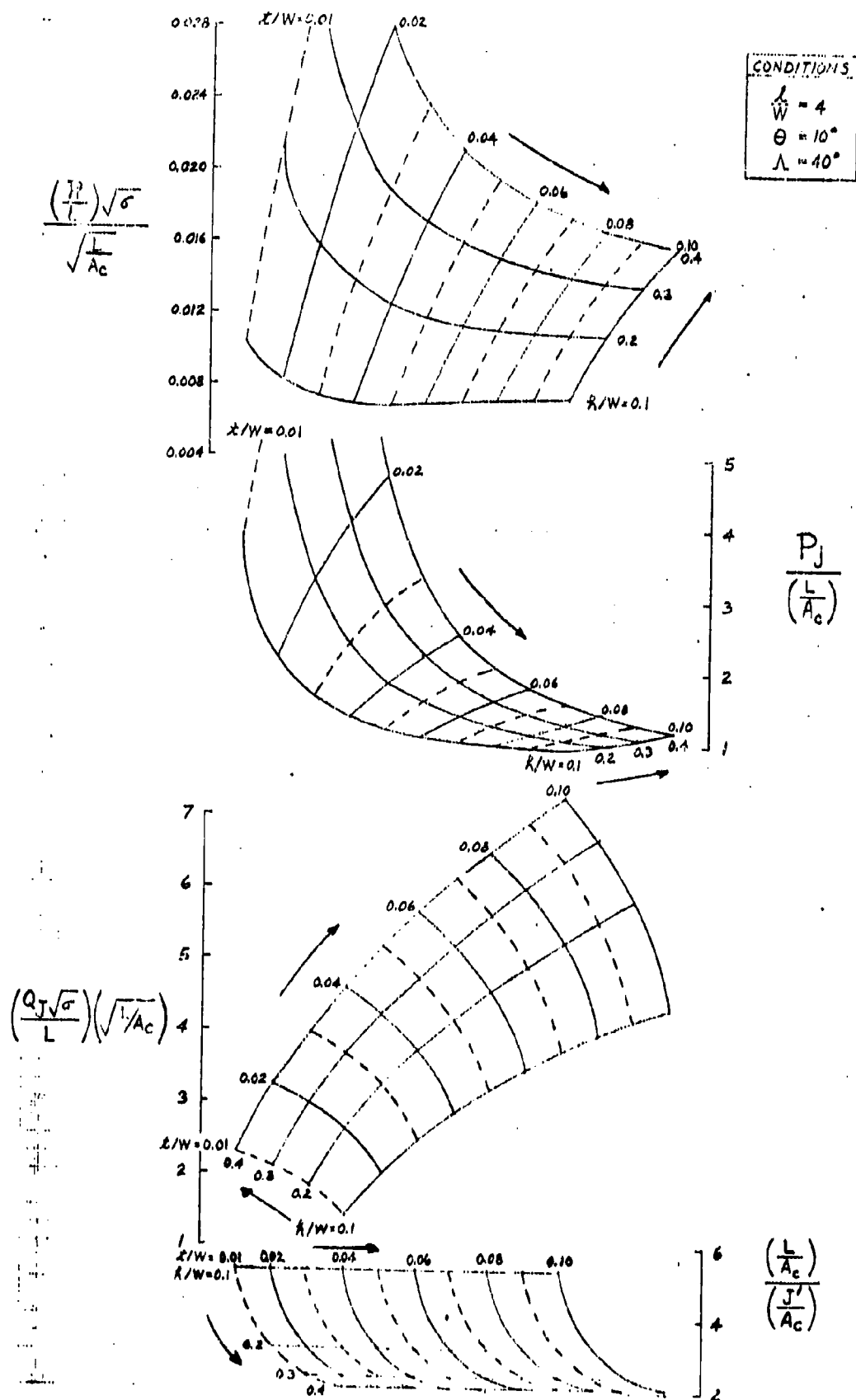
$$\frac{P_j}{\left(\frac{L}{A_c}\right)}$$

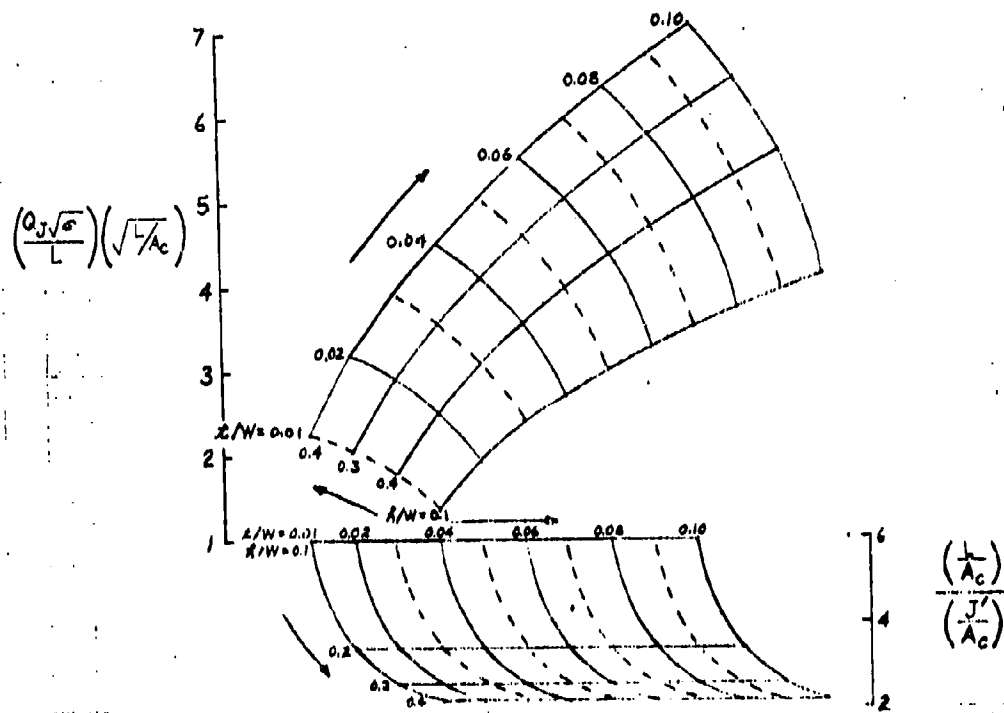
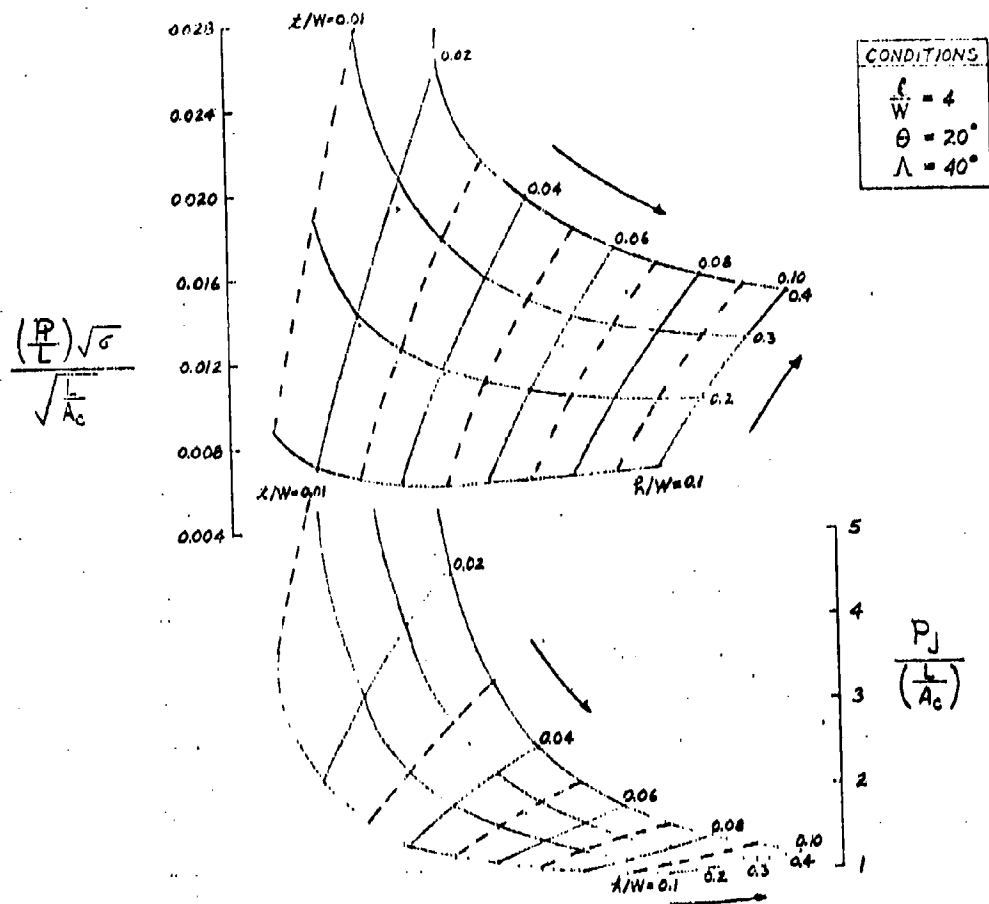
$$\frac{\left(\frac{L}{A_c}\right)}{\left(\frac{J'}{A_c}\right)}$$

FIGURE 6A

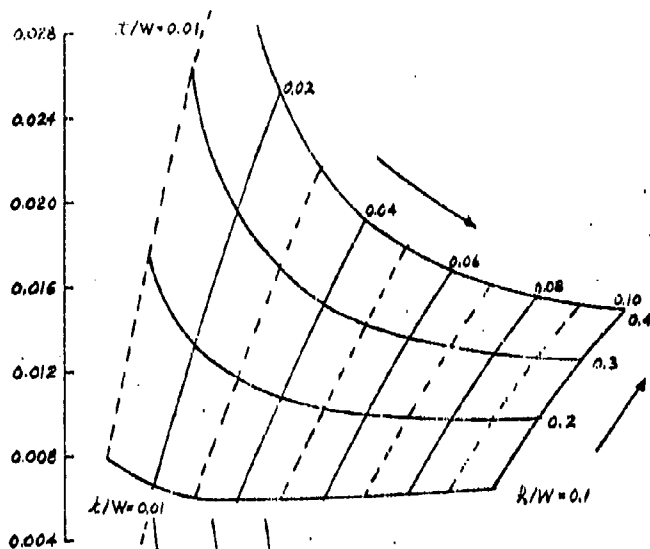




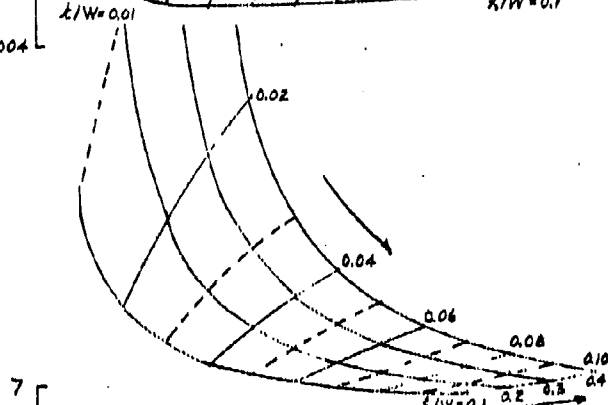




$$\frac{\left(\frac{P}{L}\right)\sqrt{\sigma}}{\sqrt{\frac{L}{A_c}}}$$



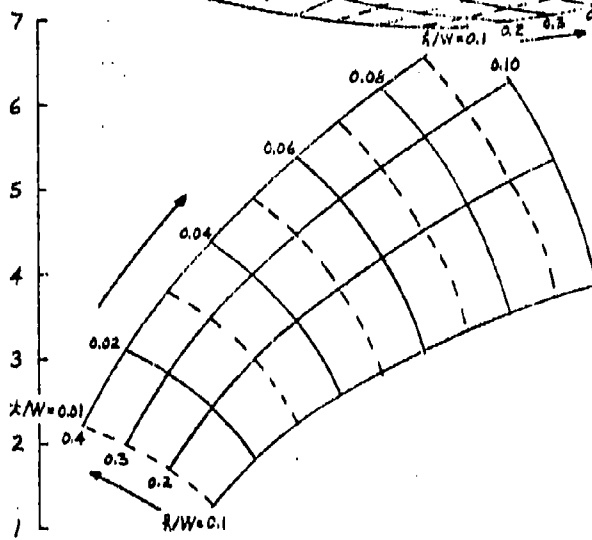
CONDITIONS:  
 $\frac{\lambda}{W} = 4$   
 $\theta = 30^\circ$   
 $\lambda = 40^\circ$



5  
4  
3  
2  
1

$$\frac{P_J}{\left(\frac{L}{A_c}\right)}$$

$$\left(\frac{Q_J \sqrt{\sigma}}{L}\right) \left(\sqrt{\frac{L}{A_c}}\right)$$



8  
6  
4  
2

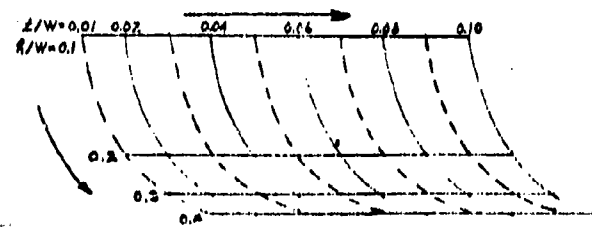
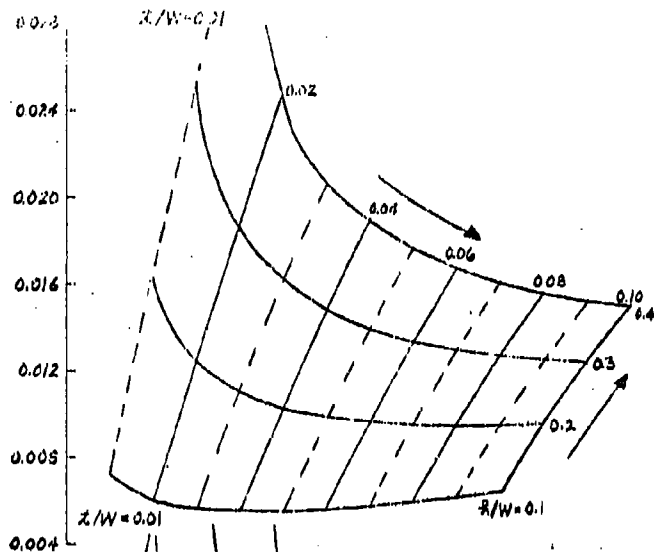
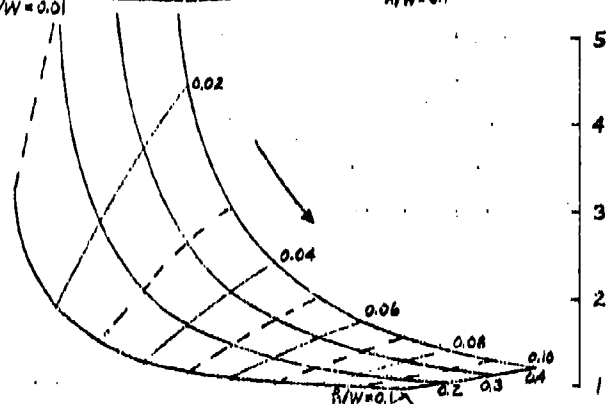
$$\frac{\left(\frac{L}{A_c}\right)}{\left(\frac{J'}{A_c}\right)}$$


FIGURE 10A

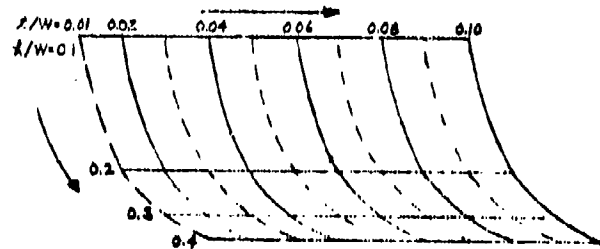
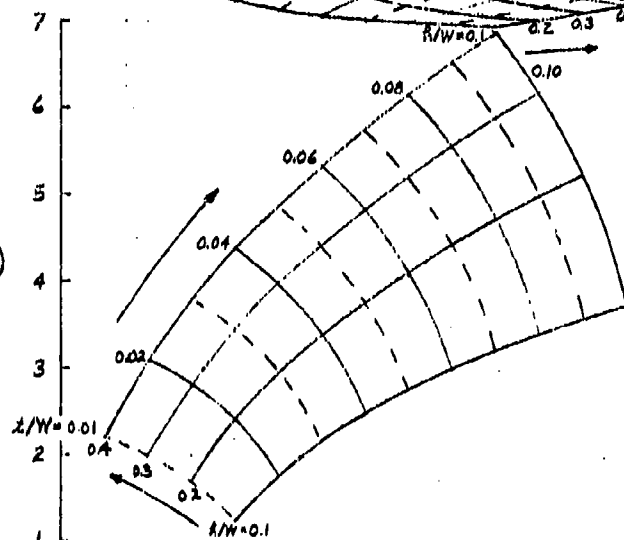
$$\frac{\left(\frac{P}{L}\right)\sqrt{\sigma}}{\sqrt{\frac{L}{A_c}}}$$



CONDITIONS  
 $\frac{l}{W} = 4$   
 $G = 40^\circ$   
 $\Lambda = 40^\circ$



$$\left(\frac{Q_T \sqrt{\sigma}}{L}\right) \left(\sqrt{\frac{L}{A_c}}\right)$$



$$\frac{\left(\frac{L}{A_c}\right)}{\left(\frac{J'}{A_c}\right)}$$

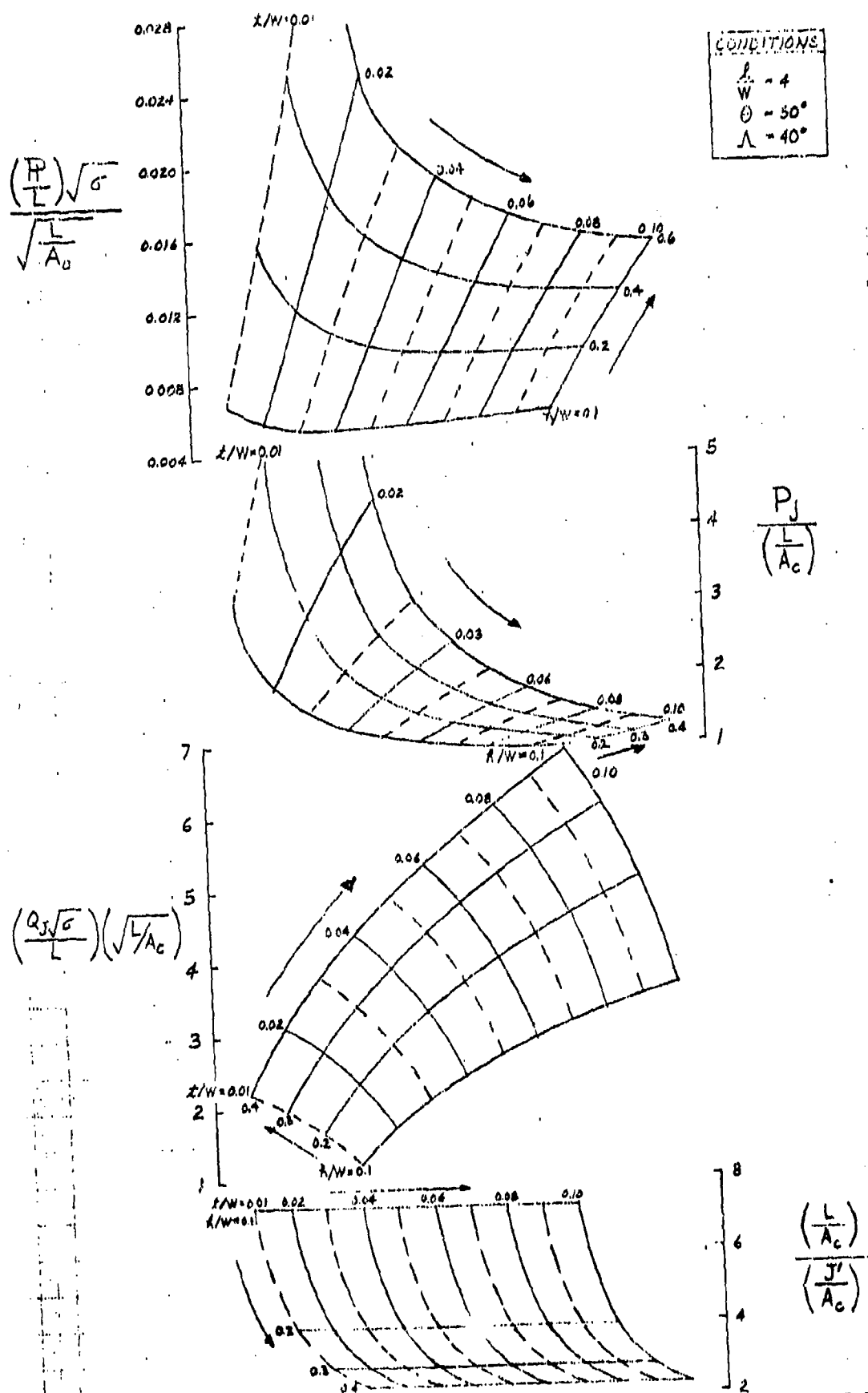


FIGURE 12A

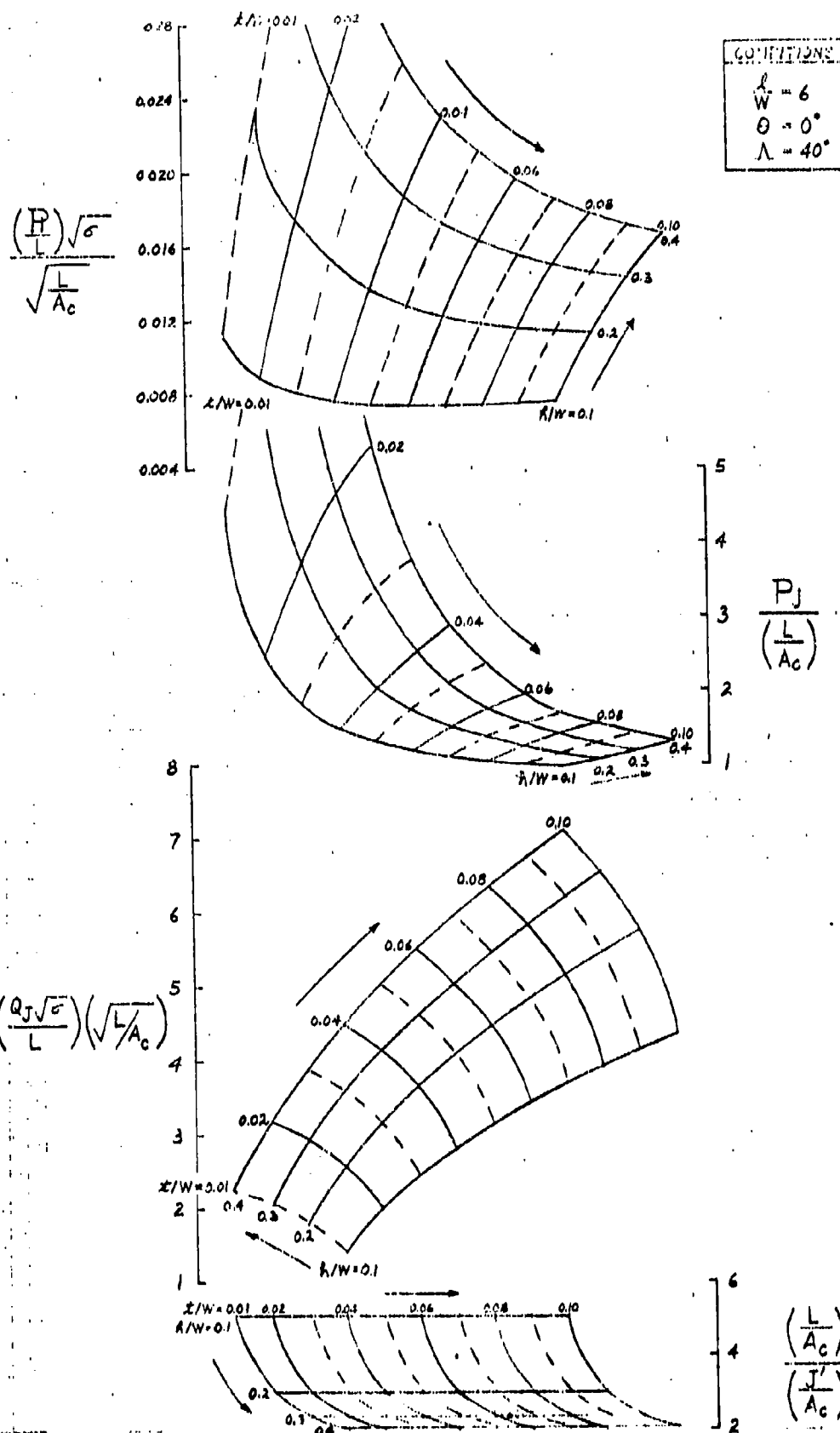


FIGURE 13A

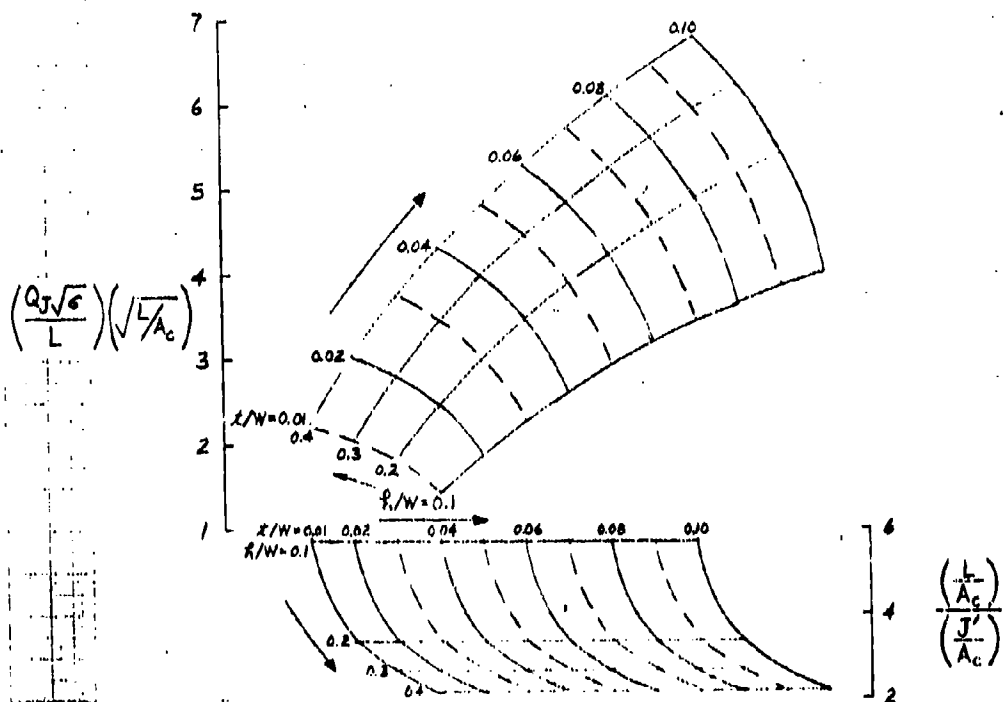
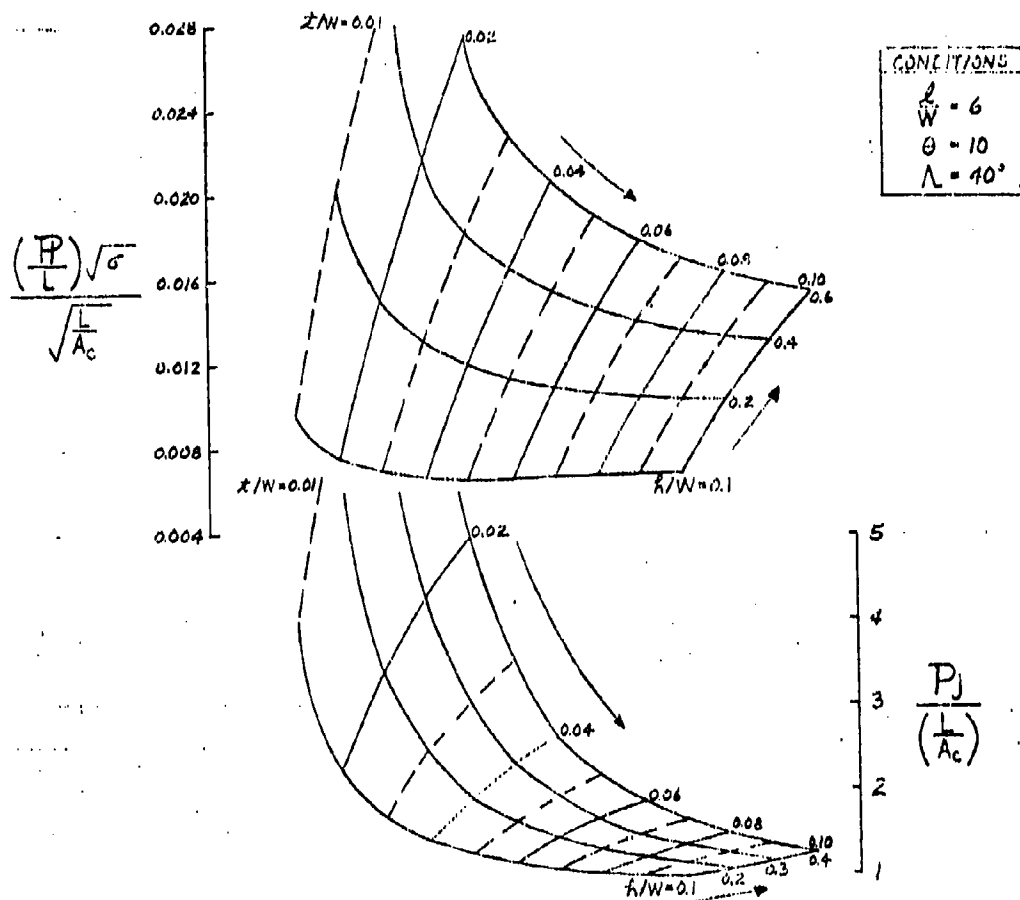
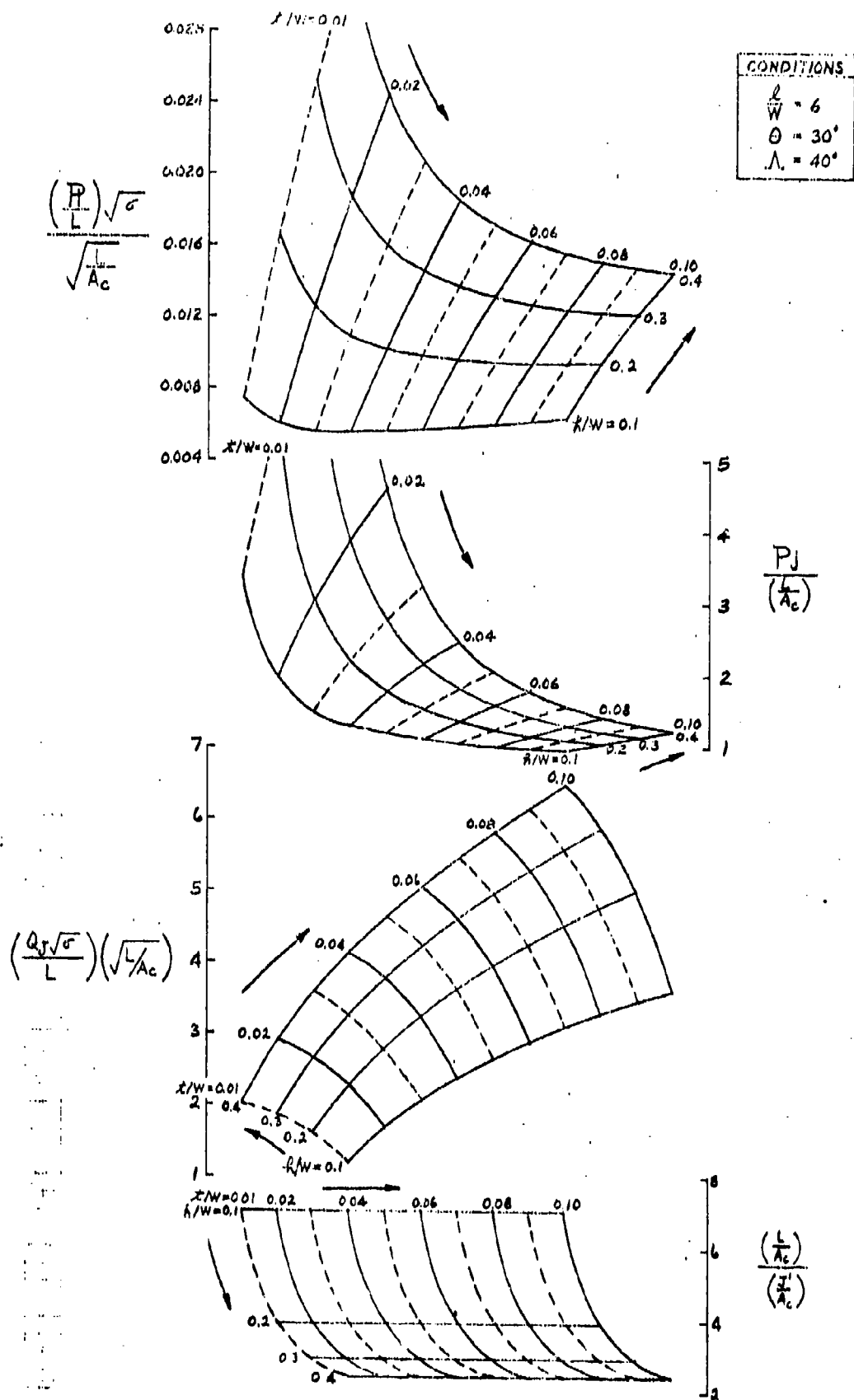
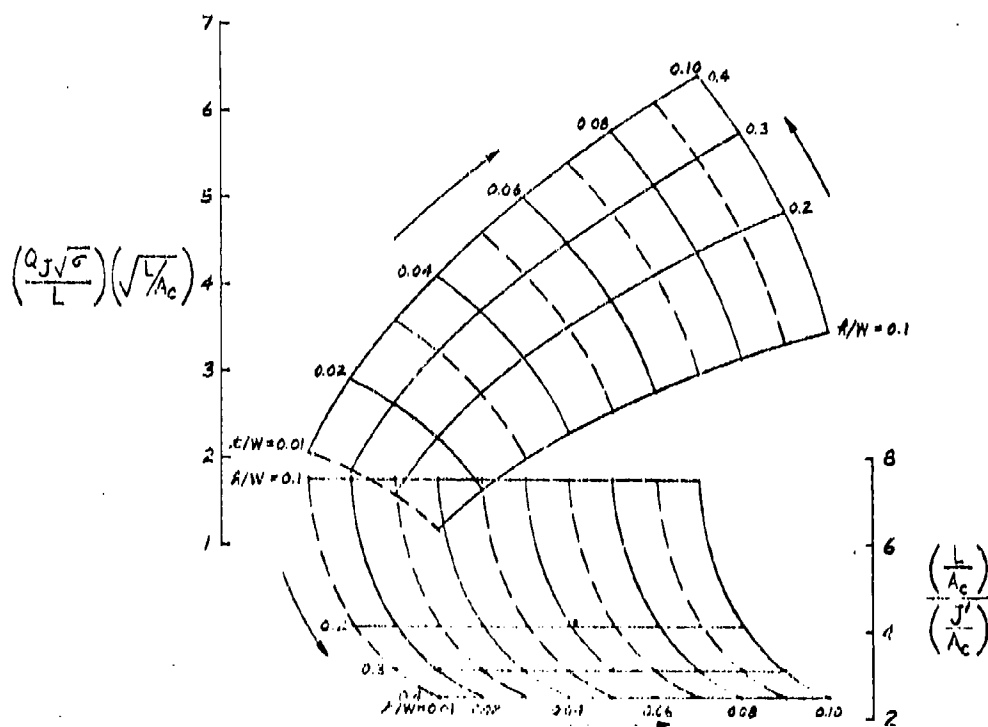
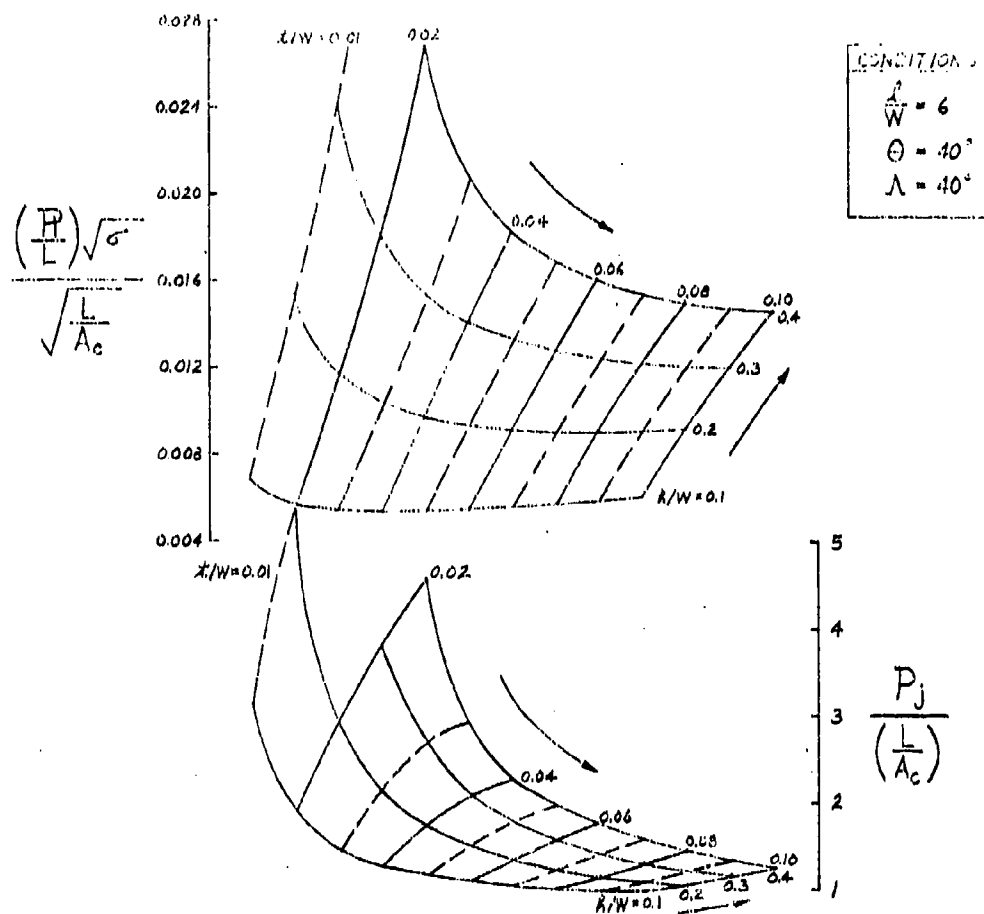


FIGURE 14A









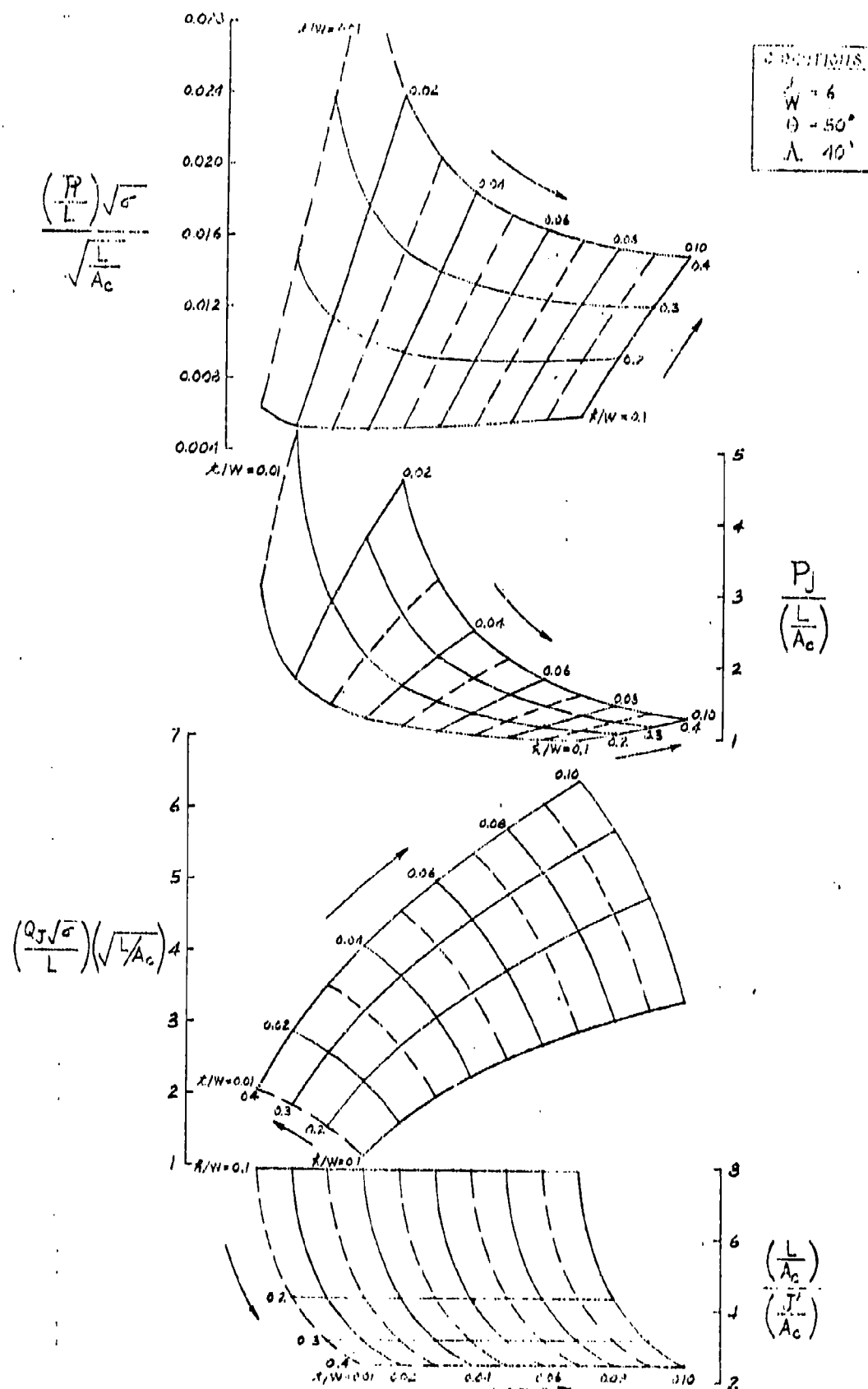


FIGURE 18A

APPENDIX B  
B1.0 STABILITY & CONTROL

Control of the PJ-ACLS vehicle at low speed will require the generation of forces and moments to supplement the low effectiveness of conventional aerodynamic controls. The need for this is particularly marked if the cushion system is designed to provide a large portion of the total vehicle support during ground-borne maneuvers. In this case the conventional landing gear is off-loaded and becomes less effective for vehicle control.

One means of generating additional control inputs to the PJ-ACLS vehicle is to vary the angle of the peripheral jet which sustains the cushion pressure. Inward or outward rotation of the jet all around its periphery changes the vertical cushion force at a given height. When the cushion is offset from the vehicle center of gravity this change of vertical force will cause incremental pitching and rolling moments. For vehicle control near the ground the generation of side-force and yawing moment is equally important and these can be produced by changing the in-plane cushion force through asymmetric variation of the peripheral jets. In this mode of control the inward jet angle is increased on one side of the cushion and reduced on the opposite side.

This stability and control analysis has investigated the use of symmetrical and asymmetrical peripheral jet angle control for the spanloader vehicle configuration. This work is a natural application and extension of the data contained in Reference 2. The Barratt theory is first extended to include asymmetric peripheral jet conditions. Then, the effectiveness of peripheral jet angle control is assessed for single unconstrained and constrained cushion vehicles. Finally, equations and a computer program are formulated for estimating the control forces and moments generated by symmetrical and asymmetrical variation of peripheral jet angle on a multi-cushion supported vehicle. These equations are then used to assess the controllability of a large spanloader PJ-ACLS vehicle, as shown in Figure 1B.

SPEED	0.75 MACH
PAYLOAD	548,327 LB
RANGE	3,000 NM
OPERATING WT.	591,877 LB
ZERO FUEL WT.	1,140,204 LB
FUEL	358,045 LB
GROSS WT.	1,498,000 LB
ENGINE THRUST	59,500 LB
ASPECT RATIO	5.90
SWEEP ANGLE	40°
WING AREA	18,560 SQ. FT.

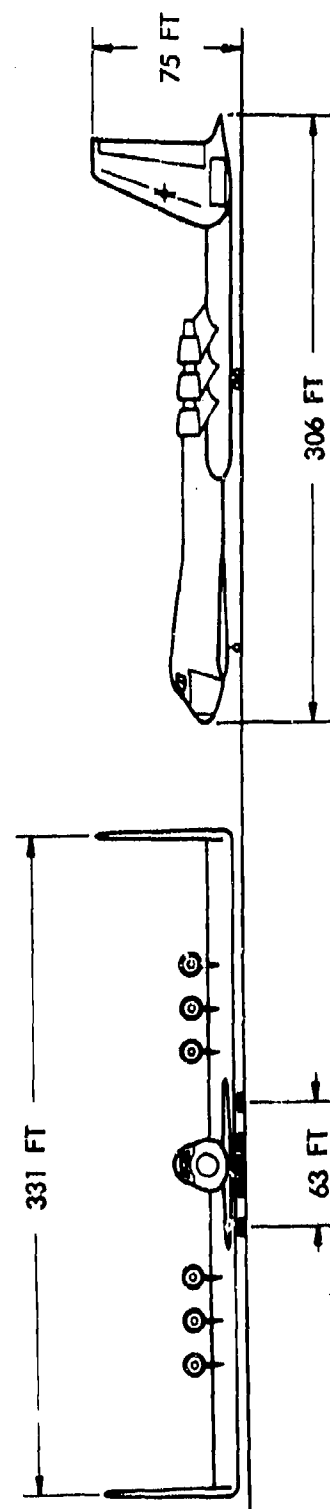
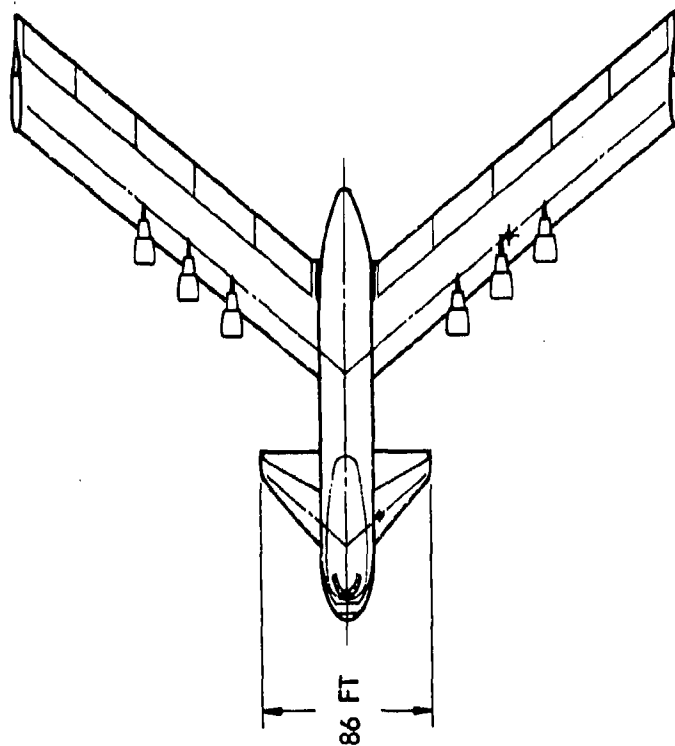


Figure 1B. PJ-ACLS Baseline Spanloader

## B2.0 ASYMMETRIC PERIPHERAL JET THEORY

The theory of air cushion landing systems for aircraft is presented by Digges in Reference 2. This reference covers various types of cushion generating systems and presents a number of different theories for estimating the basic performance characteristics of cushion vehicles. Section 2.3 of Reference 2 lists the assumptions which have been applied to all the peripheral jet theories developed in the report. Two of these principal assumptions concerning vehicle force equilibrium must be discarded in the asymmetric peripheral jet theory. These are:

Assumption 2.3.2.1., "The ACLS is symmetric and the opposite sides have identical flow, stiffness and geometric characteristics."

Assumption 2.3.2.5., "The net vertical thrust from the peripheral jet is negligible."

Control of an ACLS vehicle requires the generation of asymmetric forces and moments and, if these are derived from varying the angle of the peripheral jet, the assumption of symmetry cannot be generally retained. Also, the in-plane control forces generated by peripheral jet control may be derived mainly or totally from the peripheral jet thrust which must therefore be retained in the vehicle force equilibrium equation.

### B2.1 UNCONSTRAINED CUSHION VEHICLE

Figure 2B defines the geometry and force system for an unconstrained rectangular peripheral jet cushion vehicle. The vehicle weight,  $W$ , is completely supported by the cushion pressure and the vertical jet thrust. Also, the side force and rolling moment are zero.

Instantaneous rotation of the side jets results in the condition shown in Figure 3B. The upper figure shows the situation prior to vehicle motion response. The right jet inward inclination is increased and the left jet angle is reduced by an amount  $\delta\theta$ . This causes a cushion pressure gradient as indicated, a rolling moment to the left and an out-of-balance jet side force. The unconstrained vehicle rolls to reduce the cushion pressure

FIGURE 2B RECTANGULAR PERIPHERAL JET

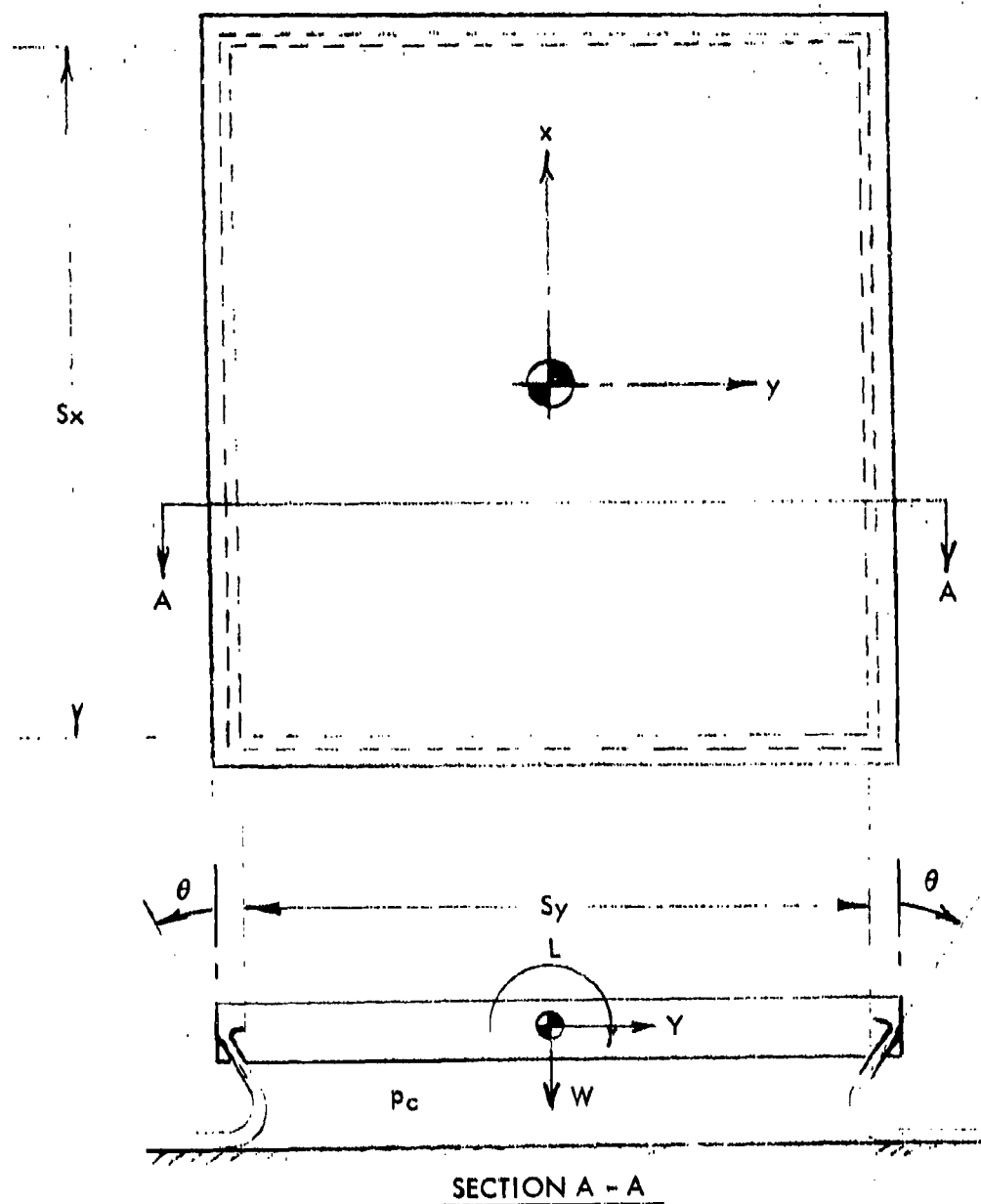
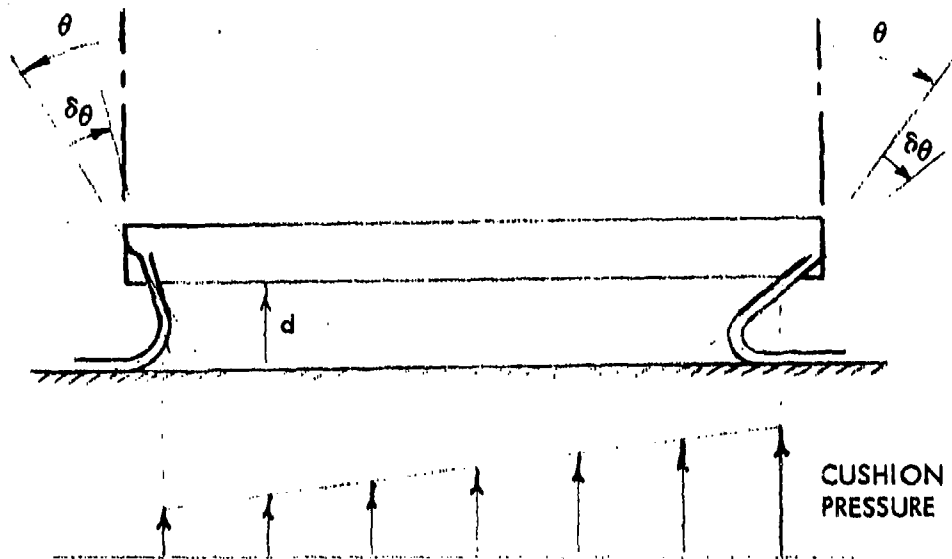
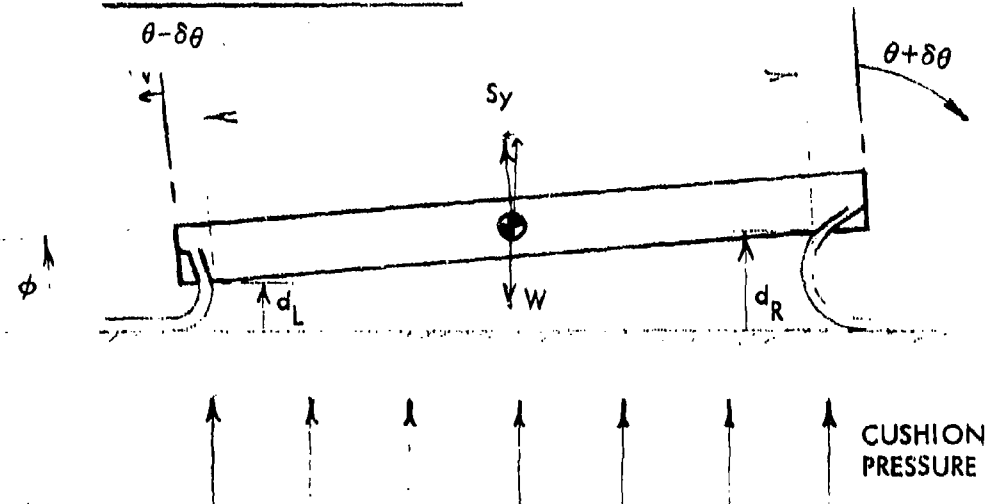


FIGURE 3B ASYMMETRIC PERIPHERAL JET CONTROL  
(VEHICLE UNCONSTRAINED)

a) CONTROL APPLICATION



b) VEHICLE EQUILIBRIUM





gradient as shown in the lower figure, and in this condition the vehicle weight is completely supported by the cushion pressure and the vertical jet thrust. The small rolling moment due to the difference in vertical thrust between the right and left jets is balanced by a small cushion pressure gradient and the only sustained out-of-balance is a side force shown in Equation 1 as:

$$Y = \frac{J'}{S_x + S_y} \left[ S_x \sin(\delta\theta - \phi) \left[ \cos\theta + \frac{6d}{S_y} \sin\theta \right] - S_y \sin\phi \right] \quad (1)$$

where  $J'$  is the total peripheral jet reaction and  $d$  is the average height of the cushion.

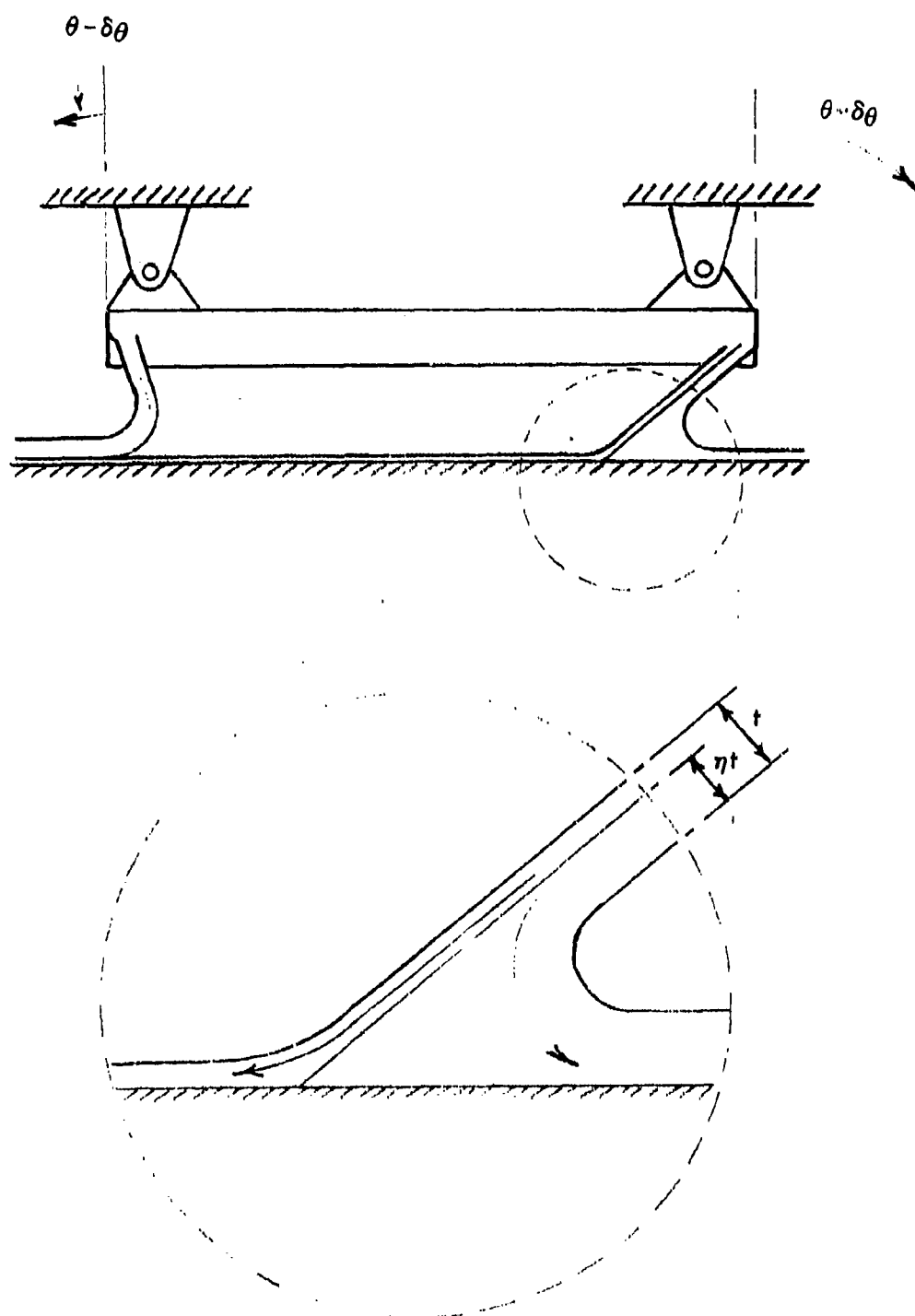
This equation indicates that the side force is totally due to the asymmetric jet reaction and that the vehicle response,  $\phi$ , in roll reduces the side force effectiveness of the jet angle variation,  $\delta\theta$ .

## B2.2 CONSTRAINED CUSHION VEHICLE

If the ACLS cushion device is attached to another vehicle, such as the spanloader aircraft, it is constrained to move with or relative to the supporting vehicle. Thus, when the peripheral jet angle is varied for control, the cushion may be prevented from tilting to seek its own equilibrium, and the peripheral jet flow behavior will be modified from that assumed for an unconstrained cushion vehicle.

Figure 4B shows a flow condition for a rectangular peripheral jet where the side-jet angles are varied asymmetrically and the cushion vehicle is constrained to hold its height and its level attitude. As before, the right jet inclination is increased and the left jet angle is reduced by an amount  $\delta\theta$ . Because of the reduced left jet angle, the equilibrium cushion pressure drops and only part of the right jet is turned outwards to sustain this pressure. The remaining part of the right jet flows under the vehicle and produces a net mass flow to the left. This splitting of the right jet is shown in the lower part of Figure 4B. Only part of the jet thickness,  $\eta t$  is turned through the angle to sustain the reduced cushion pressure. The thickness factor  $\eta$  and the net side force produced are derived in Appendix A which gives:

FIGURE 4B ASYMMETRIC PERIPHERAL JET CONTROL  
(VEHICLE CONSTRAINED)



$$\eta = 1 - \cos \theta \sin \delta \theta \quad (2)$$

$$Y = J' \left[ \frac{S_x}{S_x + S_y} \right] \cos \theta \sin \delta \theta \quad (3)$$

When the side force is non-dimensionalized by division by the initial vertical cushion force,  $Z_i$ , as shown in Appendix A, the result is:

$$\frac{Y}{Z_i} = \frac{\sin \delta \theta}{1 + \frac{S_y}{S_x} + \frac{S_y (1 + \sin \theta)}{2d \cos \theta}} \quad (4)$$

Also in Appendix A, the change in vertical force which accompanies the generation of the side force is found to be:

$$\frac{\Delta Z}{Z_i} = \frac{(\cos \delta \theta - 1) + \left[ \frac{S_y}{2d \cos \theta} \right] [\sin (\theta - \delta \theta) - \sin \theta]}{1 + \frac{S_y}{S_x} + \frac{S_y (1 + \sin \theta)}{2d \cos \theta}} \quad (5)$$

If the fore and aft jets are varied to produce an X force the equations for the rectangular peripheral jet are similar with the terms  $S_x$  and  $S_y$  being interchanged.

### B3.0 MULTI-CUSHION VEHICLE SUPPORT

The single constrained cushion relationships derived on Pages 125 - 126 and described in Section B2.2 have been incorporated into a system of equations for computing the forces and moments for a constant chord, straight swept spanloader airplane having a number of cushions distributed under the wing along the span. The multi-cushion geometry is defined in Figure 5B and the equations are developed on Pages 126 - 129. This gives the non-dimensional control forces and moments in terms of the percentages of total cushion support, the vehicle geometry, and the single constrained cushion force ratios developed in Section B2.0. The equations are:

$$\frac{X}{W} = \left[ \frac{\Sigma F_c}{W} \right] \left[ \frac{X_1}{Z_i} \cos \Lambda + \frac{Y_1}{Z_i} \sin \Lambda \right] \quad (6)$$

$$\frac{Y}{W} = \left[ \frac{\Sigma F_c}{W} \right] \left[ \frac{Y_1}{Z_i} \cos \Lambda + \frac{X_1}{Z_i} \sin \Lambda \right] \quad (7)$$

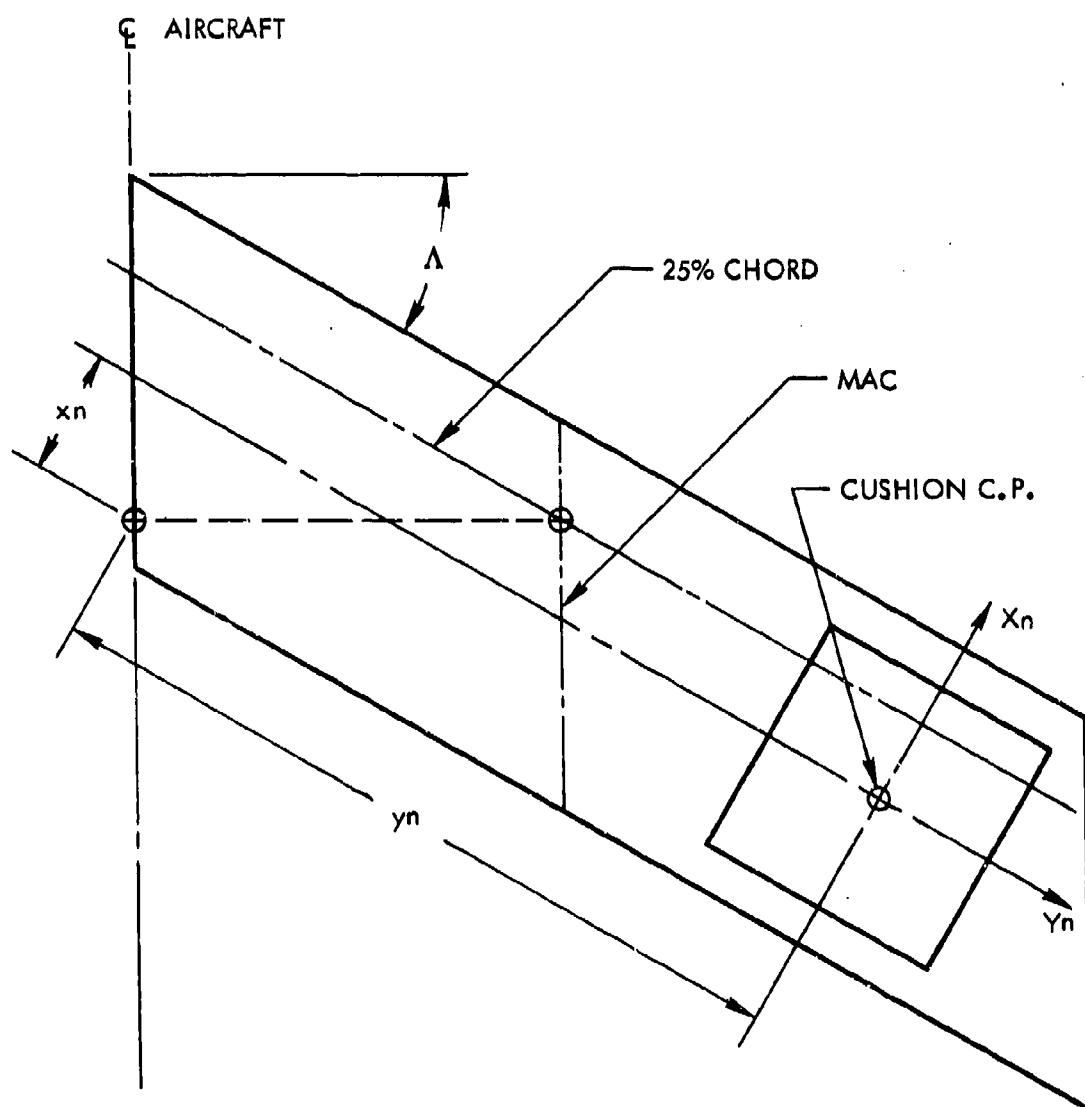
$$\frac{Z}{W} = \left[ \frac{F_c}{W} \right] \left[ \frac{\Delta Z_1}{Z_i} \right] \quad (8)$$

$$\frac{L}{Wb} = \left[ \frac{\Sigma F_c}{W} \right] \left[ \frac{\Delta Z_1}{Z_i} \right] \left[ \left( -\frac{Sy}{b} \right) \cos \Lambda + \left( \frac{X}{b} \right) \sin \Lambda \right] \quad (9)$$

$$\frac{M}{Wc} = \left[ \frac{\Sigma F_c}{W} \right] \left[ \frac{\Delta Z_1}{Z_i} \right] \left[ \left( \frac{X}{c} \right) \cos \Lambda - \left( \frac{Sy}{c} \right) \sin \Lambda \right] \quad (10)$$

$$\frac{N}{Wh} = \left[ \frac{\Sigma F_c}{W} \right] \left[ \frac{Y_1}{Z_i} \left( \frac{X}{b} \right) + \frac{X_1}{Z_i} \left( \frac{Sy}{b} \right) \right] \quad (11)$$

FIGURE 5B MULTI-CUSHION GEOMETRY



It is seen that all the forces and moments produced by peripheral jet angle control are directly proportional to the amount of total cushion support being used by the PJ-ACLS vehicle.

These equations have been incorporated in a computer program to produce control effectiveness estimates for cushion supported vehicles of the type defined by the geometry of Figure 5B. Vehicle, cushion, and peripheral jet configuration data are input to provide non-dimensional force and moment data output.

#### B4.0 SPANLOADER CONTROL EFFECTIVENESS RESULTS

The multi-cushion peripheral jet angle control program was run to produce control effectiveness results for a spanloader PJ-ACLS vehicle defined as follows:

##### Vehicle Configuration

Wing Span	330.0 Feet
Wing Chord	55.0 Feet
Wing Sweepback	40.0 Degrees

##### Cushion Configuration

Cushion Inboard Edge	30% Wing semi-span
Cushion Outboard Edge	80% Wing semi-span
Cushion Forward Edge	15% wing chord
Cushion Aft Edge	75% wing chord
Cushion + Jet Support	100% Gross weight

##### Jet Configuration

Number of Cushions/Wing	One
Jet Inward Inclination	30.0 Degrees
Jet Height Above Ground	5.0 Feet

#### B4.1 EFFECTS OF JET ANGLE DEFLECTION

A variation of jet inclination angle,  $\delta^\circ$ , from zero to 30 degrees was inserted and the effects on the vehicle forces and moments were determined. These results are presented in Figure 6B through 13B.

FIGURE 6B

SPANLOADER PERIPHERAL JET AOLSCONTROL EFFECTIVENESS OF JET ANGLE VARIATION

## VEHICLE DATA

SPAN = 330.0 FT

CHORD = 55.0 FT

SWEEP = 40.0 DEG

## CUSHION DATA

WIDTH = 30 TO 20 %GS

LENGTH = 15 TO 75 %

SUPPORT = 100.0 %GW

## JET DATA

NO/WING = 1

ANGLE = 30.0 DEG

HEIGHT = 5.0 FT

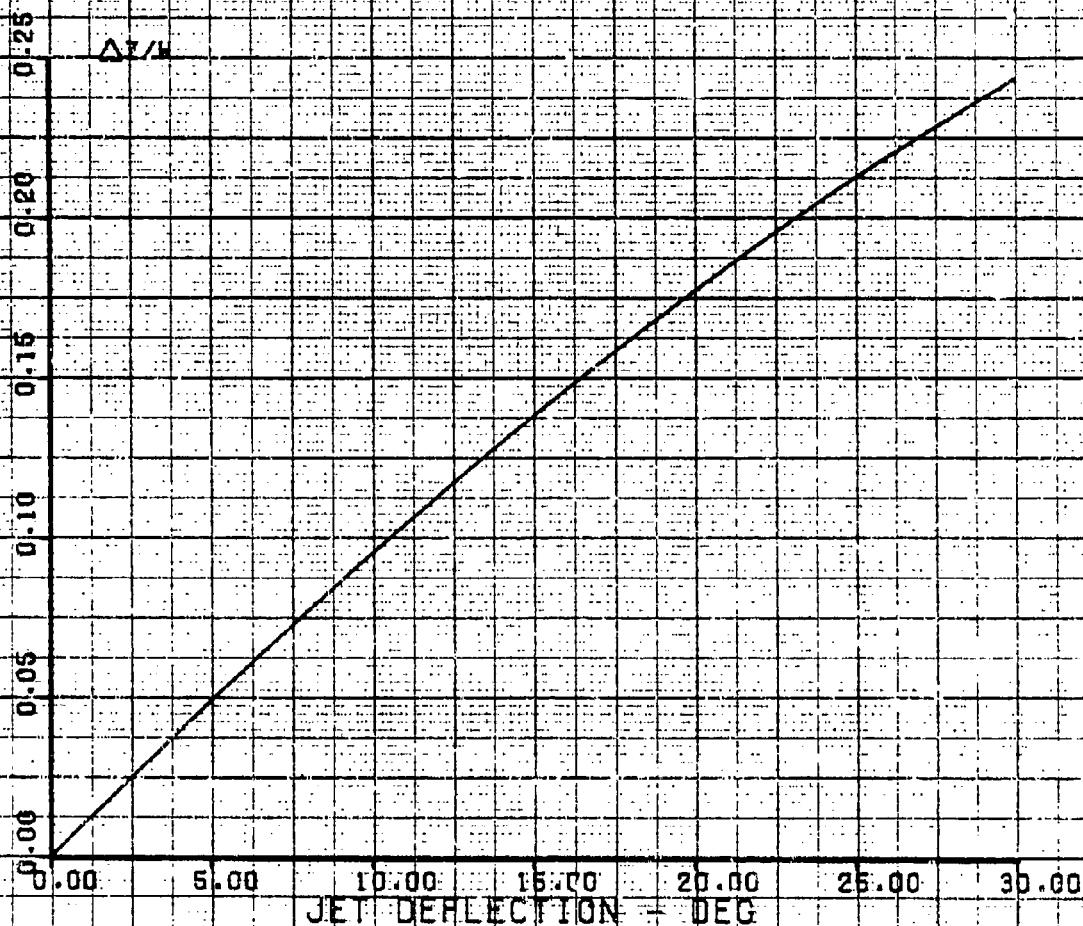




FIGURE 7B

SPANLOADER PERIPHERAL JET AOLS

## CONTROL EFFECTIVENESS OF JET ANGLE VARIATION

## VEHICLE DATA

SPAN - 330.0 FT

CHORD - 55.0 FT

SWEEP - 40.0 DEG

## CUSHION DATA

WIDTH - 80 TO 80 %SS

LENGTH - 15 TO 75 %C

SUPPORT - 100.0 %OW

## JET DATA

NO WIND - 1

ANGLE - 30.0 DEG

HEIGHT - 5.0 FT

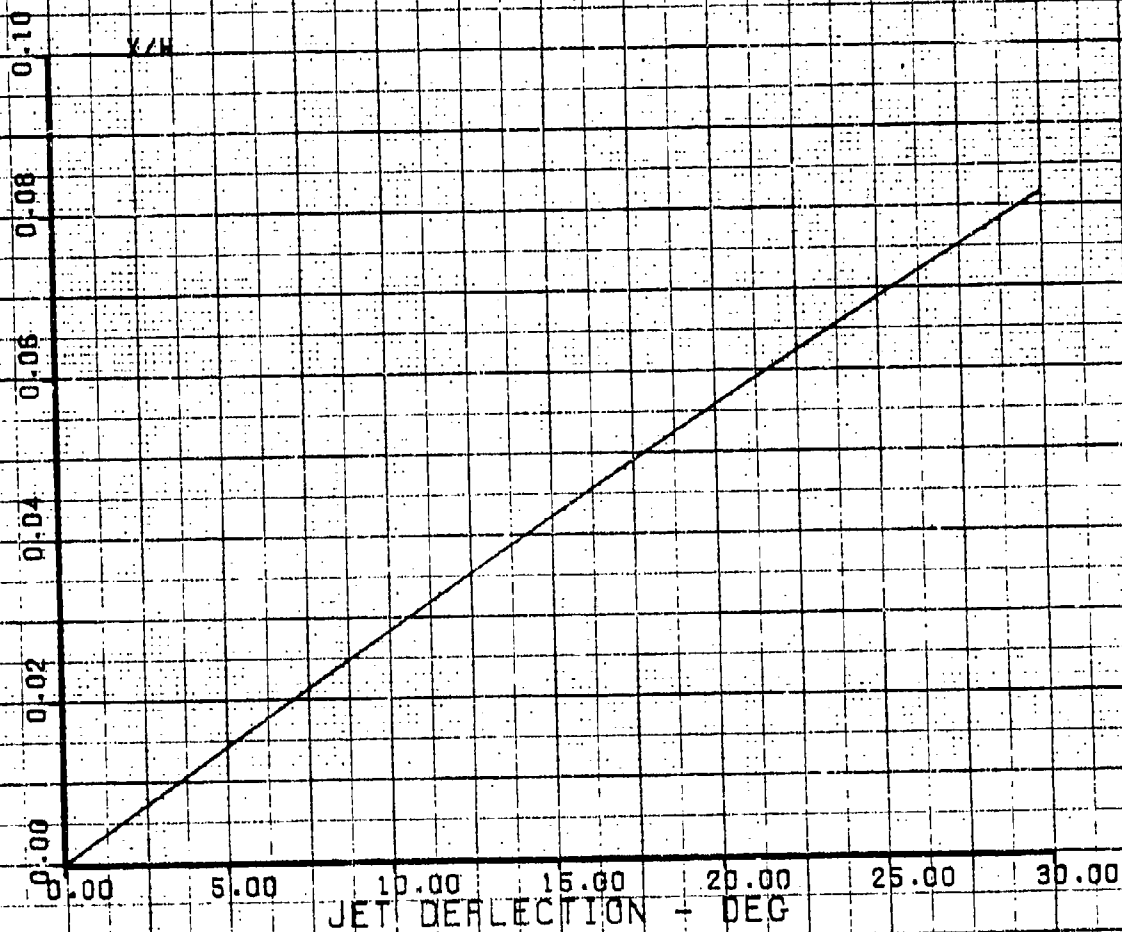


FIGURE 8B

# SPANLOADER PERIPHERAL JET ROLLS

## CONTROL EFFECTIVENESS OF JET ANGLE VARIATION

### VEHICLE DATA

SPAN = 330.0 FT

CHORD = 55.0 FT

SWEEP = 40.0 DEG

### CUSHION DATA

WIDTH = 30 TO 80 %SS

LENGTH = 15 TO 75 %C

SUPPORT = 100.0 %OW

### JET DATA

NO/WING = 1

ANGLE = 30.0 DEG

HEIGHT = 5.0 FT

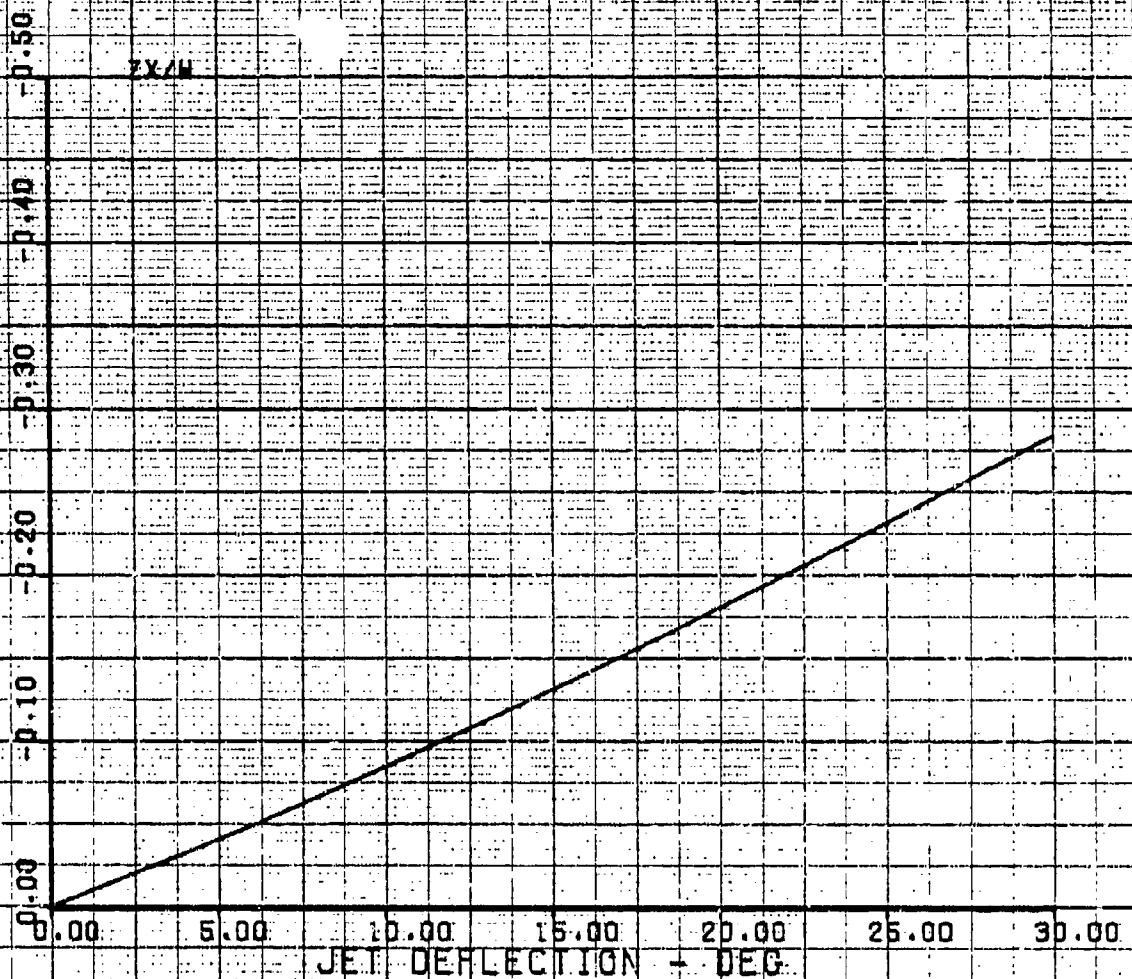


FIGURE 9B

# SPANLOADER PERIPHERAL JET ACLS

## CONTROL EFFECTIVENESS OF JET ANGLE VARIATION

### VEHICLE DATA

SPAN - 330.0 FT

CHORD - 55.0 FT

SWEEP - 40.0 DEG

### CUSHION DATA

WIDTH - 30 TO 80 %SS

LENGTH - 15 TO 75 %C

SUPPORT - 100.0 %OW

### JET DATA

NO. JET - 1

ANGLE - 50.0 DEG

HEIGHT - 5.0 FT

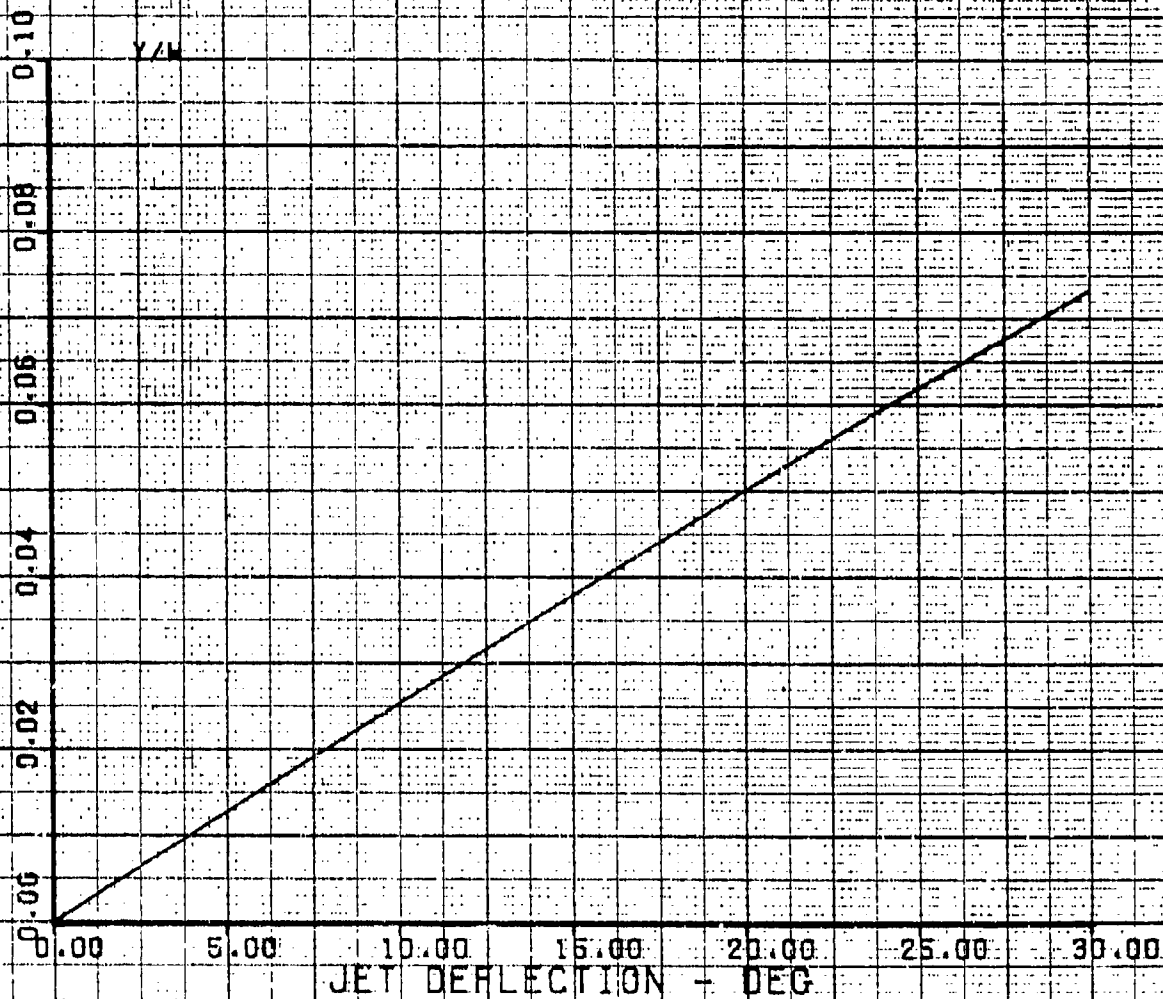


FIGURE 10B

# SPAN LOADER PERIPHERAL JET ACLS

## CONTROL EFFECTIVENESS OF JET ANGLE VARIATION

### VEHICLE DATA

SPAN - 330.0 FT

CHORD - 55.0 FT

SWEEP - 40.0 DEG

### CUSHION DATA

WIDTH - 30 TO 80 %SS

LENGTH - 15 TO 75 %C

SUPPORT - 100.0 %GW

### JET DATA

NO/WING - 1

ANGLE - 30.0 DEG

HEIGHT - 5.0 FT

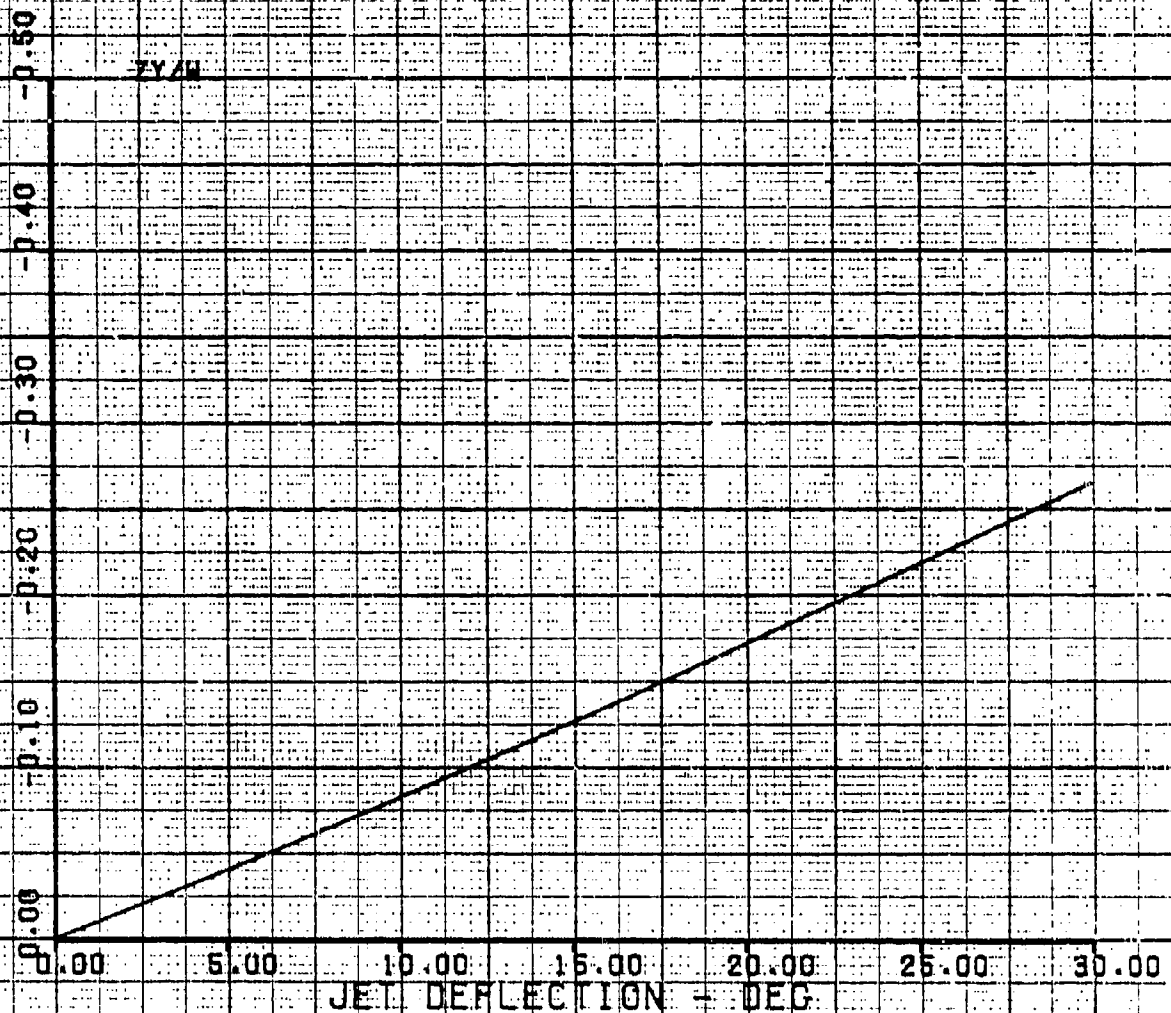


FIGURE 11B

## SPANLOADER PERIPHERAL JET ACS

## CONTROL EFFECTIVENESS OF JET ANGLE VARIATION

## VEHICLE DATA

SPAN - 330.0 FT

CHORD - 55.0 FT

SWEEP - 40.0 DEG

## CUSHION DATA

WIDTH - 80 TO 80 %SS

LENGTH - 15 TO 75 %C

SUPPORT - 100.0 %GW

## JET DATA

NO/WIND - 1

ANGLE - 30.0 DEG

HEIGHT - 5.0 FT

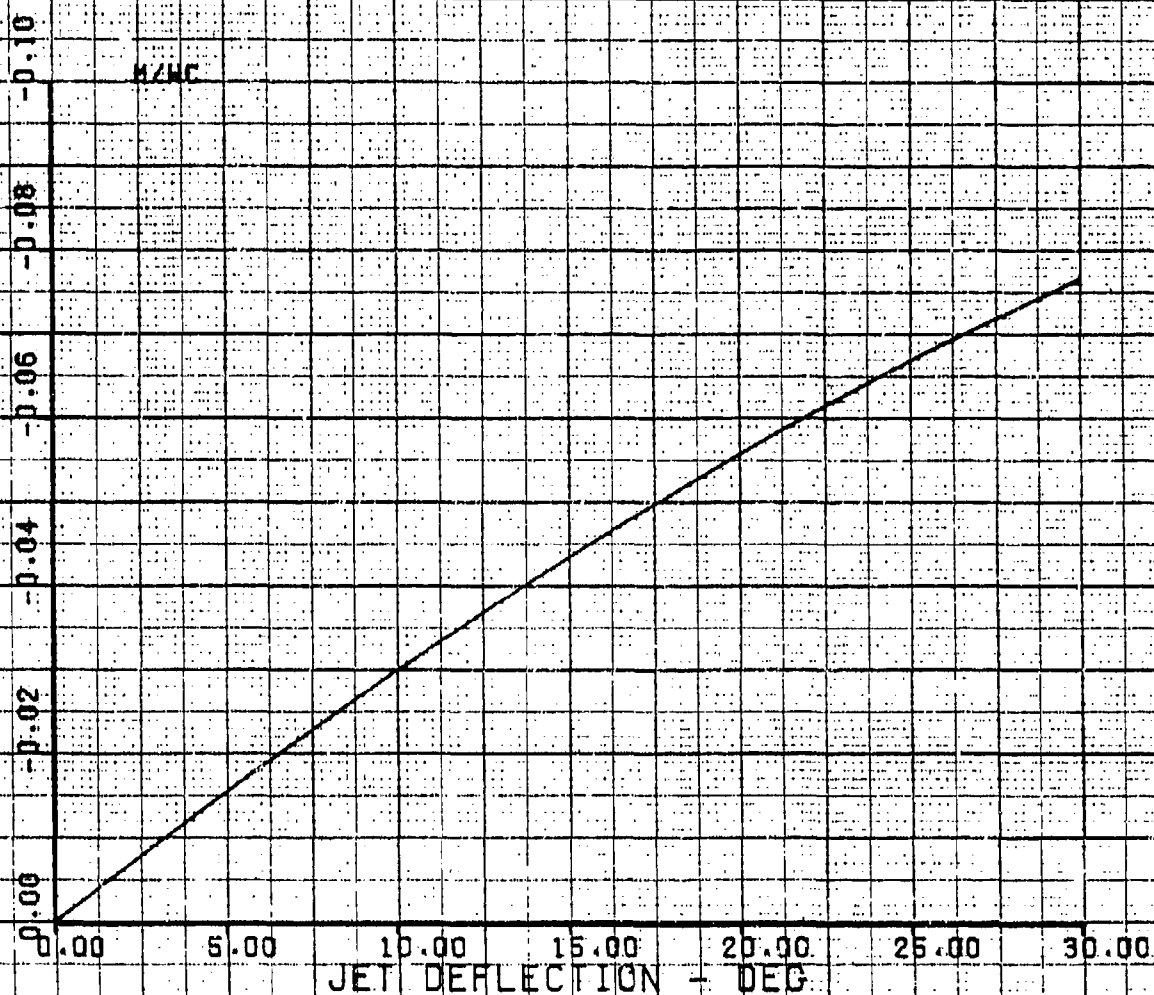


FIGURE 12B

## SPAN LOADER PERIPHERAL JET AOLS

## CONTROL EFFECTIVENESS OF JET ANGLE VARIATION

## VEHICLE DATA

SPAN - 330.0 FT

CHORD - 55.0 FT

SWEEP - 10.0 DEG

## CUSHION DATA

WIDTH - 80 TO 80 %SS

LENGTH - 15 TO 75 %C

SUPPORT - 100.0 %GW

## JET DATA

NO/WING - 1

ANGLE - 90.0 DEG

HEIGHT - 5.0 FT

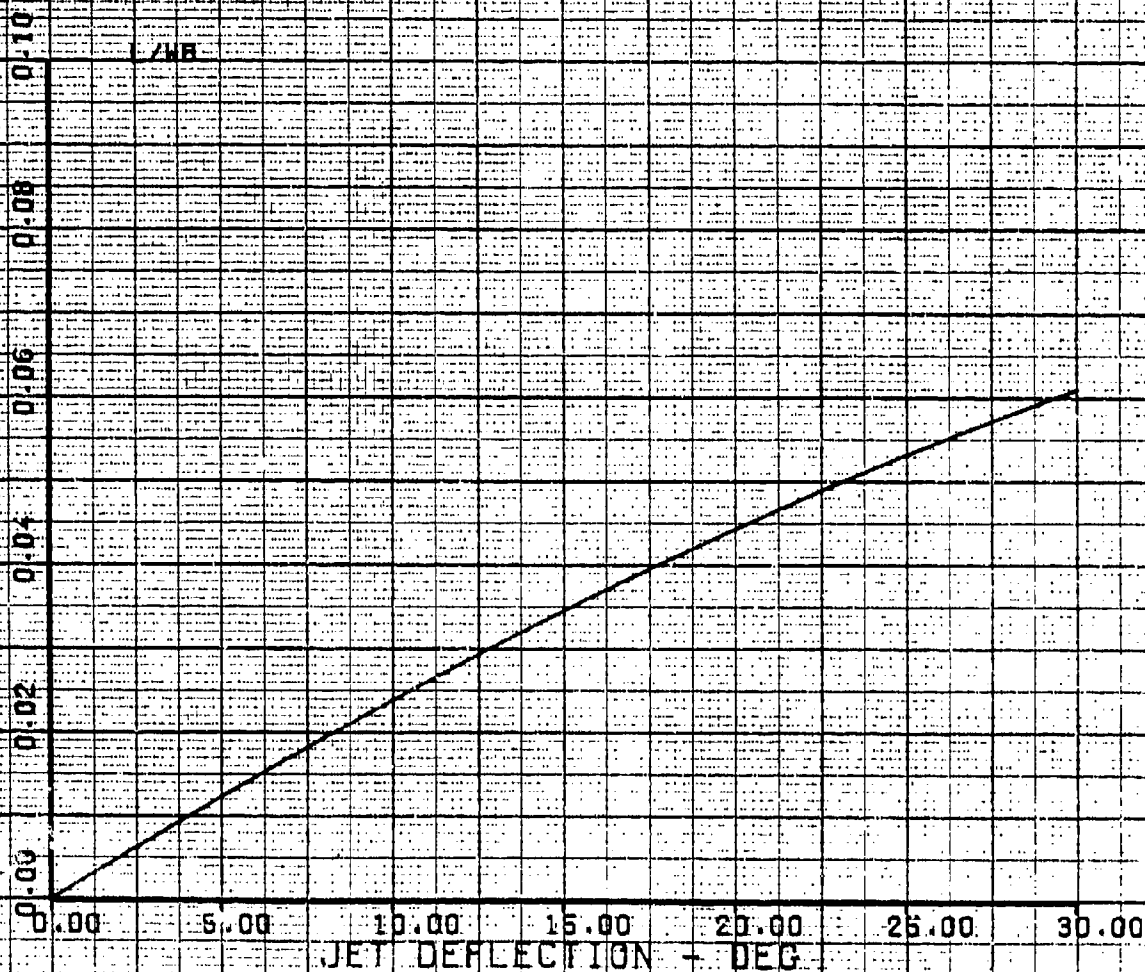


FIGURE 13B

# SPANLOADER PERIPHERAL JET AOLS

## CONTROL EFFECTIVENESS OF JET ANGLE VARIATION

### VEHICLE DATA

SPAN - 330.0 FT

CHORD - 55.0 FT

SWEEP - 40.0 DEG

### CUSHION DATA

WIDTH - 30 TO 80 %SS

LENGTH - 15 TO 75 %C

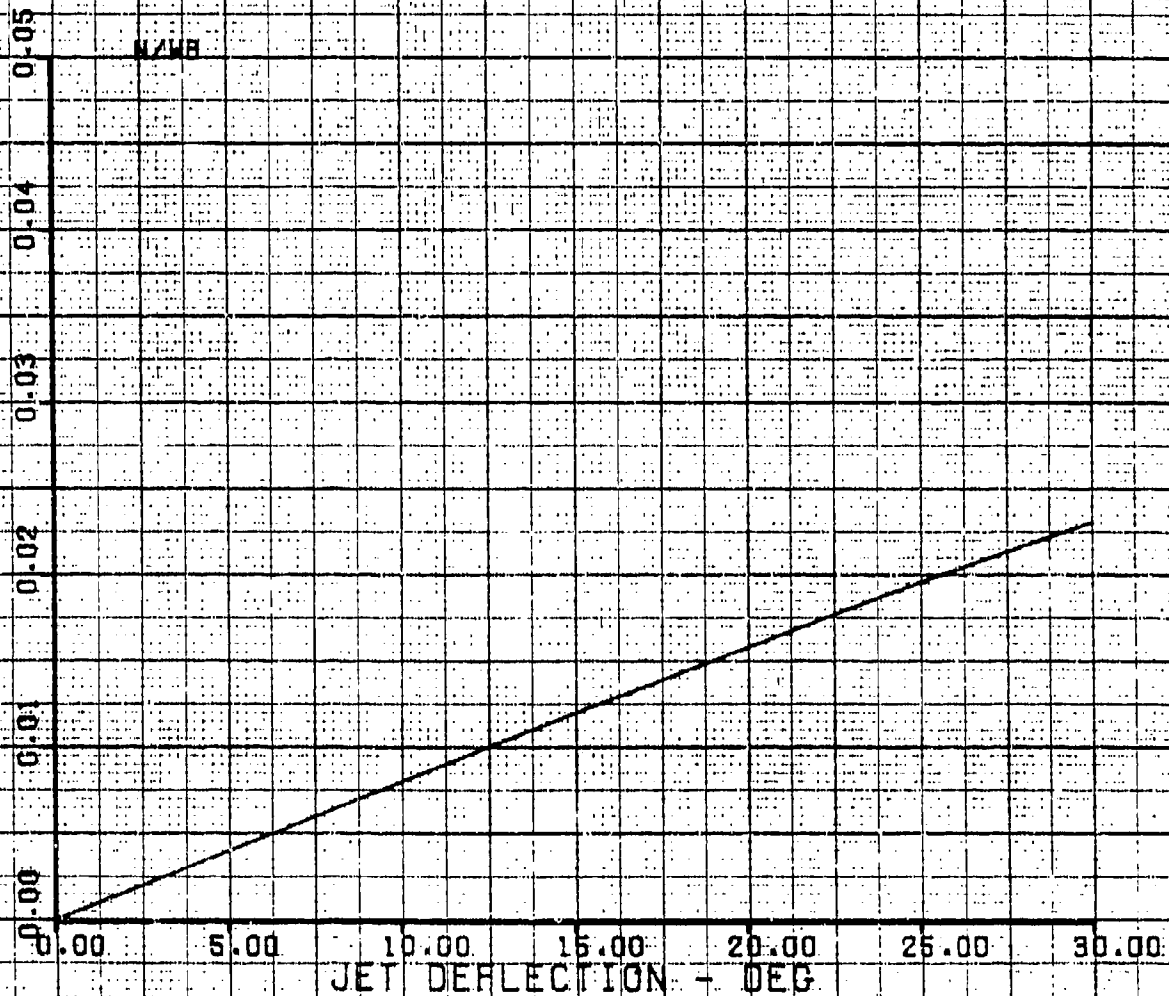
SUPPORT - 100.0 %OM

### JET DATA

NO/MINO - 1

ANGLE - 30.0 DEG

HEIGHT - 5.0 FT



#### B4.1.1 Vertical Force Change

The change of vertical force divided by the vehicle weight,  $\Delta Z/W$ , is plotted against jet deflection angle in Figure 6B. This shows that, when the jets are rotated inwards, the vertical force increases and reaches 24.4% of the vehicle weight for a jet deflection of 30 degrees.

#### B4.1.2 Forward Force

Figure 7B presents the forward force divided by vehicle weight,  $X/W$ , versus jet deflection angle. In this case the jet angle is modulated asymmetrically to produce the maximum effect in the X direction. It is seen that, for a jet deflection of 30 degrees, the X force to weight ratio is only about 8.1%. Figure 8B shows the change of vertical force caused by control action to produce the X force just discussed. This shows that the generation of the 8.1% X force/weight ratio caused a 28.5% loss of vertical force.

#### B4.1.3 Side Force

The side-force/weight ratio,  $Y/W$ , is presented in Figure 9B. Only 7.3% is produced for a jet deflection of 30 degrees. Figure 10B indicates that the control deflection to produce this side force ratio resulted in a loss of vertical force equivalent to 26.5% of the vehicle weight.

#### B4.1.4 Pitching Moment

The pitching moment about the quarter chord of the MAC is presented in Figure 11B. The moment divided by the product of the vehicle weight and the mean aerodynamic chord reaches a value of -0.077 for a 30-degree deflection angle.



#### B4.1.5 Rolling Moment

Rolling moment about the vehicle center-line non-dimensionalized by weight times span is shown in Figure 12B. The value reached 0.061 for a 30-degree deflection angle.

#### B4.1.6 Yawing Moment

Yawing moment about the quarter chord of the MAC divided by weight times span is presented in Figure 13B. This shows a value of 0.023 for a jet deflection of 30 degrees.

#### B4.1.7 Summary of Jet Angle Deflection Effect

The analysis indicates that jet angle deflection can produce significant changes of lift, pitching moment, and rolling moment. The effect on the in-plane forces X and Y is very small and the yawing moment, which is derived from a combination of X and Y forces, is also relatively small.

#### B4.2 THE EFFECTS OF VEHICLE HEIGHT (100% CUSHION SUPPORT)

The non-dimensional control forces and moments due to jet angle deflection are estimated for a range of vehicle heights from zero to 45 feet. In this case, instead of varying the incremental jet angle from zero to 30 degrees, only the value corresponding to the 30-degree control deflection is estimated. It is seen from Figures 6B through 13B that each control force and moment ratio increases smoothly with jet deflection angle, so the value at any given angle can be taken as a measure of control effectiveness. The results shown in Figures 14B and 15B apply to a situation where, at each height, the cushion and jet support are together equal to the total vehicle weight. This type of presentation gives control effectiveness information for vehicles designed to "hover" at the stated height.

FIGURE 148

## SPAN LOADER PERIPHERAL JET ACLS

## LONGITUDINAL DATA

## VEHICLE DATA

SPAN = 380.0 FT

CHORD = 55.0 FT

SWEEP = 40.0 DEG

## CUSHION DATA

WIDTH = 30 TO 80 %S

LENGTH = 15 TO 75 %C

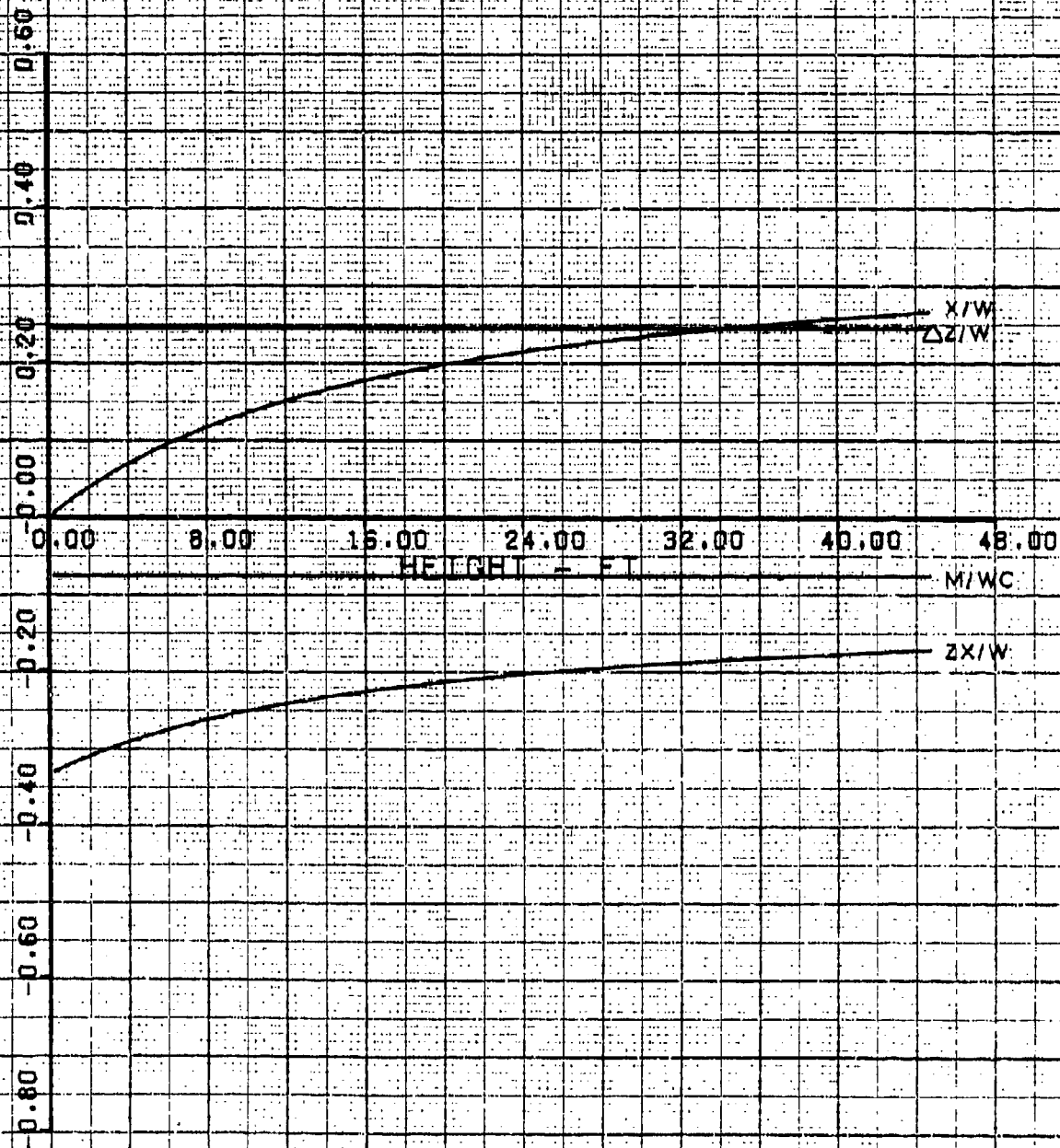
SUPPORT = 100.0 %W

## JET DATA

NO/WING = 1

ANGLE = 30.0 DEG

DEF ANG = 30 DEG



14 AUG 78 18:48:40

FIGURE 15B

## SPANLOADER PERIPHERAL JET ACLS

## LATERAL DATA

## VEHICLE DATA

SPAN = 380.0 FT

CHORD = 55.0 FT

SWEEP = 40.0 DEG

## CUSHION DATA

WIDTH = 80 TO 80 %SS

LENGTH = 15 TO 75 %C

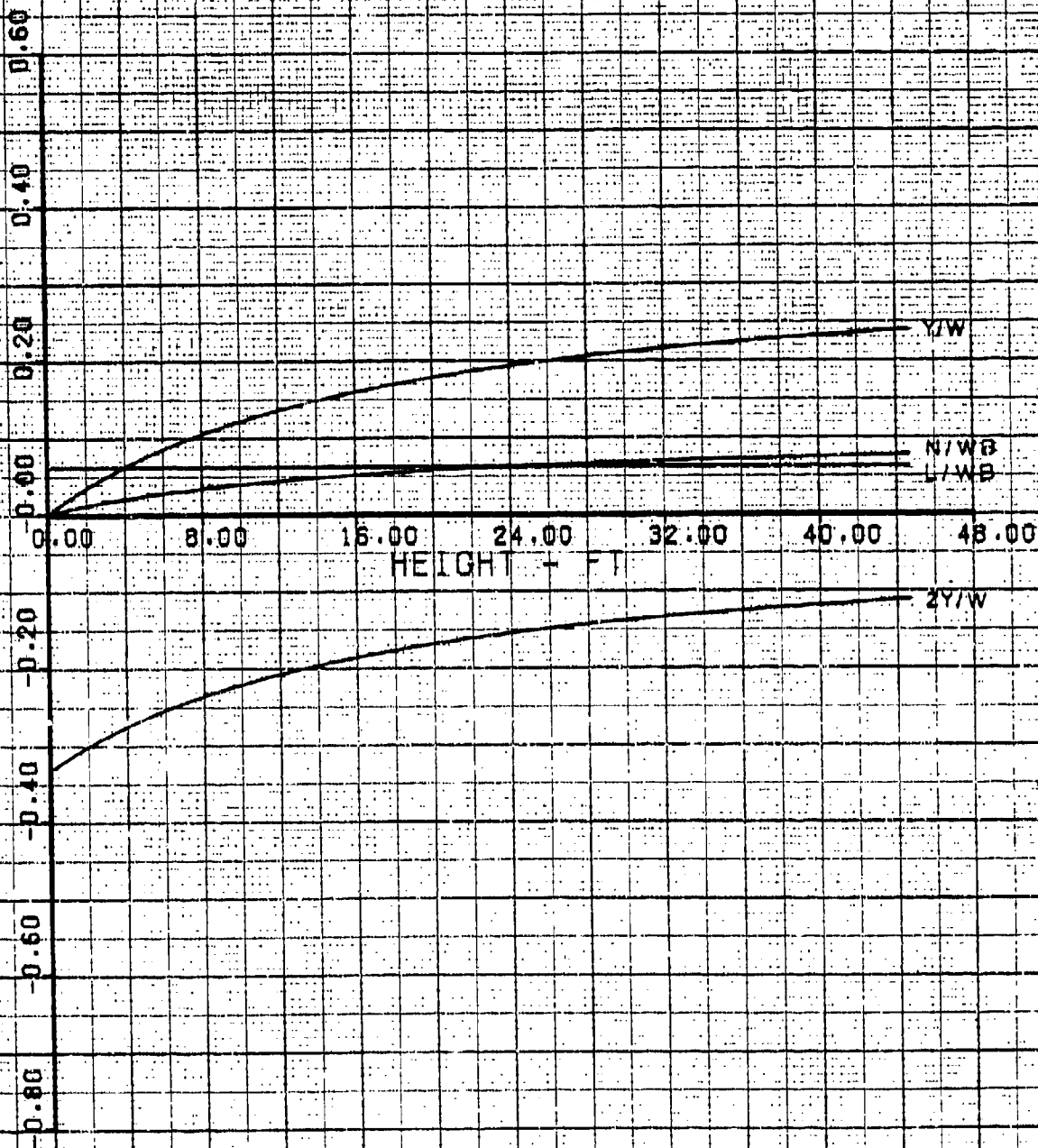
SUPPORT = 100.0 %DW

## JET DATA

NO/WING = 1

ANGLE = 30.0 DEG

DEF ANG = 30 DEG



#### B4.2.1 Longitudinal Control Effectiveness

Information on the longitudinal control force and moment ratios is presented in Figure 14B.

**Vertical Force** - The non-dimensional vertical force  $Z/W$  due to the given jet deflection does not vary with height. This is a direct consequence of the Barratt theory, the 100% support constraint, and the fact that the initial jet inclination and the jet pressure,  $p_j$ , are being held constant as height varies. The constant support and constant  $p_j$  define a fixed value of  $p_c/p_j$ . This and the Barratt theory define a fixed value of  $(t/d)(1 + \sin \theta)$  and, since  $\theta$  is fixed, the jet thickness must increase with height,  $d$ . So, under the constraints imposed, the same point on the Barratt  $p_c/p_j$  curve applies throughout the height range in Figures 14B and 15B. Thus the effect of varying jet deflection on the vertical cushion force is the same at all heights.

**Pitching Moment** - The non-dimensional pitching moment  $M/Wc$  is directly proportional to  $Z/W$  and likewise does not change with height when the support level is constrained.

**Forward Force** - The non-dimensional forward force  $X/W$  due to the control deflection increases with increasing height. To support the vehicle at large values of height with a fixed initial jet angle, the jet reaction must increase. Thus, when the jet is rotated for control, a larger value of the in-plane X force results. The value falls to zero at zero height because, under the stated constraints, a jet of zero thickness (i.e. zero reaction) can sustain the cushion pressure  $p_c$  at zero height.

**Loss of Lift Due to X Force** - The non-dimensional loss of lift due to generating the X force (i.e.  $ZX/W$ ), reduces as height is increased. Since the X force itself is increasing, the cross coupling between the in-plane and vertical force changes is reduced significantly as vehicle height increases. At large values of height a smaller proportion of the support is generated by the cushion since the jet reaction is greater. So, the loss of cushion pressure due to jet rotation is less, and the adverse cross coupling is reduced.

#### B4.2.2 Lateral Control Effectiveness

Information on the lateral control force and moment ratios is presented in Figure 15B.

**Rolling Moment** - The rolling moment ratio  $L/WB$  does not vary with the height under the stated support constraints. It is directly proportioned to  $Z/W$  which was discussed in Paragraph B4.2.1.

**Side Force** - The variation of the non-dimensional side force  $Y/W$  with height is similar to the variation of  $X/W$  discussed in Section B4.2.1.

**Yawing Moment** - The non-dimensional yawing moment  $N/WB$  varies with height like  $X/W$  and  $Y/W$  because it is a linear function of those two in-plane non-dimensional forces.

**Loss of Lift Due to Y Force** - The non-dimensional loss of lift due to generating the Y force (i.e.  $ZY/W$ ), varies like  $ZX/W$  which was discussed in Section B4.2.1.

#### B4.2.3 Summary of Vehicle Height Effect

This section of the analysis has shown that, for vehicles designed to hover at large heights, the increased jet reactions lead to improved in-plane force and yawing moments for a given peripheral jet control deflection. The vertical force control remains the same and the adverse coupling between asymmetric jet control and vertical force is reduced as height is increased.

#### B4.3 EFFECT OF HEIGHT (VARYING SUPPORT)

An analysis was performed to determine the control effectiveness of jet rotation over a range of heights when the jet reaction levels remain constant. In this case, the variation of vehicle support with height follows the Barratt  $p_c/p_i$  curve. So, the support decreases as height above the ground is increased. The longitudinal and lateral forces and moments due to a 30-degree incremental jet deflection are presented in Figure 16B and 17B. The vehicle support is 100% at a height of 5 feet.

FIGURE 16B

## SPAN LOADER PERIPHERAL JET ACES

## LONGITUDINAL DATA

## VEHICLE DATA

SPAN = 350.0 FT

CHORD = 55.0 FT

SHEEP = 40.0 DEG

## CUSHION DATA

WIDTH = 80 TO 80 %SS

LENGTH = 15 TO 75 %C

SUPPORT = VARIABLE %GW

## JET DATA

NO/WING = 1

ANGLE = 30.0 DEG

DEF ANG = 30 DEG

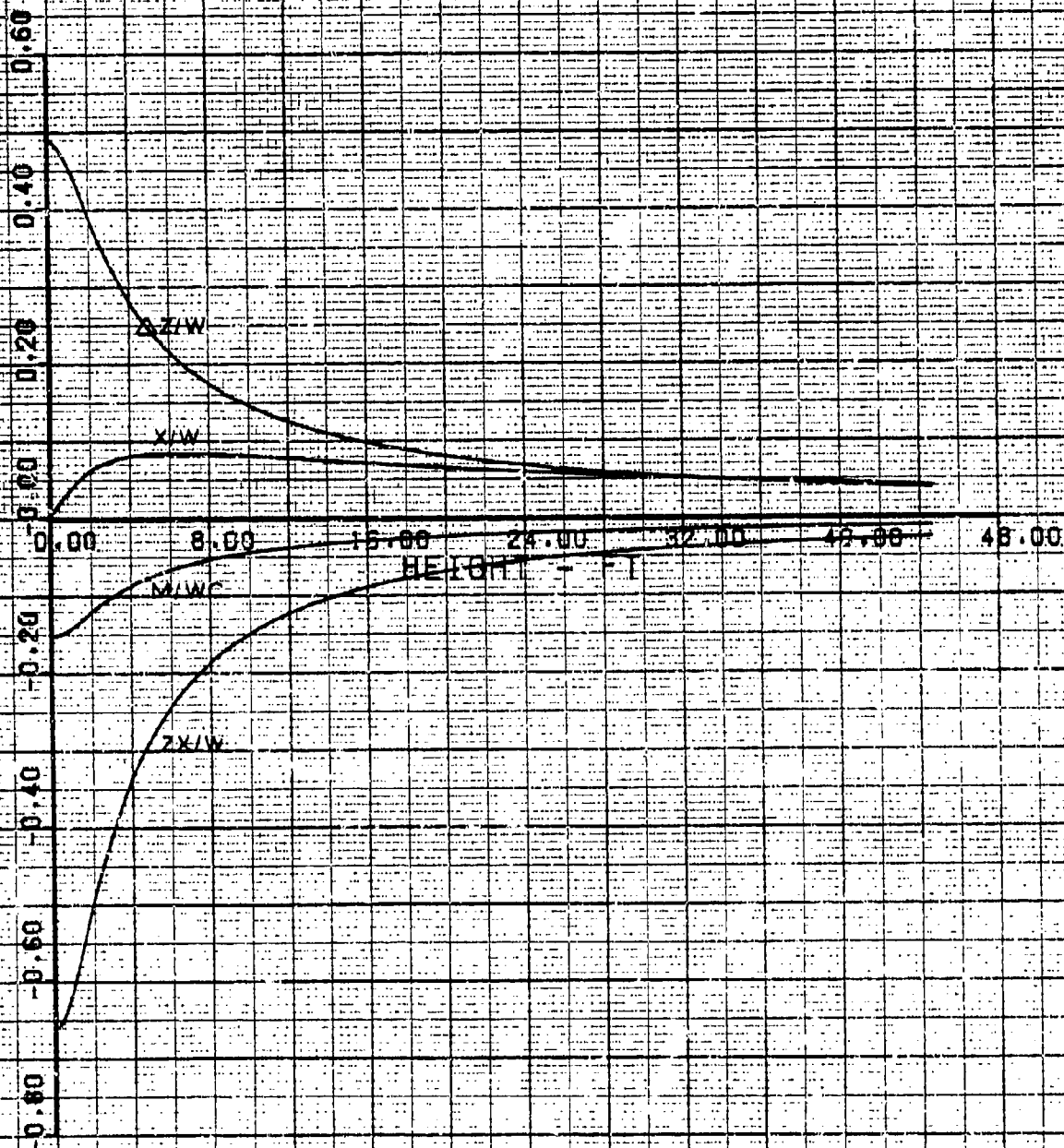


FIGURE 17B

## SPAN CATER PERIPHERA JET ACLS

## LATERAL DATA

## VEHICLE DATA

SPAN = 380.0 FT

CHORD = 55.0 FT

SWEEP = 40.0 DEG

## CUSHION DATA

WIDTH = 30 TO 80 %SS

LENGTH = 15 TO 75 %C

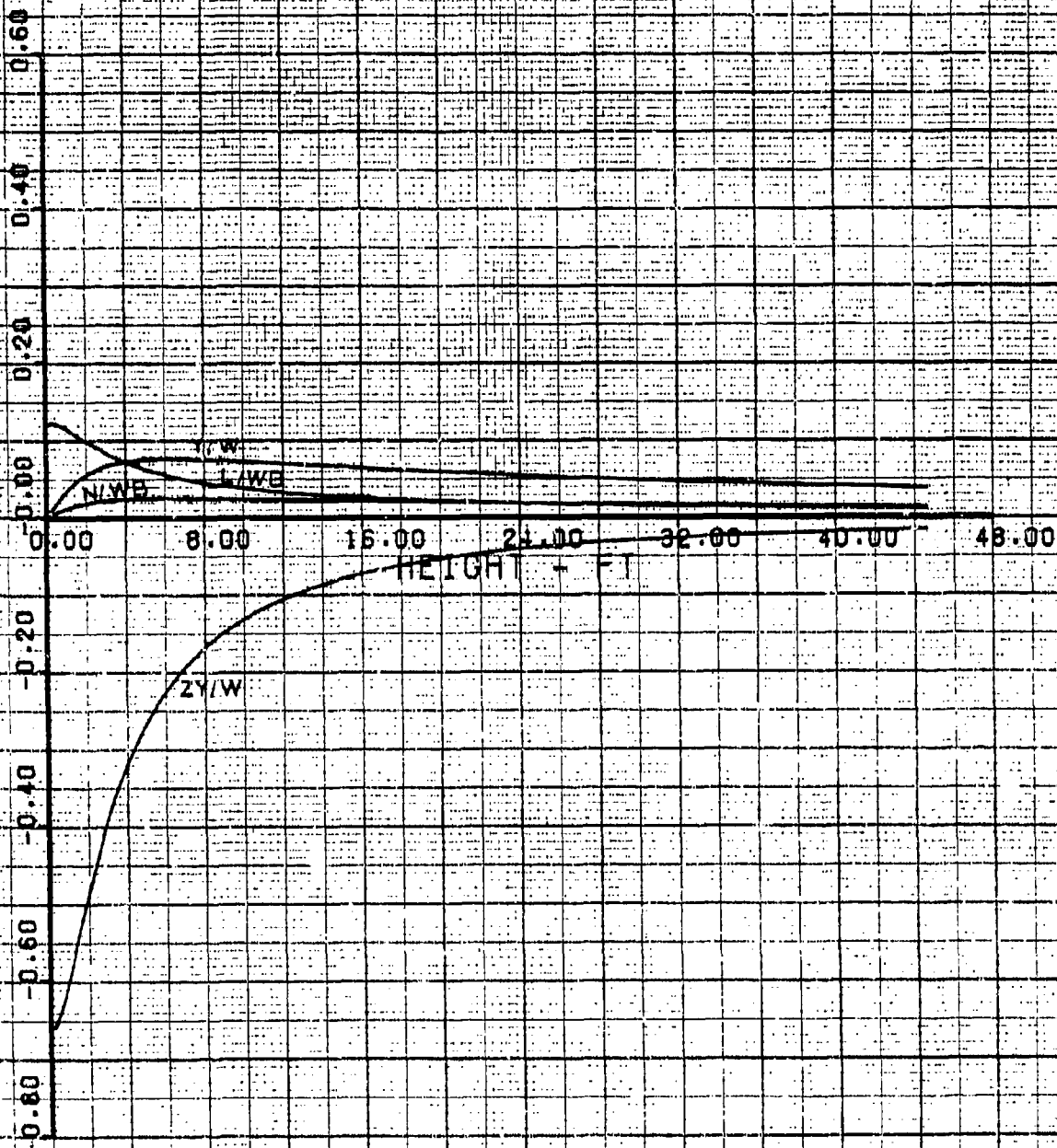
SUPPORT = VARIABLE %GW

## JET DATA

NO. JETTING = 1

ANGLE = 30.0 DEG

DEL. ANG = 30 DEG



It is seen that the vertical force ratio  $Z/W$  has a shape similar to the Barratt  $p_c/p_i$  curve. As height is reduced the value increases because the percentage of cushion support to the vehicle increases. Other curves which follow this form are the pitching and rolling moments  $M/WC$  and  $L/WB$ . These are both directly proportioned to  $Z/W$ . The cross coupling terms  $ZX/W$  and  $ZY/W$  also follow the Barratt shape because they represent a loss of cushion lift which increases as the percentage of total cushion support increases.

The in-plane forces  $X/W$  and  $Y/W$  together with the yawing moment  $N/WB$  all follow a similar form as height is varied. Their shape is a consequence of factoring the 100% support values of Figures 14B and 15B by the varying percent support derived from the Barratt curve. The significant fact is that these in-plane forces and moments do not change much with variation of height above the height at which the support is 100% (in this case 5 feet).

#### B4.4 EFFECT OF INITIAL JET INCLINATION

This effect was explored by repeating the analysis for initial jet angles of 20 and 40 degrees. The results are presented in Figures 18B through 25B. Comparison with the corresponding data in Figures 14B through 17B indicates that all the trends are similar and no significant difference in jet deflection control effectiveness results in this range of initial jet angles from 20 to 40 degrees.



FIGURE 18B

## SPAN LOADER PERIPHERAL JET ACOLS

## LONGITUDINAL DATA

## VEHICLE DATA

SPAN = 380.0 FT

CHORD = 55.0 FT

SWEEP = 40.0 DEG

## CUSHION DATA

WIDTH = 80 TO 80 X65

LENGTH = 15 TO 75 %C

SUPPORT = 100.0 %W

## JET DATA

NO/WING = 1

ANGLE = 20.0 DEG

DEF ANG = 30.0 DEG

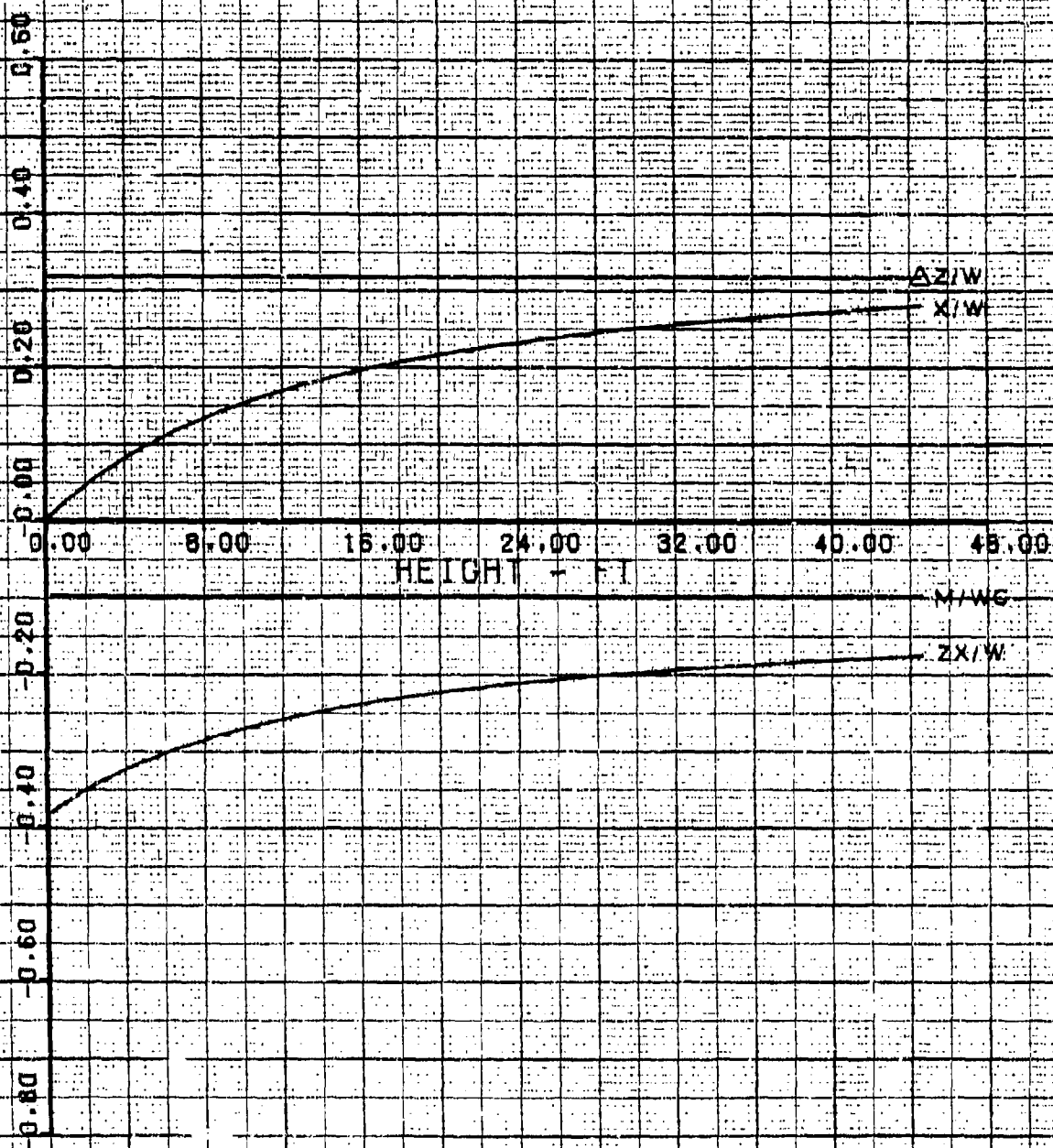


FIGURE 19B

## SPAN LOADER PERIPHERA JET ACIS

## LATERAL DATA

## VEHICLE DATA

SPAN = 330.0 FT

CHORD = 55.0 FT

SWEEP = 40.0 DEG

## CUSHION DATA

WIDTH = 30 TO 80 %SS

LENGTH = 15 TO 75 %C

SUPPORT = 100.0 %GW

## JET DATA

NO/WING = 1

ANGLE = 20.0 DEG

DEF ANG = 30 DEG

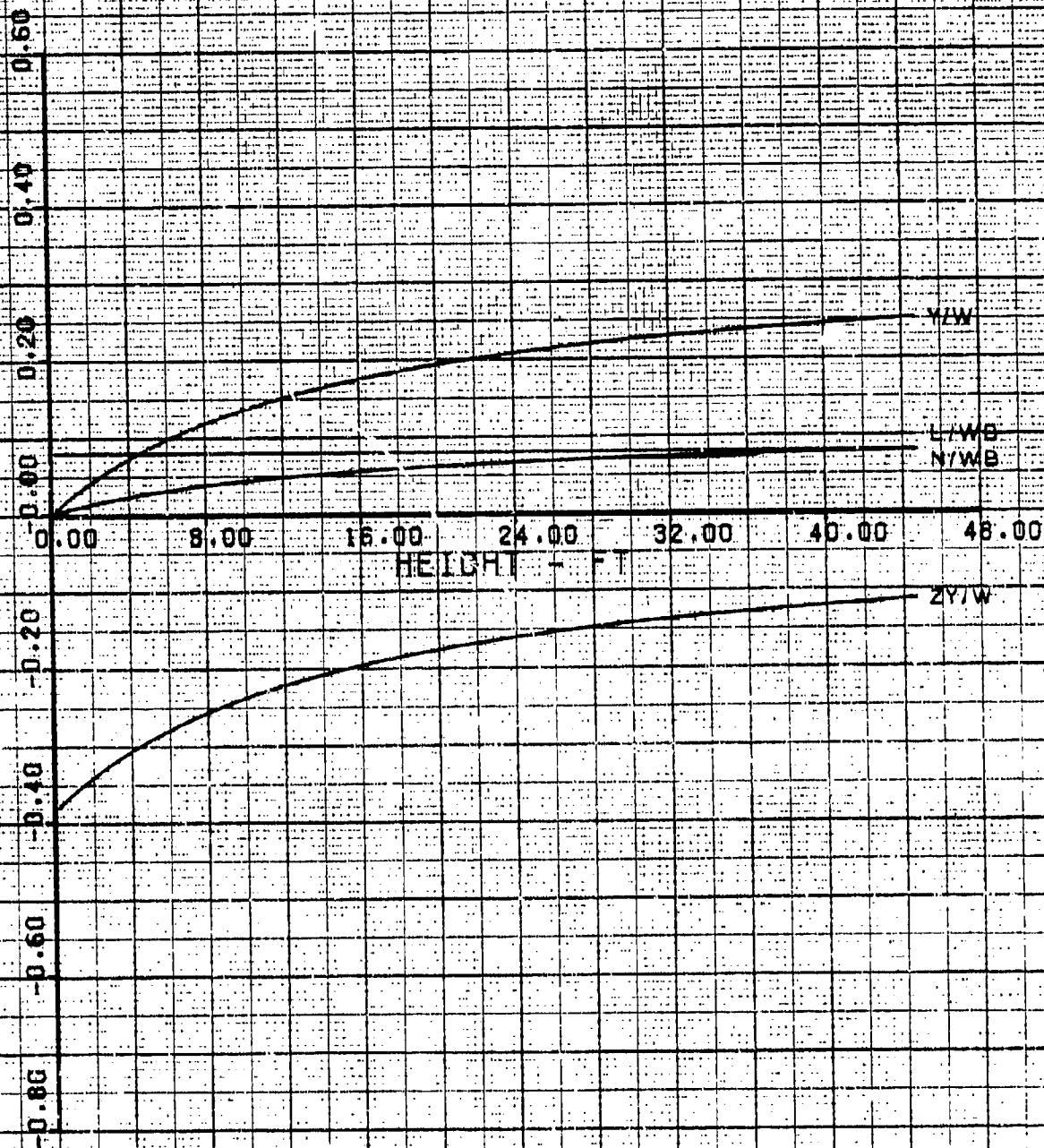


FIGURE 20B

## SPAN LOADER PERIPHERAL JET ACIS

## LONGITUDINAL DATA

## VEHICLE DATA

SPAN = 330.0 FT

CHORD = 55.0 FT

SWEEP = 40.0 DEG

## CUSHION DATA

WIDTH = 80 TO 80 %SS

LENGTH = 16 TO 75 %C

SUPPORT = VARIABLE %GW

## JET DATA

NO/WING = 1

ANGLE = 20.0 DEG

DEF ANG = 30 DEG

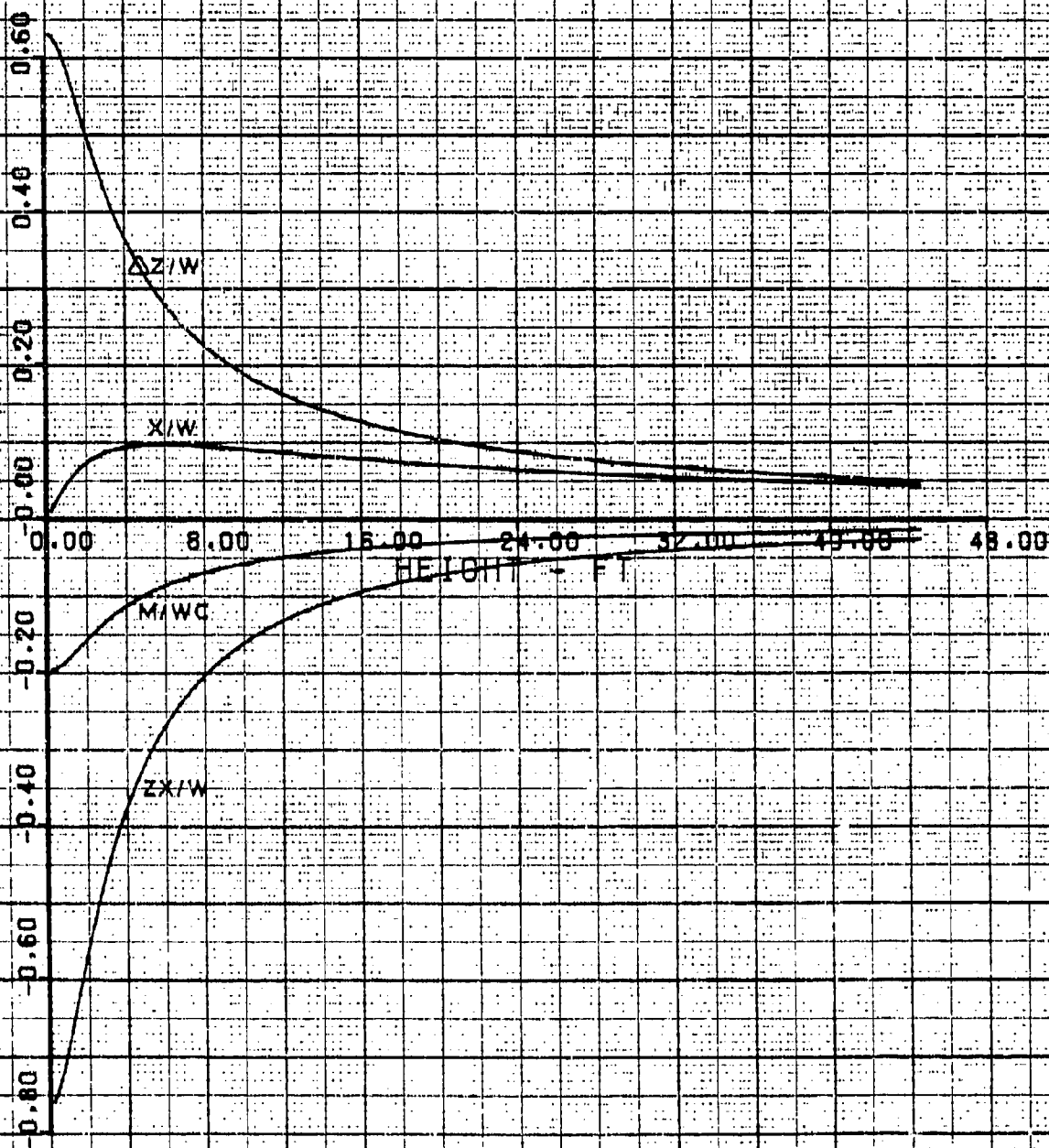


FIGURE 21B

## SPAN LOADER PERIPHERA JET ACES

## LATERAL DATA

## VEHICLE DATA

SPAN = 330.0 FT

CHORD = 66.0 FT

SWEEP = 40.0 DEG

## CURSION DATA

WIDTH = 30 TO 80 %SS

LENGTH = 15 TO 75 %C

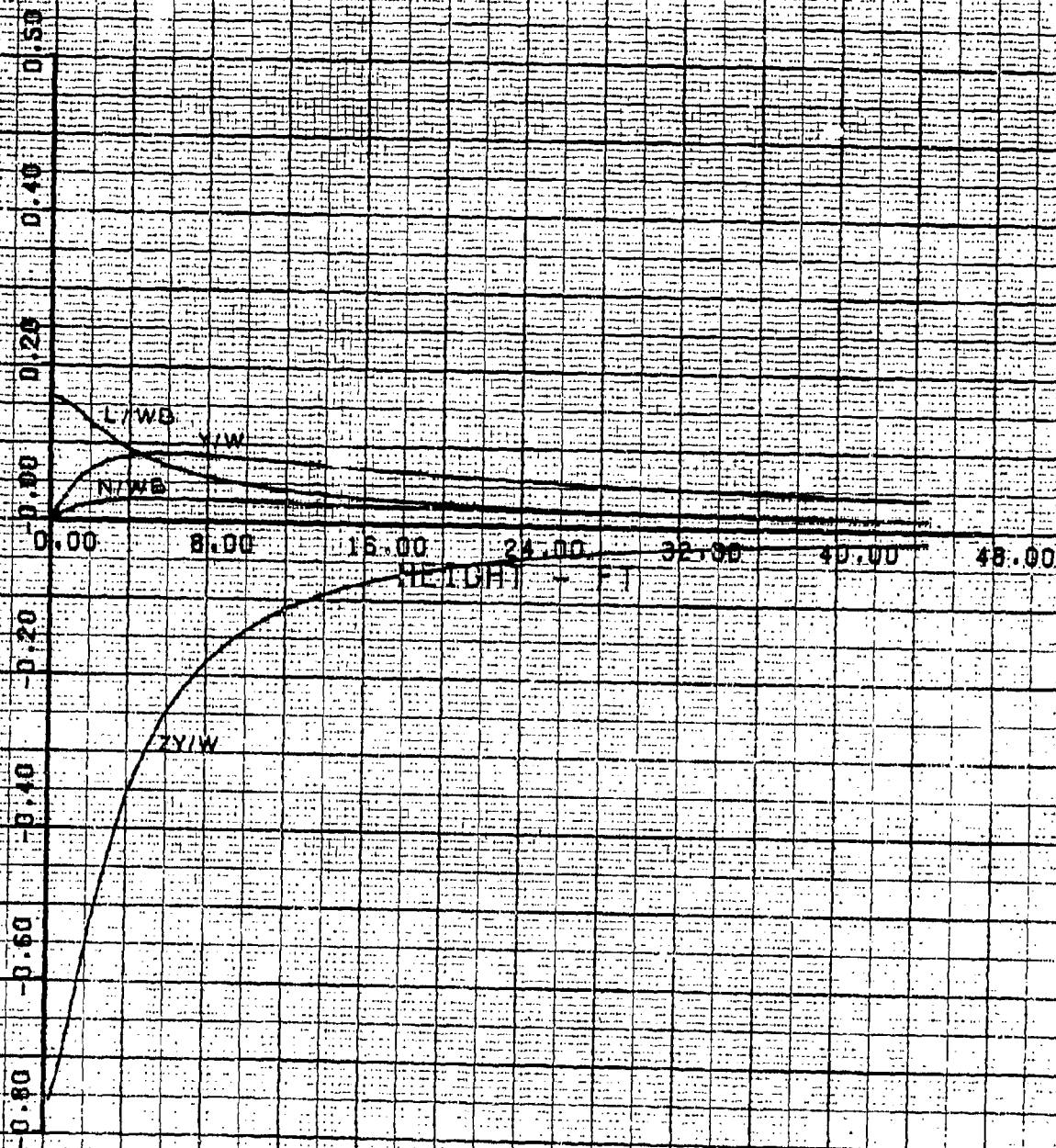
SUPPORT = VARIABLE %OW

## JET DATA

NO/WING = 1

ANGLE = 20.0 DEG

DEL ANG = 30 DEG



14 AUG 79 18:53:00

FIGURE 22B

## SPAN LOADER PERIPHERAL JET ACIS

## LONGITUDINAL DATA

## VEHICLE DATA

SPAN = 330.0 FT

CHORD = 55.0 FT

SWEEP = 40.0 DEG

## CUSHION DATA

WIDTH = 80 TO 80 %SS

LENGTH = 15 TO 75 %C

SUPPORT = 100.0 %DW

## JET DATA

NO/WING = 1

ANGLE = 40.0 DEG

DEL ANG = 30 DEG

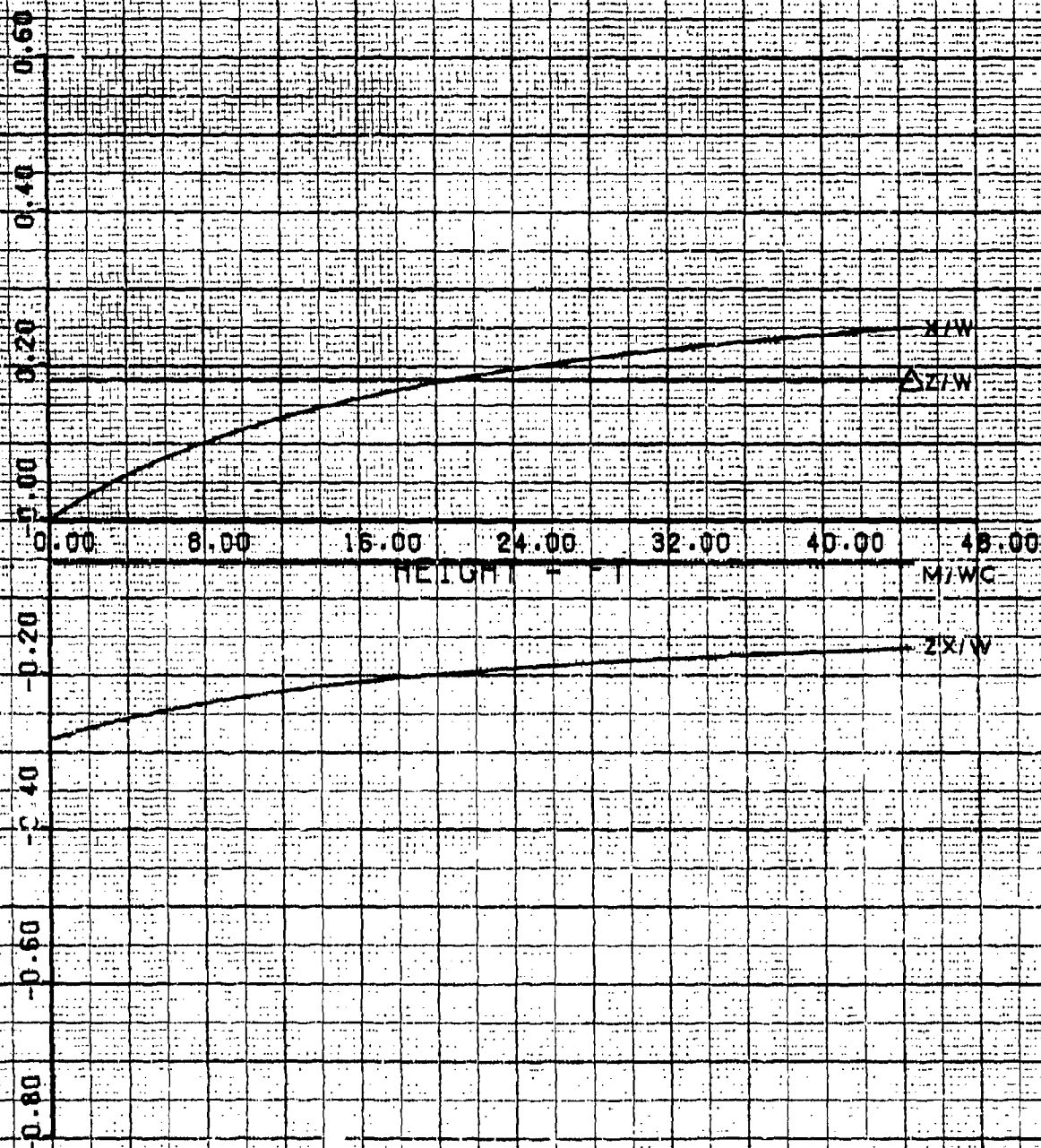


FIGURE 23B

## SPAN LOADER PERIPHERAL JET ACLS

## LATERAL DATA

## VEHICLE DATA

SPAN = 380.0 FT

CHORD = 55.0 FT

SWEEP = 40.0 DEG

## CUSHION DATA

WIDTH = 30 TO 80 %S

LENGTH = 15 TO 75 %C

SUPPORT = 100.0 %ZW

## JET DATA

NO/WING = 1

ANGLE = 40.0 DEG

DEL ANG = 30 DEG

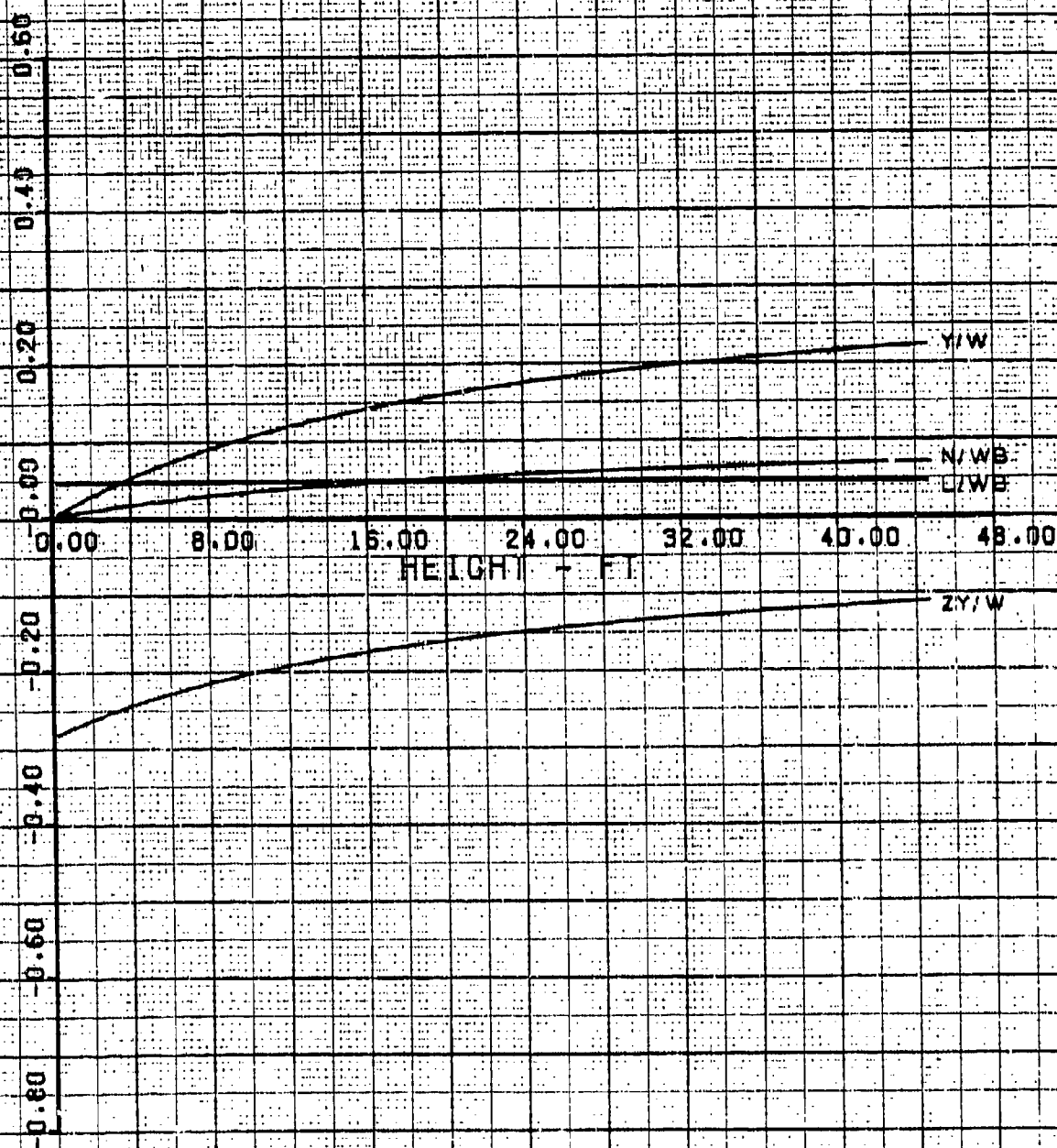




FIGURE 24B

## SPAN LADER PERIPHERAL JET ACLS

## LONGITUDINAL DATA

## VEHICLE DATA

SPAN = 380.0 FT

CHORD = 55.0 FT

SWEEP = 40.0 DEG

## CUSHION DATA

WIDTH = 30 TO 80 %SS

LENGTH = 15 TO 75 %C

SUPPORT = VARIABLE %OW

## JET DATA

NO/WIND = 1

ANGLE = 40.0 DEG

DEL ANG = 30 DEG

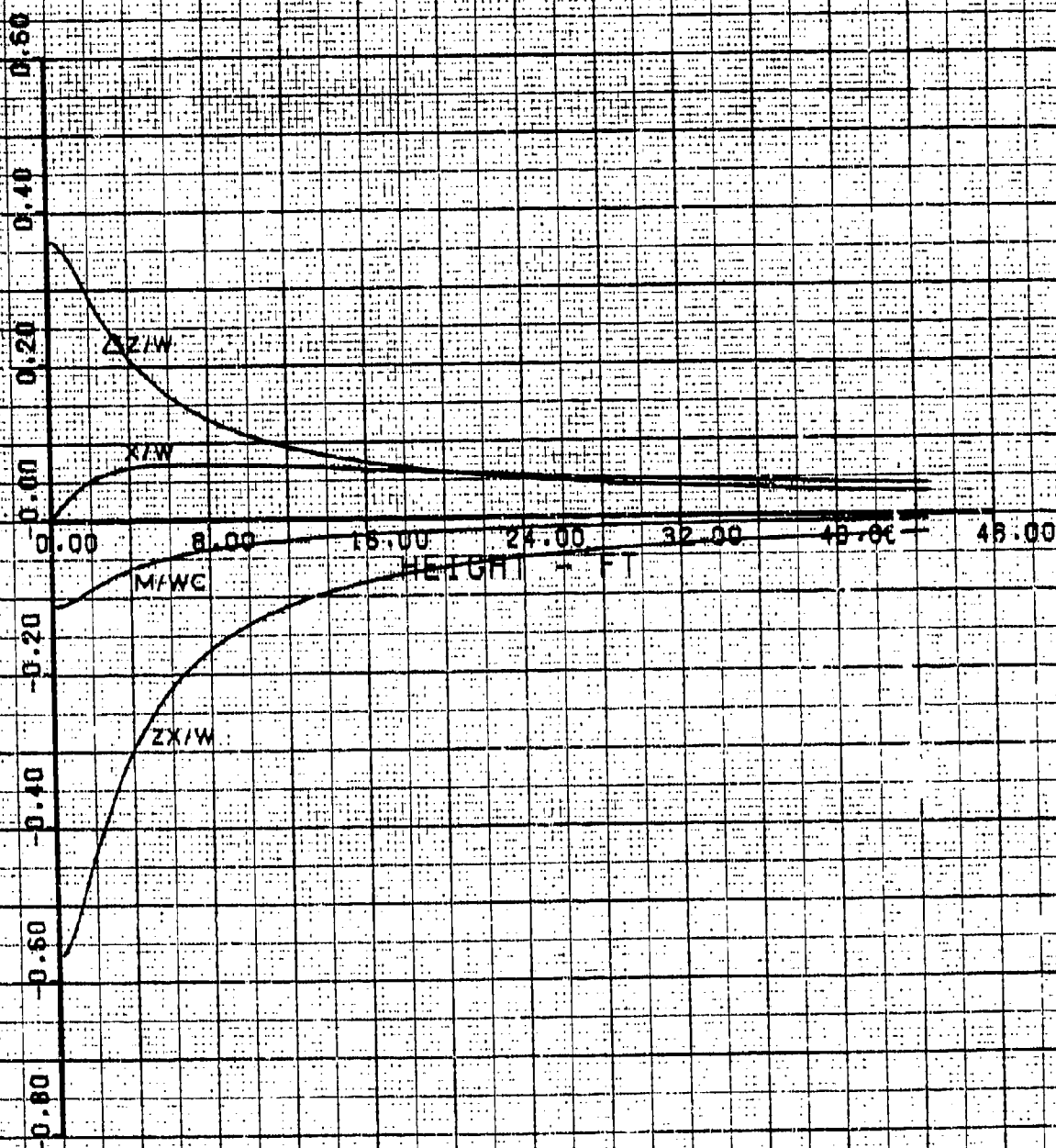


FIGURE 25B

## SPANLOADER PERIPHERAL JET ACIS

## LATERAL DATA

## VEHICLE DATA

SPAN = 390.0 FT

CHORD = 55.0 FT

SWEEP = 40.0 DEG

## CUSHION DATA

WIDTH = 80 TO 80 %SS

LENGTH = 15 TO 75 %C

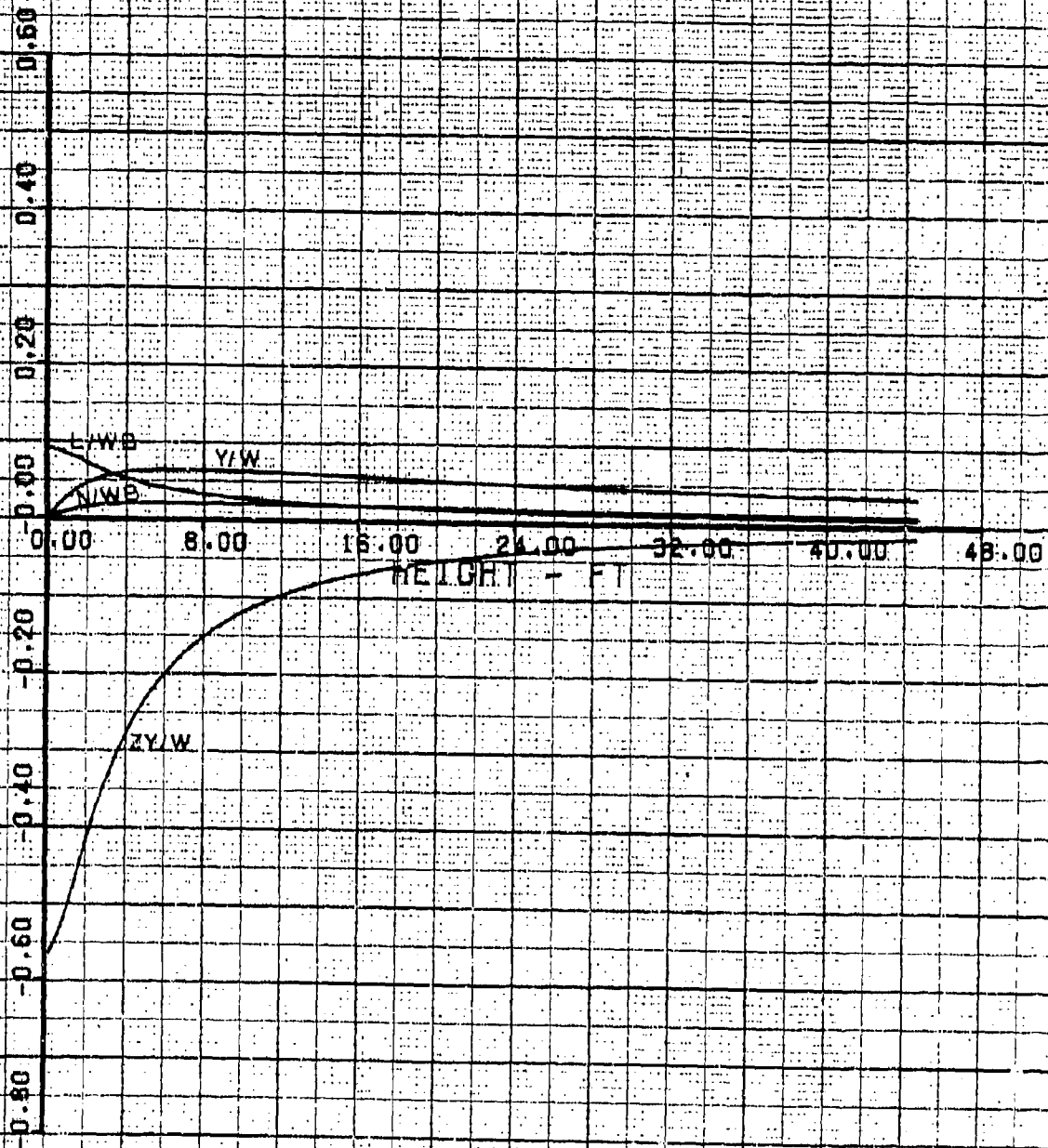
SUPPORT = VARIABLE %DW

## JET DATA

NO/WING = 1

ANGLE = 40.0 DEG

DEL ANG = 30 DEG





## B5.0 CONCLUSIONS

This stability and control analysis of the effectiveness of peripheral jet angle control on a spanloader PJ-ACLS vehicle has indicated that:

1. The vertical force, rolling moment, and pitching moment due to jet deflection arise mainly from the change of cushion pressure.
2. The forward force, sideforce, and yawing moments due to jet deflection arise mainly from the unbalanced in-plane jet reaction terms.
3. For realistic vehicle/cushion configurations, the jet reaction terms are small, and only small in-plane forces and yawing moments can be generated by control of the jet deflection angle.
4. For vehicles designed to 'hover' at large heights above the ground, the increased jet thrust leads to improved controllability from jet angle variation.
5. A large loss of lift is caused by variation of the jet deflection angle to generate in-plane forces and moments.
6. All forces and moments generated by varying the jet deflection angle are proportional to the level of cushion support provided.
7. Due to all of the above conclusions, it is considered that, unless the vehicle is designed to have a high level of ACLS support at a large height above the ground, vehicle control by peripheral jet angle variation should not be implemented.

B6.0 UNCONSTRAINED CUSHION VEHICLE

For the tilted unconstrained single cushion vehicle shown in Figure 3B the equilibrium equations are:

Vertical Force

$$W = p_c S_x S_y \cos \phi + J'_L \cos [\theta - (\delta \theta - \phi)] + J'_R \cos [\theta + (\delta \theta - \phi)] + 2J'_F \cos \theta$$

$$J'_L = J'_R = J' \frac{S_x}{2(S_x + S_y)} = \text{reaction of one side jet}$$

$$J'_F = J' \frac{S_y}{2(S_x + S_y)} = \text{reaction of one fwd or aft jet.}$$

Then:

$$W = p_c S_x S_y \cos \phi + J' \frac{S_x}{2(S_x + S_y)} 2 \cos \theta \cos (\delta \theta - \phi) + J' \frac{S_y}{2(S_x + S_y)} 2 \cos \theta$$

For small values of  $\delta \theta - \phi$ ,  $\cos (\delta \theta - \phi) \approx 1$  giving:

$$W \approx p_c S_x S_y \cos \phi + J' \cos \theta \quad (\text{B.1.})$$

Rolling Moment - Assuming a linear residual pressure gradient under the cushion:

$$\left( \frac{p_{cR} - p_{cL}}{2} \right) \left( \frac{S_y}{\delta} \right) (S_x S_y) = J'_L \cos [\theta - (\delta \theta - \phi)] \frac{S_y}{2} - J'_R \cos [\theta + (\delta \theta - \phi)] \frac{S_y}{2}$$

which becomes:

$$\left( \frac{p_{cR} - p_{cL}}{2} \right) \left( \frac{S_y}{\delta} \right) (S_x S_y) = \frac{J' S_x S_y}{4(S_x + S_y)} [\cos [\theta - (\delta \theta - \phi)] - \cos [\theta + (\delta \theta - \phi)]]$$

This gives the pressure difference between the right and left cushion sides as:

$$p_{c_R} - p_{c_L} = \frac{6J'}{S_y(S_x + S_y)} \sin \theta \sin(\delta\theta - \phi) \quad (B.2.)$$

This small cushion pressure gradient balances the rolling moment due to the asymmetric peripheral jets.

### Side Force

$$Y = p_{c_R} d_R S_x - p_{c_L} d_L S_x - \frac{p_{c_R} + p_{c_L}}{2} S_x S_y \sin \phi + \text{jet reaction term}$$

Now let  $p_{c_R} = p_c + \delta p$  and  $p_{c_L} = p_c - \delta p$  then:

$$Y = p_c (d_R - d_L) S_x - p_c S_x S_y \sin \phi + \delta p (d_R + d_L) S_x + \text{jet reaction term}$$

But  $d_R - d_L = S_y \sin \phi$  so:

$$Y = \delta p (d_R + d_L) S_x + \text{jet reaction terms.}$$

$$\text{Now } \delta p = \left( \frac{p_{c_R} - p_{c_L}}{2} \right)$$

$$d_R + d_L = 2d$$

So,

$$Y = (p_{c_R} - p_{c_L}) d S_x + \text{jet reaction terms.}$$

Substituting from equations (B.2) and defining the jet reaction terms gives:

$$Y = \frac{6J' d S_x}{S_y(S_x + S_y)} \sin \theta \sin(\delta - \theta) + J'_R \sin[\theta + (\theta - \delta\phi)] - J'_L \sin[\theta - (\theta - \delta\phi)] - 2J'_F \sin \phi$$

which simplifies to:

$$Y = \frac{J'}{(S_x + S_y)} \left\{ S_x \sin(\delta\theta - \phi) \left[ \cos\theta + \frac{\delta d}{S_y} \sin\theta \right] - S_y \sin\phi \right\} \quad (B.3)$$

#### D7.0 CONSTRAINED CUSHION VEHICLE

For the constrained single cushion vehicle shown in Figure 4B, the application of the Barrett theory to the right and left jets gives:

$$\frac{f}{d} [1 + \sin(\theta - \delta\theta)] = \eta \frac{f}{d} [1 + \sin(\theta + \delta\theta)] - (1 - \eta) \frac{f}{d} [1 - \sin(\theta + \delta\theta)]$$

which leads to:

$$\eta = 1 - \cos\theta \sin\delta\theta \quad (B.4)$$

Also, the side force due to the difference in horizontal reaction between the left and right jets is:

$$\begin{aligned} Y &= J'_R \sin(\theta + \delta\theta) - J'_L \sin(\theta - \delta\theta) \\ &= \frac{J' S_x}{2(S_x + S_y)} 2 \cos\theta \sin\delta\theta \end{aligned}$$

or:

$$Y = J' \frac{S_x}{(S_x + S_y)} \cos\theta \sin\delta\theta \quad (B.5)$$

The change of vertical force caused by asymmetrical jet control is found by subtracting the initial vertical force from the resulting vertical force. Also the initial vertical force may be used as a non-dimensionalizing parameter.

The vertical force produced by asymmetrical jet variation is:

$$Z = p_c S_x S_y + J'_R \cos(\theta + \delta\theta) + J'_L \cos(\theta - \delta\theta) + 2J'_p \cos\theta$$

$$Z = \frac{J' S_x S_y [1 + \sin(\theta - \delta\theta)]}{2d(S_x + S_y)} + \frac{J' S_x \cos \theta \cos \delta\theta}{S_x + S_y} + \frac{J' S_y \cos \theta}{S_x + S_y} \quad (B.6)$$

The initial vertical force is found by putting  $\delta\theta = 0$  which gives:

$$Z_i = \frac{J' S_x S_y [1 + \sin \theta]}{2d(S_x + S_y)} + J' \cos \theta \quad (B.7)$$

Dividing B.6 by B.7 gives

$$\frac{Y}{Z_i} = \frac{J' \frac{S_x}{S_x + S_y} \cos \theta \sin \delta\theta}{J' \frac{S_x S_y [1 + \sin \theta]}{2d(S_x + S_y)} + J' \cos \theta}$$

which reduces to:

$$\frac{Y}{Z_i} = \frac{\sin \delta\theta}{1 + \frac{S_y}{S_x} + \frac{S_y(1 + \sin \theta)}{2d \cos \theta}} \quad (B.8)$$

Similarly, subtracting (B.7) from (B.6) and dividing the result by (B.7) gives:

$$\frac{\Delta Z}{Z_i} = \frac{(\cos \delta\theta - 1) + \frac{S_y}{2d \cos \theta} [\sin(\theta - \delta\theta) - \sin \theta]}{1 + \frac{S_y}{S_x} + \frac{S_y(1 + \sin \theta)}{2d \cos \theta}} \quad (B.9)$$

Equations (B.8) and (B.9) give the non-dimensional side force and the non-dimensional change of vertical force due to asymmetric side jet rotation. If the fore and aft jets are varied to produce an X force, the equations for the rectangular peripheral jet are similar to those derived above with the terms  $S_x$  and  $S_y$  being interchanged.

#### B8.0 MULTI-CUSHION EQUATIONS

Figure 5B shows the geometry for the  $n^{\text{th}}$  cushion situated on a straight swept wing. The wing sweep angle is  $\Lambda$  and the cushion centroid is situated relative to the mean

aerodynamic quarter chord position as shown. Assuming geometric symmetry about the vehicle centerline and assuming that the cushion edge jets are manipulated in the most favorable combination, the overall forces and moments which can be generated by peripheral jet angle control are:

$$\text{Forward Force,} \quad X = 2 \left[ \cos \Lambda \sum_{n=1}^n X_n + * \sin \Lambda \sum_{n=1}^n Y_n \right]$$

$$\text{Side Force,} \quad Y = 2 \left[ \cos \Lambda \sum_{n=1}^n Y_n + * \sin \Lambda \sum_{n=1}^n X_n \right]$$

$$\text{Vertical Force,} \quad \Delta Z = 2 \sum_{n=1}^n \Delta Z_n$$

$$\text{Rolling Moment,} \quad L = 2 \left[ \cos \Lambda \sum_{n=1}^n \Delta Z_n Y_n + \sin \Lambda \sum_{n=1}^n \Delta Z_n X_n \right]$$

$$\text{Pitching Moment,} \quad M = 2 \left[ \cos \Lambda \sum_{n=1}^n \Delta Z_n X_n - \sin \Lambda \sum_{n=1}^n \Delta Z_n Y_n \right]$$

$$\text{Yawing Moment,} \quad N = 2 \left[ \sum_{n=1}^n Y_n X_n + \sum_{n=1}^n X_n Y_n \right]$$

\*sign assumes most favorable control of edge jets.

For cushion segments of the same size and configurations:

$$\sum_{n=1}^n X_n = n X_1$$

$$\sum_{n=1}^n Y_n = n Y_1$$

$$\sum_{n=1}^n \Delta Z_n = n \Delta Z_1$$

Then:

$$\sum_{n=1}^n \Delta Z_n Y_n = \Delta Z_1 \sum_{n=1}^n Y_n = n \Delta Z_1 S_y$$

$$\sum_{n=1}^n \Delta Z_n X_n = n \Delta Z_1 X_1$$

$$\sum_{n=1}^n Y_n X_n = n Y_1 X_1$$

$$\sum_{n=1}^n X_n Y_n = n X_n S_y$$

Substituting back into the force and moment equations and non-dimensionalizing gives:

$$\frac{\text{Forward Force}}{\text{Vehicle Weight}} = \frac{X}{W} = 2n \left[ \frac{X_1}{W} \cos \Lambda + \frac{Y_1}{W} \sin \Lambda \right]$$

$$\frac{\text{Side Force}}{\text{Vehicle Weight}} = \frac{Y}{W} = 2n \left[ \frac{Y_1}{W} \cos \Lambda + \frac{X_1}{W} \sin \Lambda \right]$$

$$\frac{\text{Vertical Force}}{\text{Vehicle Weight}} = \frac{\Delta Z}{W} = 2n \frac{\Delta Z_1}{W}$$

$$\frac{\text{Rolling Moment}}{\text{Weight X Span}} = \frac{L}{Wb} = 2n \frac{\Delta Z_1}{W} \left[ \left( \frac{S_y}{b} \right) \cos \Lambda + \left( \frac{x}{b} \right) \sin \Lambda \right]$$

$$\frac{\text{Pitching Moment}}{\text{Weight X Chord}} = \frac{M}{Wc} = 2n \frac{\Delta Z_1}{W} \left[ \left( \frac{x}{c} \right) \cos \Lambda - \left( \frac{S_y}{c} \right) \sin \Lambda \right]$$

$$\frac{\text{Yawing Moment}}{\text{Weight X Span}} = \frac{N}{Wb} = 2n \left[ \frac{Y_1}{W} \left( \frac{x}{b} \right) + \frac{X_1}{W} \left( \frac{S_y}{b} \right) \right]$$

Now the ratio of total cushion support over vehicle weight is:

$$\frac{\Sigma F_c}{W} = \frac{2n Z_1}{W}$$

where  $Z_i$  is the initial support provided by one cushion element.

Using this term in the above non-dimensional equations gives:

$$\frac{X}{W} = \frac{\Sigma F_c}{W} \left[ \frac{X_1}{Z_1} \cos \Lambda + \frac{Y_1}{Z_1} \sin \Lambda \right]$$

$$\frac{Y_F}{W} = \frac{\Sigma F_c}{W} \left[ \frac{Y_1}{Z_1} \cos \Lambda + \frac{X_1}{Z_1} \sin \Lambda \right]$$

$$\frac{\Delta Z}{W} = \frac{\Sigma F_c}{W} \left[ \frac{\Delta Z_1}{Z_1} \right]$$

$$\frac{L}{Wb} = \frac{\Sigma F_c}{W} \frac{\Delta Z_1}{Z_1} \left[ \left( \frac{S_y}{b} \right) \cos \Lambda + \left( \frac{x}{b} \right) \sin \Lambda \right]$$

$$\frac{N}{Wb} = \frac{\Sigma F_c}{W} \frac{\Delta Z_1}{Z_1} \left[ \left( \frac{x}{c} \right) \cos \Lambda - \left( \frac{S_y}{c} \right) \sin \Lambda \right]$$

$$\frac{N}{Wb} = \frac{\Sigma F_c}{W} \left[ \frac{Y_1}{Z_1} \left( \frac{x}{b} \right) + \frac{X_1}{Z_1} \left( \frac{S_y}{b} \right) \right]$$

This final equation set expresses the non-dimensional forces and moments in terms of:

1. The percentage cushion support,  $(\Sigma F_c/W)$
2. The vehicle geometry,  $b, c, \Lambda, x, S_y$ .
3. The single constrained cushion control force ratios derived in Section B2.0.



## APPENDIX C

### CUSHION AIR SUPPLY COMPONENT SIZING, PERFORMANCE, AND WEIGHTS

The determination of the fan requirements, and the system power and weight requirements was accomplished as a part of the comprehensive PJ-ACLS computer program. The supply system calculations are based on the equations defining the system component characteristics of Figures 25 through 27. The system component weights are functions of the required fan power, which in turn is a function of the fan flow and pressure required for the peripheral jet. The following summarizes the steps defining the required fan performance, and the system power and weight requirements.

(1) Fan Pressure,  $P_F$

$$P_F = P_J + P_I + P_{EX} = \left( 1 + \frac{P_I}{P_J} + \frac{P_{EX}}{P_J} \right) P_J$$

where:

- $P_F$  = Pressure rise across fan, PSF
- $P_J$  = Peripheral jet total pressure, relative to ambient, obtained from Appendix A, PSF
- $P_I$  = Fan inlet pressure loss, PSF
- $P_{EX}$  = Fan exhaust pressure loss, PSF

Estimating, for a typical installation as shown in Figure 25:

$$P_I/P_J = .051 \text{ \&}$$

$$P_{EX}/P_J = .071$$

then:

$$P_F = \left( 1 + \frac{.051 + .071}{P_J} \right) P_J = 1.122 P_J$$

(2) Fan Flow,  $Q_F$

$$Q_F = f \left[ (P_F)^{1/2} \right] = 5368 (P_F)^{1/2}$$

where:

$Q_F$  = Fan flow capacity per fan, at design point, CFM

(3) Number of Fans Required, NO. FAN

$$\text{NO. FAN} = \frac{Q_J \text{ TOT}}{Q_F} = \frac{120 Q_J}{Q_F}$$

where:

NO. FAN = Number of fans required per aircraft

$Q_J \text{ TOT}$  = Total jet airflow required per aircraft, CFM

$Q_J$  = Jet airflow required per semispan, obtained from Appendix A, CFS

(4) Fan Power Requirements,  $\text{BHP}_F$

$$\text{BHP}_F = f \left[ (P_F)^{3/2} \right] = 0.209 (P_F)^{3/2}$$

where:

$\text{BHP})_F$  = Brake horsepower required per fan

(5) Turboshaft Engine Power Requirements, SHP/ENG.

$$\text{SHP/ENG} = \frac{(\text{NO. FANS}) (\text{BHP})_F (\% \text{ Oversize}_{TS}/100)}{(\text{NO. TS}) (\eta_{GB}/100) (1 - \Delta\eta_{TS}/100)}$$

where:

NO. TS = Total number of turboshaft engines per aircraft = 8

$\% \text{ Oversize}_{TS}$  = Percent engine oversize to provide engine-out capability

$\eta_{GB}$  = Gearbox efficiency, %

$\Delta\eta_{TS}$  = Percent loss in engine power due to engine inlet and exhaust penalties

To provide engine-out capability, each engine is oversized to handle twice the required design load. Assuming an engine emergency power capability of 110% of engine rating, the required engine rating is  $2/1.1 = 1.82$  or 182% of the required design load.

also assuming:

$\eta_{GB}$  = 98% &

$\Delta\eta_{TS}$  = 5%

then:

$$\text{SHP/ENG} = \frac{(\text{NO. FANS}) (\text{BHP})_F (1.82)}{(8) (.98) (.95)} = (0.244) (\text{NO. FAN}) (\text{BHP}_F)$$

(6) Total Fan Weight, WTFAN

$$\text{WTFAN} = (\text{NO. FAN}) (\text{WFAN})$$

where:

WTFAN = Total fan weight per aircraft

WFAN = Fan weight per fan

$$= f(P_F, Q_F) = f(P_F), \text{ for a given fan size}$$

$$= 1.38 P_F$$

(7) Total Turboshaft Engine Weight, WTTS

$$\text{WTTS} = (\text{NO. TS}) (\text{WTS})$$

where:

WTTS = Total turboshaft engine weight per aircraft

WTS = Turboshaft engine weight per engine

$$= f(\text{SHP/ENG}) = 0.11675 (\text{SHP/ENG})$$

NO. TS = Total number of turboshaft engines per aircraft = 8

hence:

$$\text{WTTS} = (8) (.11675) (\text{SHP/ENG}) = 0.934 (\text{SHP/ENG})$$

(8) Total Gearbox Weight, WTGB

$$WTGB = (NO. GB) (WGB)$$

where:

WTGB = Total gearbox weight per aircraft

NO. GB = Total number of gearboxes per aircraft = 8

WGB = Gearbox weight per gearbox

$$= f(GR, SHP/ENG) = (.00588 GR + .01) (SHP/ENG)$$

GR = Gearbox gear ratio

$$= N_{TS}/N_F$$

$N_{TS}$  = Turboshaft speed, RPM

$$= f(SHP/ENG) = 24009 - 1.433 \left(\frac{SHP}{ENG}\right) + .00003254 \left(\frac{SHP}{ENG}\right)^2$$

$N_F$  = Fan Speed, RPM

$$= f \left[ (P_F)^{1/2} \right] = (221) (P_F)^{1/2}$$

(9) Total Uninstalled Air Supply System Weight, WT AIRU

$$WTAIRU = WTFAN + WTTS + WTGB$$

where:

WT AIRU = Total uninstalled air supply system weight per aircraft

WTFAN = Total fan weight per aircraft from step (6)

WTTS = Total turboshaft engine weight per aircraft from step (7)

WTGB = Total gearbox weight per aircraft from step (8)

(10) Total Installed Air Supply System Weight, WT AIRI

Assuming the weight required to install the air supply system is approximately 25% of uninstalled weight:

$$WT\ AIRI = 1.25\ WT\ AIRU$$

(11) Cushion Fuel Weight, W FUEL

$$WFUEL = \frac{(SFC) (SHP/ENG) (NO. TS) (\Delta t)}{(\% \text{ Oversize}_{TS}/100)}$$

where:

- WFUEL = Total fuel weight, per aircraft, per mission,  
as required to power turboshaft engines
- SFC = Specific fuel consumption of turboshaft  
engines = 0.32
- NO. TS = Total number of turboshaft engines = 8
- $\Delta t$  = Total time of cushion operation per aircraft  
mission
- $\% \text{ Oversize}_{TS}$  = Percent engine oversize to provide engine-out  
capability = 182% (from step (5))

assuming:

$$\Delta t = .45 \text{ hour} = 27 \text{ min.}$$

then:

$$WFUEL = \frac{(0.32) (8) (.45) (SHP/ENG)}{1.82} \approx 0.64 (SHP/ENG)$$

As explained previously, the fan dimensions, shown on Figure 25 , are based on the maximum fan size which can be accommodated by the available installation space. The fan inlet flow geometry, and the minimum fan spacing, shown on Figure 7, were selected primarily on the basis of compatibility with acceptable inlet losses and flow characteristics at the fan inlet. A minimum fan spacing of 2 feet assures a fan inlet approach-flow area approximately equal to or greater than the fan inlet area. With respect to turbo-shaft engine size, the required dimensions for the selected baseline systems, are determined from Figure 26.

#### SYSTEM CONSTRAINTS

The feasible PJ-ACLS design envelope may be constrained by fan speed limit, and/or by the maximum space available for fan installation.

Fan Speed Limit - The maximum available fan pressure, and in turn the maximum available peripheral jet pressure, is dictated by the fan speed limit. For a given cushion and jet geometry:

$$P_J \text{ required} = f(\text{Lift Required})$$

$$\text{Max Lift Available} = f \left[ (P_J) \text{ max. available} \right]$$

$$\begin{aligned}
 &= f \left[ (P_F) \text{ max. available} \right] \\
 &= f (\text{Fan Speed Limit})
 \end{aligned}$$

Therefore, the maximum lift available from the cushion is constrained by the requirement that:

$$\begin{aligned}
 P_J \text{ required} &\leq P_J \text{ max. available} \\
 &= f(\text{Fan Speed Limit})
 \end{aligned}$$

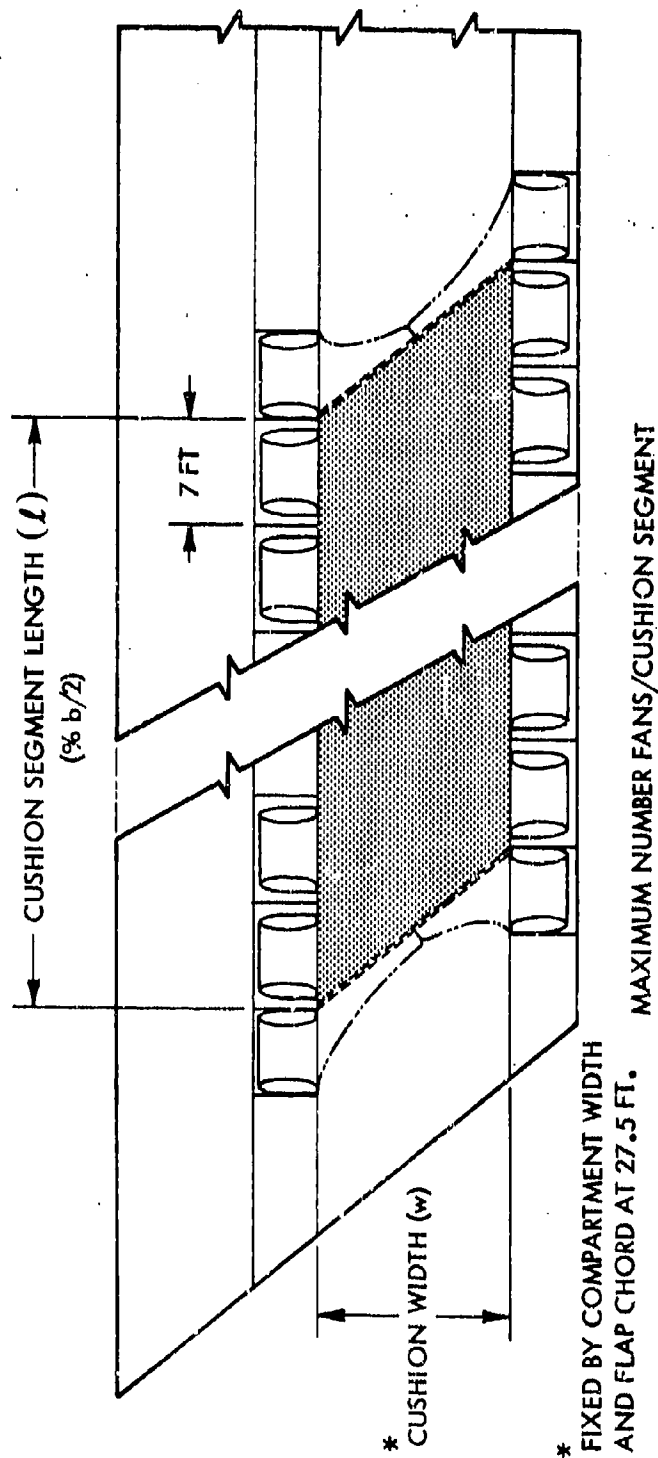
For a centrifugal fan, the fan speed is limited primarily by structural considerations and depends on fan and installation design. For the purposes of this study, it is assumed that the limiting parameter is fan tip speed and that:

$$\text{Fan Tip Speed Limit} = 800 \text{ ft/sec}$$

The results of the present study, Figure 32, shows the optimum cushion to lie well within this fan speed limit.

Fan Space Limit - The number of fans required to provide the required jet flow must not exceed the number of fans which can be fitted into the available installation space. Based on the fan installation as previously described and as shown on Figure 1C, the number of fans possible is limited by the spanwise (cushion lengthwise) space available per cushion segment. Referring to Figure 1C, the maximum number of fans possible is therefore defined as follows:





$$\text{Limit/seg} = \left[ \frac{l}{7} \right]$$

MAXIMUM NUMBER FANS/AIRCRAFT

$$\text{NUMBER FANS} = (4) (\text{Limit/seg}) + 8$$

Figure 1C. Cushion Fan Space Limit

$$\begin{aligned}\text{LIMIT/Aircraft} &= (4) (\text{LIMIT/Seg}) + 8 \\ \text{LIMIT/Seg} &= \ell / (\Delta \ell)_{\text{FI}} \\ &= \ell / \left[ (\Delta \ell)_F + (\Delta \ell)_{\text{FSPACE}} \right]\end{aligned}$$

where:

$$\begin{aligned}\text{LIMIT/Aircraft} &= \text{Maximum number of fans possible per aircraft} \\ \text{LIMIT/Seg} &= \text{Maximum number of fans possible per cushion segment} \\ \ell &= \text{Cushion length (or segment length)} \\ \Delta \ell_{\text{FI}} &= \text{Spanwise space required per fan installation} \\ &= \Delta \ell_F + \Delta \ell_{\text{FSPACE}} \\ \Delta \ell_F &= \text{Fan width} = 5 \text{ ft.} \\ \Delta \ell_{\text{FSPACE}} &= \text{Minimum spacing required between fans} = 2 \text{ ft.}\end{aligned}$$

therefore:

$$\text{LIMIT/Aircraft} = (4) \left[ \frac{\ell}{(5) + (2)} \right] + 8 = (4) \left( \frac{\ell}{7} \right) + 8$$

To ascertain adequate available space for fan installation, this space-limited number of fans must be equal to or greater than the number of fans required as calculated in Step (3) above. Referring to Figure 2C, it is seen that the fan space limit constrains the selected baseline -40 inch configuration to a total aircraft weight greater than what would otherwise be the minimum.

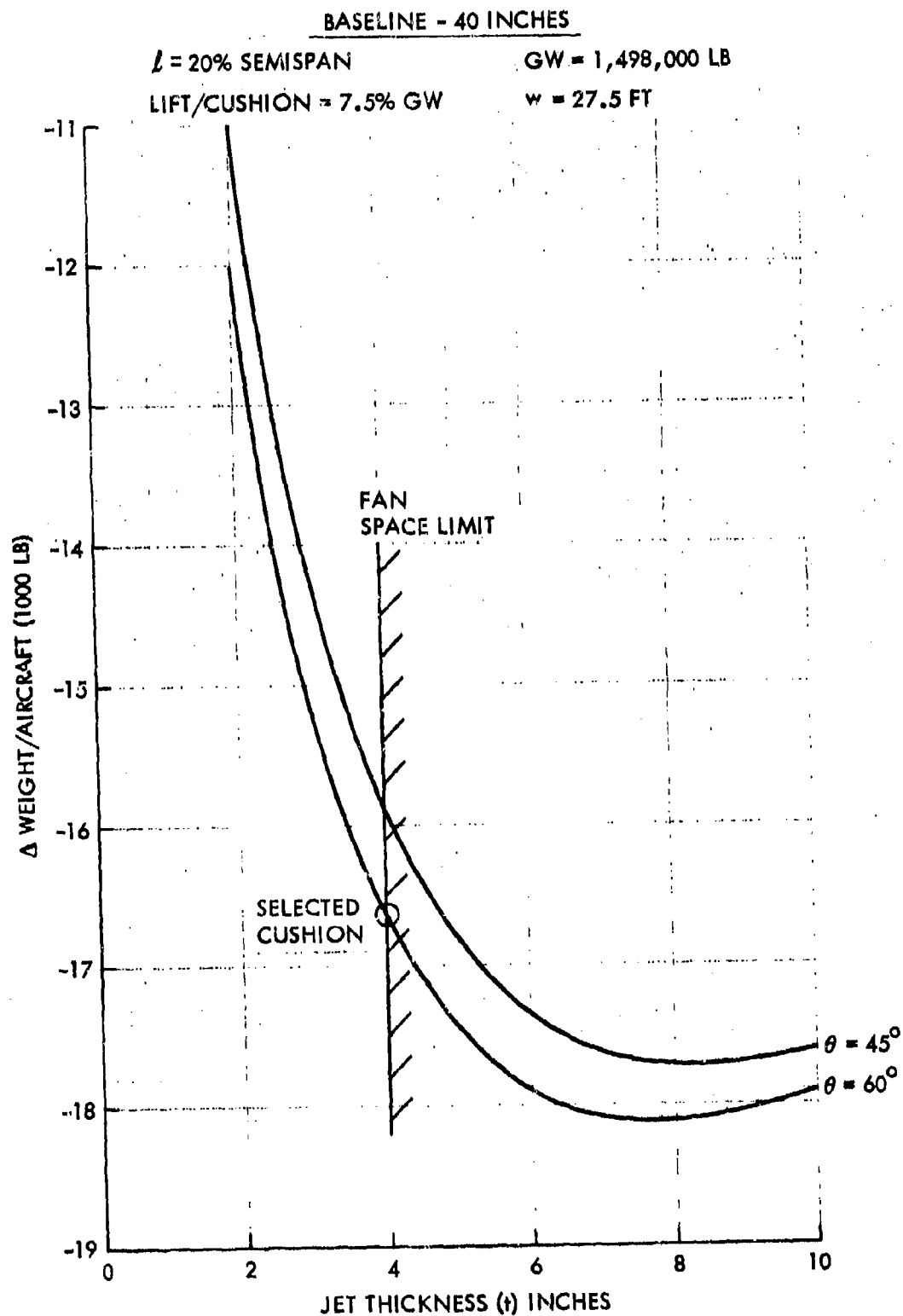


Figure 2C. Delta Aircraft Weight vs Jet Thickness & Angle

It should be pointed out that by selecting excess pressure fans, the number of fans required can be reduced to the limit number; but only at a net increase in total aircraft weight. By selecting fans with higher pressure capability than would be necessary to provide the required jet pressure when assuming a 7.1 percent fan exhaust pressure loss per Step (1) above, the flow pumping capacity per fan would be increased, thereby reducing the total number of fans required. In this case the correct jet pressure could be provided by designing increased losses into the fan exhaust system. This approach would allow the cushion jet to then be sized at the jet thickness for minimum aircraft weight (see Figure 20). Analyses show, however, that the weight decrement produced by optimizing jet thickness is much less than the increase in weight required due to the higher power, less efficient fan installation. For example, for the baseline -40 inches configuration of Figure 29, at 60 degrees  $\theta$ , the weight decrement which would be realized by increasing the jet thickness from the 4-inch space limited thickness, to the approximate 8-inch thickness at the minimum weight point, is only about 1500 pounds; while, the total increase in installed air supply system and fuel weight required to reduce the number of fans to the space-limited number, with the 8-inch thickness jet, is approximately 58,500 pounds. Thus this design approach would result in a net increase in aircraft weight of approximately 57,000 pounds, as related to the selected baseline -40 inch configuration. The selected configuration therefore remains the minimum weight design.

## REFERENCES

1. Johnston, W. M., et al., "Technical and Economic Assessment of Span-Distributed Loading Cargo Aircraft Concepts," Lockheed Georgia Company, NASA CR-145034, August 1976
2. Digges, K. H., "Theory of An Air Cushion Landing System for Aircraft," Air Force Flight Dynamics Laboratory, AFFDL-TR-71-50, June 1971
3. Earl, T. D., "Air Cushion Landing Gear Feasibility Study," Air Force Flight Dynamics Laboratory, AFFDL-TR-67-32, May 1967
4. Anon., "A Study of Radial-Flow Fans for GEM Propulsion System Applications," U. S. Army Transportation Research Command, TRECOM Tech Report 64-33, July 1964
5. Anon., "Preliminary Performance and Installation Data for the STS487 Turboshaft Engine," Pratt & Whitney Aircraft, CDS-11, March 1976
6. Anon., "Preliminary Performance and Installation Data for the STF 477 Turbofan Engine," Pratt & Whitney Aircraft, CDS-6
7. Anon., "Allison PD370-22, Advanced Turboprop Engine," Detroit Diesel Allison, EDR 8798, June 1976
8. Dau, K., et al., "Aerodynamics of a Rectangular Wing with a Peripheral Jet for Air-Cushion Take-off and Landing," AFFDL-TR-65-59, September 1965
9. Dau, K., "Characteristics of a Rectangular Wing with a Peripheral Jet in Ground Effect," Part I, UTIA Tech. Note No. 56, September 1961
10. Davis, J. M., "Characteristics of a Rectangular Wing with a Peripheral Jet in Ground Effect," Part II, UTIA Tech. Note No. 59, May 1962
11. Surry, D., "Characteristics of a Rectangular Wing with a Peripheral Jet in Ground Effect," Part III, UTIA Tech. Note No. 77, August 1964
12. Braden, J. A., "Flight Sciences, Conceptual Research Program," Lockheed-Georgia Company LG78ER0030, Vol. 11a, Project 78R470, March 1978
13. Braden, J. A., Conceptual Research - "Evaluation of Highly Integrated Aero-Propulsive Concepts," Lockheed Georgia Co., LG79ER0006, Project 79R471, March 1979